A Novel Method of Characterizing Polymer Membranes Using Upstream Gas Permeation Tests

by

Mukhtar Al-Ismaily

Thesis submitted to the Faculty of Graduate and Postdoctoral Studies in partial fulfillment of the requirements for the degree of

Master of Applied Science

in the Department of Chemical & Biological Engineering

Faculty of Engineering

University of Ottawa

October, 2011

Abstract

Characterization of semi-permeable films promotes the systematic selection of membranes and process design. When acquiring the diffusive and sorption properties of gas transport in non-porous membranes, the time lag method is considered the conventional method of characterization. The time lag method involves monitoring the transient accumulation of species due to permeation on a fixed volume present in a downstream reservoir.

In the thesis at hand, an alternative approach to the time lag technique is proposed, termed as the short cut method. The short cut method appoints the use of a two reservoir system, where the species decay in the upstream face of the membrane is monitored, in combination with the accumulation on the downstream end. The early and short time determination of membrane properties is done by monitoring the inflow and outflow flux profiles, including their respective analytical formulas. The newly proposed method was revealed to have estimated the properties at 1/10 the required time it takes for the classical time lag method, which also includes a better abidance to the required boundary conditions.

A novel design of the upstream reservoir, consisting of a reference and working volume, is revealed, which includes instructional use, and the mechanics involved with its operation. Transient pressure decay profiles are successfully obtained when the reference and working volumes consisted of only tubing. However when tanks were included in the volumes, large errors in the decay were observed, in particular due to a non-instantaneous equilibration of the pressure during the start up. This hypothesis was further re-enforced by examining different upstream tank-based configurations.

In the end, a validated numerical model was constructed for the purpose of simulating the two reservoir gas permeation system. A modified form of the finite differences scheme is utilized, in order to account for a concentration-dependent diffusivity of penetrants within the membrane. Permeation behavior in a composite membrane system was disclosed, which provided a new perspective in analyzing the errors associated with the practical aspect of the system.

Résumé

La caractérisation des films semi-perméable favorise la sélection systématique des membranes et la conception de procédés. Lors de l'acquisition des propriétés de diffusion et de sorption pour le transport de gaz dans des membranes non-poreuses, la méthode de temps de latence (ou décalage temporel) est considérée comme la méthode conventionnelle de caractérisation. Cette méthode consiste à surveiller l'accumulation d'espèces chimiques à l'état transitoire causée par la perméation dans un volume fixe présent dans un réservoir en aval.

Dans la présente thèse, une approche alternative à la technique du temps de latence est proposée appelée la méthode du raccourci. La méthode du raccourci comprend l'utilisation d'un système à deux réservoirs, où la dégradation chimique des espèces en amont de la membrane et les espèces accumulées en aval sont contrôlées.

Les propriétés à court et long terme des membranes sont estimées en contrôlant les profils des flux d'entrée et de sortie, y compris leurs formules analytiques respectives. La méthode nouvellement proposées s'est révélée pouvoir estimer les propriétés à 1/10ème fois le temps requis par la méthode classique de décalage temporel, qui respecte aussi mieux des conditions limites.

Une nouvelle conception du réservoir en amont est proposée : celle-ci est comprend un volume de référence et un volume actif, accompagnée d'un guide d'instruction et de la mécanique de son fonctionnement. Les profils de chute de pression à l'état transitoire sont obtenus lorsque le volume de référence et les volumes de travail sont seulement composés de tubes. Cependant, quand des citernes ont été incluses dans les volumes, des erreurs

importantes dans la chute de pression ont été observées, particulièrement en raison d'une équilibration non instantanée de la pression durant le démarrage de l'expérience Cette hypothèse a été renforcée en examinant différentes configurations de citernes en amont de la membrane.

À la fin, un modèle numérique validé a été mis en place dans le but de simuler le système à deux réservoirs de perméation de gaz. Une forme modifiée de la méthode numérique de différences finies est utilisée, afin de tenir compte de la dépendance de la diffusivité sur la concentration des espèces pénétrants la membrane. Le comportement de perméation dans un système composite de membrane a été divulgué, qui a fourni une nouvelle perspective dans l'analyse des erreurs liées à l'aspect pratique du système.

Statement of Collaborators

The short cut method by utilizing the idea of average fluxes was originally conceived by Dr. Hanz Wijmans of Membrane Technology & Research Inc., and the two-volume concept of monitoring low permeation rates in the upstream is owed to my supervisor Dr. Bogulaw Kruczek. The downstream reservoir employed in this project was adopted by former PhD graduate Siamak Lashkari.

I acknowledge that the remainder of the work, which includes the mathematical developments, coding of the numerical model, the numerical methods utilized, and the thesis write-up was done entirely by me.

Mukhtar S. Al-Ismaily

Signature: _____ **Date: _____**

Acknowledgements

I would like to take this opportunity to thank the people that helped me with my Master's studies here in the University of Ottawa.

Foremost, I'd like to express my utmost gratitude to Dr. Boguslaw Kruczek for allowing me to embark on this project, and for his expertise, kindness, and most of all, for his patience. His continued support and guidance in this project was immense, and I couldn't have imagined a better mentor for my graduate work.

I would like to thank Qiang Wang for his time and effort on his training for synthesizing the membranes. I'd also like to thank former Ph.D. graduate Siamak Lashkari for assisting me with troubleshooting the original system, and the major relevance his Ph.D. work had on my research.

I would like to thank Dr. Thibault who was always there to offer his help whenever I encountered certain obstacles at the course of my research. Special thanks to friend Addis Zewde for providing me with the French translation to the abstract.

I'd like to express my gratitude to my thesis examiners Dr. Marc Dube, Dr. Arturo Macchi, and Dr. Poupak Mehrani for their questions, insightful comments, and their support

Special Thanks to the Ministry of Manpower, Oman for sponsoring my Master's education here in the University of Ottawa. This would have not been possible without their unparalleled support.

I would like to admire the support and love of my father, my mother, and siblings Salima and Qais for their patience and inspiration during these difficult times.

This thesis is especially dedicated to my former late colleagues Samir Ali and Mehrdad Khazabi who always stood behind me and knew I would succeed. Gone now but never forgotten.

Table of Contents

List of Tables

List of Figures

CHAPTER 1

INTRODUCTION

1.1 Literature Review

1.1.1 Transport in Non-Porous Membranes

A membrane is basically a semi-permeable barrier between two phases. Transport of species from one phase to the other across the membrane is by the gradient of chemical potential, which depending on the circumstances and conditions of separation may simplify to the gradient of concentration of species, temperature, voltage, or pressure. The current project revolves around the use of dense non-porous membranes, where transportation of species is commonly driven by a concentration gradient across the membrane. The transport of penetrant molecules to the other side of the membrane is typically referred to

as 'permeation'. The types of membrane processes that utilize non porous membranes include pervaporation, and gas/vapour separation [1].

Non porous polymer films are a special class of membranes capable of separating molecules of approximately the same size (similar order of magnitude). The basis of separation are the differences in the diffusivity and solubility within the polymer membrane, or where at certain cases (glassy polymers) the extent of interaction between the polymer and permeate is what determines the degree of separation. Examples include the separation of N_2 and O_2, or hexane and heptane, where the conventional use of porous membranes is ineffective. Examples for the applicational use of non-porous membranes are [2]:

- Ammonia production plants equipped with membrane system used for the recovery and recirculation of H_2 from the purge gas.
- Pre-purification of natural gas by permeation of acid compounds such as CO_2 and H_2S
- The enrichment of O_2 or N_2 from air, which served itself as a good competitor to well-established adsorption and cryogenic-based processes.

Transportation of gas, vapour, and liquid components through dense non porous membranes is commonly classified via a mechanism known as the 'Solution Diffusion Model'. The transportation of gas molecules will be the focus of this project

$$P = D \cdot S \tag{1.1}$$

where S, the solubility (cm^3 (STP) cm^{-3} $cmHg^{-1}$), is a measure of the amount of penetrant that is sorbed by the membrane at equilibrium and D (cm^2/s) is the diffusivity, which is an indication of how fast the penetrant travels through the membrane, which depends on the size/shape of the penetrant and available free volume within the membrane's polymer structure. In the case of permeation of ideal gases and/or elastic polymer membranes (ideal systems), the polymer-penetrant interactions are low, hence the solubility is relatively low and the diffusivity is not concentration dependant. As a result, the penetrant concentration in a polymer is described via a linear relationship known as Henry's Law,

$$C = p \cdot S \tag{1.2}$$

where p is the partial pressure of the species on one side of the membrane, and C is its concentration within the polymer membrane. However in the case of glassy polymers, sorption of the penetrant no longer obeys Henry's Law. The most commonly accepted case of this is the concept of dual mode sorption [3], which deduces the existence of two sorption sites: Henry Sites, and Langmuir sites.

$$C = Sp + \frac{C'_H \, bp}{1 + bp} \tag{1.3}$$

where b is the hole affinity constant ($cmHg^{-1}$), and C'_H (cm^3 (STP) cm^{-3}) is the hole saturation constant. This is briefly touched upon later in Chapter 5.

As previously shown in Eq. (1.1), the permeability (P) is the product of the diffusivity and solubility coefficients. The permeability unit is defined in terms of Barrer, which is commonly used in packaging applications, and it has the base units of

[cm^3(STP)cm/cm^2·s·cmHg]. As a result, these properties (*P*, *S*, and *D*) serve as the main constituents for characterizing gas permeation in non porous polymer membranes.

The simplest way to describe the flux at any position within a slab membrane is by Fick's 1st Law of diffusion:

$$J = -D\frac{\partial C}{\partial x} \tag{1.4}$$

where *J* (cm^3(STP) cm^{-2} s^{-1}) is the penetrant flux, and *x* (cm) is the position along the membrane thickness.

On the other hand, Fick's 2nd Law of diffusion describes the concentration of species *C* as a function of position *x* and time *t*.

$$\frac{\partial C}{\partial t} = D\frac{\partial^2 C}{\partial x^2} \tag{1.5}$$

1.1.2 Constant Volume System

Knowledge of the Solubility (*S*) and Diffusivity (*D*) facilitates systematic membrane selection and design of separation processes. Despite the structure and type of membrane being used, the first step prior to its application is characterizing the membrane via the many available and well-renowned techniques.

The current focus is gas permeation in non-porous membranes, where the most common scheme being applied is Dayne's Time Lag Method [3], where *S*, *D*, and eventually *P* are obtained. In its simplest terms, the time lag method is a test that exploits the concept of 'integral permeation' [4]. Where a cell containing a membrane of known thickness is

pressurized on one side by a gas, then the extent and cumulative amount of gas permeated is measured on a receiving volume over time.

Integral permeation is notably measured by means of a mass flow meter or bubble flow meter [1]. A more sophisticated setup was later employed by Barrer [6] where the receiving volume (downstream reservoir) was initially kept under vacuum, and the integral permeation was monitored via placement of a pressure transducer. The pressure accumulation is therefore directly monitored. This is a basic representation of a classical constant volume (CV) system.

More recent/modern setups of the CV system involve usage of an accumulation tank in the downstream reservoir [7]. This was primarily used to tackle issues of high permeation rates that limit the range of available pressure transducers. Also, Stern et al. [8] implemented as similar design, but with multiple accumulation tanks (separated by valves), which provides the flexibility of accurate measurements of the permeability based on anticipated permeation rates.

Recent publications from Lashkari and Kruczek [9] concluded that the combination of accumulation tanks under high vacuum in the downstream led to major errors in estimating the membrane properties (*D, P,* and hence *S*), which is due to a 'resistance effect' on the gas accumulation. The resistance to gas accumulation implied the existence of a non-negligible pressure gradient across the downstream reservoir. This particular study and its common implications to this research are further discussed in Chapter 4.

1.1.3 Time Lag Method

The classical time lag method was developed by Daynes for membranes of slab geometry [1]. Barrer [6] employed alternative models for measuring the time lag in slab, cylindrical, and spherical geometries. In 1957, Frisch [10] utilized the asymptotic solution using numerical approximations for estimating the diffusivity and solubility. This is carried out after obtaining and achieving steady state in the pressure accumulation profile, which is collected by the constant volume system. This time lag method is applicable when the membrane permeation test complies with the following boundary conditions

$$C(x,0) = C_{Ai} \approx 0$$
$$C(0,t) = C_{A0}$$
$$C(L,t) = C_{AL} \approx 0$$

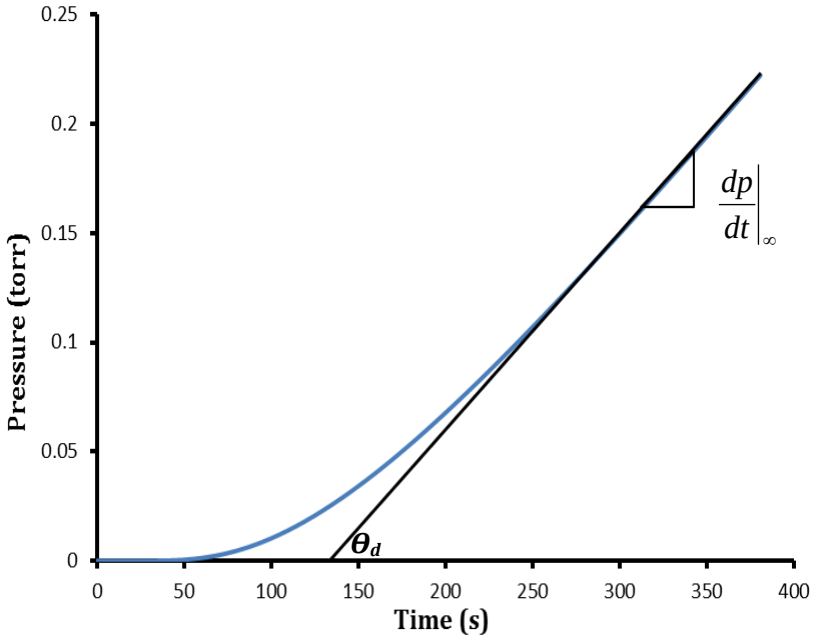

Figure 1.1 Demonstrating the time lag from the pressure accumulation plot

Rogers et al. [11] derived an analytical expression (Eq. (1.6)) that accounts for the cumulative species collected over time.

$$Q_L(t) = -A\int_0^t J_L(t)dt = \frac{ADC}{L}\left[t - \frac{L^2}{6D} + \frac{2L^2}{\pi^2 D}\sum_{n=0}^{\infty}\frac{(-1)^n}{n^2}\exp\left(-\frac{Dn^2\pi^2 t}{L^2}\right)\right] \qquad (1.6)$$

$$\lim_{t\to\infty} Q_L(t) = \frac{ADC}{L}\left[t - \frac{L^2}{6D}\right]$$

This approaches steady state as time $t \rightarrow \infty$. It leads to the following expressions (Eq. (1.7 & 1.8)), where the diffusivity and permeability are extracted from the pressure accumulation in Fig. 1.6 ***after achieving steady state***.

$$\theta_d = \frac{L^2}{6D} \qquad (1.7)$$

$$\left.\frac{dp}{dt}\right|_{\infty} = \frac{p_0 ARTP}{VL} \qquad (1.8)$$

A is the membrane cross sectional area, while V is the volume of the downstream reservoir and T is the operating temperature. The time lag (θ_d) is obtained from the x-intercept extrapolation of the steady state accumulation plot (Fig. 1.1) and $\left.\frac{dp}{dt}\right|_{\infty}$ is the slope.

1.2 Thesis Objectives

The primary objective of this thesis is to propose an alternative 'integral permeation' method for the faster determination of membrane properties, without the need of achieving steady state conditions. This involves monitoring the decay of species from the

upstream reservoir simultaneously with the pressure accumulation on the downstream reservoir. The newly developed scheme is assessed at a theoretical and practical level. This is in order analyze its credibility and feasibility with respect to the classical time lag method.

1.3 Thesis Outline

Following the current literature review, the thesis immediately embarks to the heart of this project, which is the newly proposed short cut method for the faster determination of membrane properties using the two reservoir system. Chapter 3 continues with an isolated assessment of only the upstream pressure decay profiles in an attempt to determine the transport properties, and it also serves as a prerequisite to Chapter 4. Chapter 4 provides a detailed outline on the design of the two reservoir integral permeation system, with an added emphasis on a novel design of the upstream reservoir for measuring the pressure decay. Finally, Chapter 5 serves as a guide for the development of a numerical model used to carry out the various data-backed simulations in this thesis. Chapter 6 concludes this dissertation with additional reporting on the recommendations and contributions of this project.

The appendices consist of 2 parts. Firstly is a step by step procedure involved with the derivation of the short time solution, and last is supplementary material of experimental results and calculations based on Chapter 2

References

[1] M. Mulder, Basic Principles of Membrane Technology, Second Edition. Springer, 1996, p. 158.

[2] M.R. Shah, R.D. Noble, D.E. Clough, Measurement of sorption and diffusion in nonporous membranes by transient permeation experiments, J. Mem. Sci. 287 (2007) 111–118

[3] H.A. Daynes, The process of diffusion through a rubber membrane, Proc. R. Soc. London Ser. A 97 (685) (1920) 286–307.

[4] H. Kumazawa, S.-Y. Bae, Sorption and Permeation Behavior for a Gas in Glassy Polymer Membrane Near the Glass Transition Temperature, 60 (1996) 115-121.

[5] S.W. Rutherford, D.D. Do, Review of time lag permeation technique as a method for characterization of porous media and membranes, Adsorption 3 (1997) 283.

[6] R.M. Barrer, Permeation, diffusion and solution of gases in organic polymers, Trans. Farad. Soc., 35 (1939) 628-643.

[7] K.C. O'Brien, W.J. Koros, T.A. Barbari, E.S. Sanders, A new technique for measurement of multicomponent gas transport through polymeric films, J. Membr. Sci., 29 (1986) 229-238

[8] S.A. Stern, P.J. Gareis, T.F. Sinclair, P.H. Mohr, Performance of a versatile variable-volume permeability cell. Comparison of gas permeability measurements by variable-volume and variable-pressure methods, J. Appl. Polym. Sci. 7 (1963) 2035-2051

[9] S. Lashkari, B. Kruczek, Effect of resistance to gas accumulation in multi-tank receivers on membrane characterization by the time lag method. Analytical approach for optimization of the receiver, J. Membr. Sci. 360 (2010) 442–453.

[10] H.L. Frisch, The Time Lag in Diffusion, J. Phys. Chem., 61 (1957) 93-95

[11] W.A. Rogers, R.S. Buritz, D. Alpert, Diffusion coefficient, solubility, and permeability for helium in glass, J. Appl. Phys. 257 (1954) 868–875.

CHAPTER 2

A SHORTCUT METHOD FOR FASTER DETERMINATION OF PERMEABILITY COEFFICIENT FROM TIME LAG EXPERIMENTS

M. Al-Ismaily [1], B. Kruczek[1], J.G. Wijmans[2]

[1] Department of Chemical & Biological Engineering
University of Ottawa

[2] Membrane Technology and Research, Inc.

Abstract

Time lag permeation experiments are a well-known method for the determination of permeability and diffusion coefficients of gases in polymer films. In these experiments pressurized gas is brought in contact with one side of the film and the amount of gas evolving from the opposite, low pressure, side of the film is measured as a function of time. The permeability coefficient is obtained from the steady-state permeation flux and the diffusion coefficient is obtained from the permeation flux versus time behavior through an extrapolation method. The time required to reach steady state permeation is of the order of several hours or less for most polymers, but can be on the order of weeks or even months for films prepared from low-permeability barrier polymers.

A novel method is described in this paper for the early determination of the permeability coefficient, which was revealed to yield estimates at $1/10^{th}$ the time it normally takes with the conventional time lag methods. This method requires an accurate monitoring of transient gas fluxes in and out of the tested membrane. To achieve the former a new design of the upstream side of a constant volume system was developed.

The applicability of the short cut method is demonstrated in permeation tests with nitrogen in a PPO membrane. The results show good compliance with the classical time lag and steady state methods. In the case of imprecise pressure measurements, improved accuracy of the results is observed and expected when operating at higher pressures.

Keywords: Gas Permeation, Permeability, Gas Diffusion, Constant Volume System, Time Lag

2.1 Introduction

Gas permeation through nonporous polymer films, often referred to as homogeneous membranes, is governed by the solution-diffusion mechanism. The knowledge of sorption and diffusion properties of small molecules in the membrane enables investigation of structure–property relationships. Consequently, this facilitates the systematic selection of membranes and prediction of their performances [1]. Several methods of membrane characterization have been put into use over the years. For nonporous polymeric films, the continuous monitoring of species permeating and accumulating in a constant volume system is commonly associated with the time lag method (integral permeation). The first one to conceive the time lag method was Daynes in 1920 [2]. The time lag method was then brought to prominence by Barrer [3], who described how the time required to achieve steady state permeation of a gas can be distinguished between contributions of diffusion and sorption to overall permeability, which is defined as follow:

$$P = D \cdot S \tag{2.1}$$

where P is the permeability, D is the diffusivity, and S is the solubility.

Prior to a time lag permeation experiment both sides of a polymer film are exposed to a vacuum. At time $t > 0$, the upstream side is exposed to a gas or vapor at a specified pressure p_{A0}. The gas molecules start sorbing into the high-pressure side of the film, and subsequently diffuse to the opposite vacuum/low-pressure side of the film (downstream). As a result, an accumulation and decay of species is observed in the downstream and

upstream ends, respectively, and a concentration profile develops in the film over time according to Fick's Law.

$$\frac{\partial C_A}{\partial t} = D_A \frac{\partial^2 C_A}{\partial x^2} \tag{2.2}$$

where C_A is the concentration of species A in the film, which is a function of position x and time t, and D_A is the diffusion coefficient of species A in the film. Slab geometry is assumed, and based on the following initial/boundary conditions; a concentration profile is obtained using Laplace Transforms:

$$C_A(x,0) = C_{Ai}$$
$$C_A(0,t) = C_{A0} = \text{constant}$$
$$C_A(l,t) = C_{Al} = 0$$

$$C_A(x,t) = C_{A0} \sum_{n=0}^{\infty} \left[erfc\left(\frac{2l^{3/2} n + \sqrt{l}\, x}{2l\sqrt{D_A t}} \right) - erfc\left(\frac{2l^{3/2}(n+1) + \sqrt{l}\, x}{2l\sqrt{D_A t}} \right) \right] \tag{2.3}$$

where, C_{A0} is the species concentration ot the high pressure side of the film, and l represents the thickness of the membrane film. At low pressures and ideal gas conditions, Henry's Law is often sufficient to relate the concentration of gas in the membrane to its pressure.

$$C_A = p_A \cdot S_A \tag{2.4}$$

where S_A is Henry's solubility coefficient of species A, and p_A is the gas partial pressure.

The time lag method involves monitoring the accumulation of gas species in the low pressure end (downstream) of the membrane, where evaluation of the flux (at $x = l$) is

necessary. The flux, J_A, is linearly related to the concentration gradient according the Fick's first law of diffusion:

$$J_A(x,t) = -D_A \frac{\partial C_A}{\partial x} \tag{2.5}$$

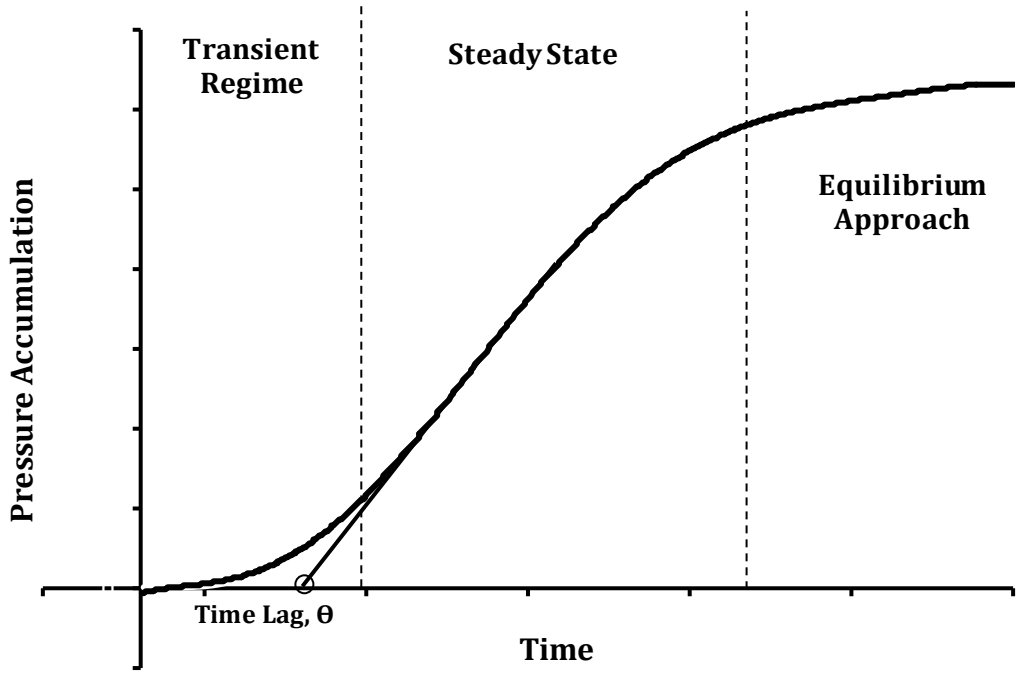

Figure 2.1 Typical pressure profile of downstream constant volume system, illustrating the 3 key regions of the permeation test.

When performing time lag experiments, an accumulation of species is observed on the downstream end of the membrane. A typical pressure profile is demonstrated in Fig. 2.1. There exists an early and highly transient short-time state, a quasi-steady state, and an equilibrium state where no net diffusion of the species occurs. From a mass balance performed on the constant volume at the downstream side of the membrane, the pressure is calculated as a function of flux as follows [4]:

$$p_A(l,t) = \frac{p_{A0} S_A RTA_f}{C_{A0} V} \int_0^t J_A(l,t)dt \tag{2.6}$$

where V is the receiving volume of the gas, T is the operating temperature, and A is the surface area of the membrane. Within integral permeation systems the gas permeability is generally calculated as follows [5]:

$$P = \frac{J_\infty \cdot l}{\Delta p} \tag{2.7}$$

$$J_\infty = \left.\frac{dp_A}{dt}\right|_\infty \frac{V}{A_f RT} \tag{2.8}$$

where Δp is the pressure difference across the membrane and the subscript ∞ denotes a quasi-steady state. Permeation rate tests do not only yield the permeability as shown in Eq. (2.7), but also the diffusion coefficient. The outflow time lag, θ_L, is obtained by extrapolating the asymptote of the linear steady state portion of the pressure profile to the time axis. In turn, the diffusion coefficient is inversely proportional to the time lag [2]:

$$D = \frac{l^2}{6\theta_L} \tag{2.9a}$$

Alternatively, the time lag method can be applied to the inflow volume by monitoring the pressure decay in the upstream, and the magnitude of the resulting time lag, which is referred to as the inflow time lag, θ_0, is twice as large but on the negative side of the time axis [4]. Consequently, the diffusion coefficient is related to the inflow time lag as follows:

$$D = -\frac{l^2}{3\theta_0} \tag{2.9b}$$

The classical time lag method described above requires reaching quasi-steady state permeation conditions, which could take hours and possibly even weeks for lower permeability barrier films. Moreover, when the quasi-steady state is reached, the second boundary condition, $C_{Al} = 0$, on which the classical time lag method is based, is no longer applicable. Although the modifications of the classical time lag method for different expressions of the 2nd boundary conditions are available in the literature [4], the common practice is to use Eq. (2.9a) regardless of the adherence of the of the experimental data to $C_{Al} = 0$. Therefore it is useful to develop tools for the determination of membrane properties under much earlier time periods not only because of time savings, but also because of a better adherence to the simplest form of the 2nd boundary condition for the governing partial differential equation.

In this paper we present a novel method for estimation of the permeability coefficient at very short times, considerably before quasi-steady state permeation conditions are attained. This method requires an accurate monitoring of transient gas fluxes in and out of the tested membrane. To achieve the former we present a new design of the upstream side of a constant volume system.

2.2 Theory

2.2.1 Shortcut method for determination of the diffusion coefficient

As a rule of thumb, in the classical time lag method the steady state permeation is attained after the time corresponding to 3 outflow time lags [6]. Rogers et al (1954) [7] have revealed an approximation where the flux profile can be manipulated into characterizing the membrane prior to reaching quasi-steady state. Based on Fick's first law of diffusion, at the downstream end of the membrane ($x = l$) the transient flux is given by:

$$J_A(l,t) = \frac{2\sqrt{D_A}C_{A0}}{\sqrt{\pi t}} \sum_{n=0}^{\infty} \exp\left(\frac{-(2n+1)^2 l^2}{4D_A t} \right) \tag{2.10}$$

At early times, the latter terms of the series are very small relative to the first term. Thus, by retaining only the first term (set $n = 0$), the following short time solution becomes applicable:

$$J_A(l,t) = \frac{2\sqrt{D_A}C_{A0}}{\sqrt{\pi t}} \exp\left(-\frac{l^2}{4D_A t} \right) \tag{2.11}$$

Eq. (2.11) is then linearized to the following form:

$$\ln\left(J_A(L,t)\sqrt{t}\right) = \ln\left(\frac{2\sqrt{D_A}C_{A0}}{\sqrt{\pi}} \right) - \frac{L^2}{4D_A t} \tag{2.12}$$

Plotting $\ln\left(J_A(l,t)\sqrt{t}\right)$ vs. t^{-1}, the diffusion coefficient can be directly recovered from the slope m, where:

$$m = -\frac{l^2}{4D_A} \tag{2.13}$$

Subsequently, knowing D_A, C_{A0} can be determined from the intercept. In turn, using Eq. (2.4), the solubility coefficient is evaluated, and then with the diffusivity and solubility, Eq. (2.1) allows calculation of the permeability. The short time solution is applicable with data points, which do not exceed a Fourier number ($Fo = D_A t / l^2$) of 0.145. For Fo > 0.145 the latter terms of the series in Eq. (2.10) begin to increase in prominence.

The method described above requires monitoring of the gas flux. However, in constant volume system the gas flux is not measured directly, but rather it is determined from the derivative of the pressure with respect to time. Consequently, it is more convenient to base the analysis on the downstream pressure, which is measured directly, rather than the downstream flux. Differentiating Eq. (2.5) with respect to time and substituting Eq. (2.10), allows re-expressing the short time solution of Rogers et al. [7] as follows:

$$\frac{dp_A(l,t)}{dt} = \frac{2\sqrt{D_A}\, p_{A0} S_A A_f RT}{V_2 \sqrt{\pi t}} \sum_{n=0}^{\infty} \exp\left(\frac{-(2n+1)^2 l^2}{4 D_A t} \right) \tag{2.14}$$

Then, integrating Eq. (2.14) from 0 to t the pressure accumulation in the receiving volume is modeled as:

$$p_A(l,t) = \frac{2 p_{A0} S_A RTA_f \sqrt{D_A}}{V_2 \sqrt{\pi}} \sum_{n=0}^{\infty} \left\{ \begin{array}{l} \left(\frac{(2n+1)\sqrt{\pi} l}{\sqrt{D_A}} \right) \cdot \left[erf\left(\frac{(2n+1) l}{2\sqrt{D_A t}} \right) - 1 \right] \\ + 2\sqrt{t} \exp\left(\frac{-(2n+1)^2 l^2}{4 D_A t} \right) \end{array} \right\} \tag{2.15}$$

Similarly to Eq. (2.10), for Fo < 0.145, Eq. (2.15) is well approximated by retaining only the first term of the series (n = 0), which leads to:

$$p_A(l,t) = \frac{4 p_{A0} S_A RTA_f \sqrt{D_A}}{V\sqrt{\pi}} \sqrt{t} \exp\left(-\frac{l^2}{4D_A t}\right) \tag{2.16}$$

Dividing Eq. (2.16) by $\sqrt{t}$ and taking the natural logarithm of both sides leads to:

$$\ln\left[\frac{p_A(l,t)}{\sqrt{t}}\right] = \ln\left[\frac{4 p_{A0} S_A RTA_f \sqrt{D_A}}{V\sqrt{\pi}}\right] - \frac{l^2}{4D_A}\frac{1}{t} \tag{2.17}$$

Plotting $\ln\left(p_A(l,t)/\sqrt{t}\right)$ against t^{-1} should yield a straight line with the slope m given by Eq. (2.13).

2.2.2 Determination of the permeability coefficient

The short cut method described above allows the determination of the diffusivity and solubility from the slope and intercept, respectively, and the permeability from the product of diffusivity and solubility. We shall now present an alternative approach for the determination of the permeability, which requires only the diffusivity but not the solubility. The rationale for this approach comes from the fact that systems associated with a slight degree of noise with data acquisition may potentially compromise the intercept value obtained, and thus the solubility and the permeability values.

Knowing the diffusion coefficient and the membrane thickness allows conversion of the experimental time into dimensionless time (Fourier number). In turn, knowing a transient permeation rate at a given Fourier number, a steady state permeation rate and thus the permeability coefficient can be estimated. The difficulty in this approach based on

the gas flux emerging from the membrane arises from the fact at very small Fourier numbers the gas either had not emerged from the membrane or the rate at which it emerges is relatively very small leading to a large error associated with the experimental gas flux. To overcome this challenge, we propose a novel procedure, in which in addition to monitoring of the gas flux emerging from the membrane, the gas flux entering the membrane is also monitored.

A cornerstone is this procedure, in which the fluxes in and out of the film as a function of the Fourier number are monitored, is shown in Fig. 2.2. The flux into the film is initially very high and decreases with time, whereas the flux out of the film starts off at zero and increases with time. Steady state permeation is achieved when fluxes in and out are the same, which in the model occurs as the Fourier number approaches 0.5, i.e. the time corresponding to three outflow time lags ($3\theta_L$). Substituting Eq. (2.3) into Eq. (2.5) and evaluating it at x = 0 yields the mathematical description of the upstream flux as a function of time:

$$J_A(0,t) = \frac{\sqrt{D_A}C_{A0}}{\sqrt{\pi t}} \sum_{n=0}^{\infty} \left[\exp\left(-\frac{(n+1)^2 l^2}{D_A t} \right) + \exp\left(-\frac{l^2 n^2}{D_A t} \right) \right] \tag{2.18}$$

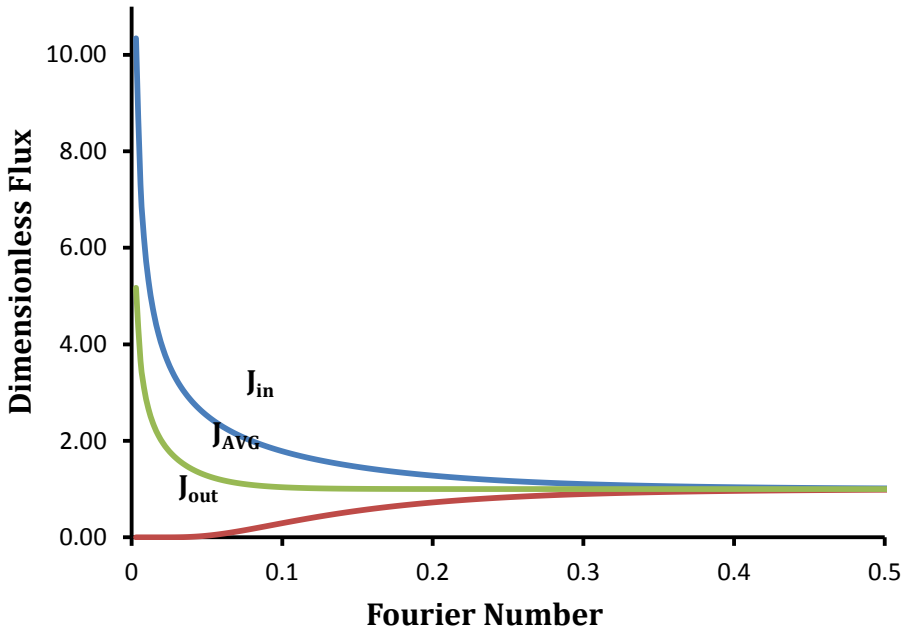

Figure 2.2 Simulated dimensionless fluxes (in, out, and average) as a function of dimensionless time (Fourier number). At Fourier number greater than 0.1 J_{in} and J_{out} become mirror images with respect to the steady state value flux. As a result, J_{AVG}, which is the arithmetic average of J_{in} and J_{out}, approaches the steady state value flux much faster than the individual fluxes.

The key feature in Fig. 2.2 is that soon after the start of the experiment, the flux profiles in and out of the film become mirror images with respect to the steady state value, J_∞. This means that an arithmetic average of the fluxes in and out of the film, J_{AVG}, approaches J_∞ much faster than the individual fluxes. The mathematical expression of J_{AVG} is obtained by combining the expressions for J_{in} and J_{out} given by Eqs. (18) and (10), respectively:

$$J_{AVG}(t) = \frac{\sqrt{D_A}C_{A0}}{2\sqrt{\pi t}} \sum_{n=0}^{\infty} \exp\left(-\frac{n^2 l^2}{D_A t}\right)\left[2\exp\left(-\frac{(n+0.25)l^2}{D_A t}\right) + \exp\left(-\frac{(2n+1)l^2}{D_A t}\right) + 1\right] \qquad (2.19)$$

For cases of dealing with ultra-low permeability barrier materials, waiting to approach steady state could get tediously long. However, by attempting to analyze the rate in which the average flux approaches steady state, a shortcut approach can be implemented for a much faster determination of the permeability.

Table 2.1 The theoretical fluxes in (J_{in}) and out (J_{out}) of the membrane as well as their arithmetic average (J_{AVG}) expressed in terms of the steady state flux (J_∞) along with the corresponding correction factors (ε) at different dimensionless times (Fourier number) in transient permeation period. The relationship between J_∞, J, and ε is given by Eq. (2.20).

Fourier Number	**Relative fluxes and the corresponding correction factors**					
	J_{in} **[%]**	ε_{in}	J_{out}**[%]**	ε_{out}	J_{AVG}**[%]**	ε_{AVG}
0.025	355.4	2.554	0.0	n/a	177.7	0.777
0.050	252.3	1.523	3.4	-0.954	127.9	0.279
0.075	205.7	1.057	14.8	-0.852	110.3	0.103
0.100	178.4	0.784	29.3	-0.707	103.9	0.039
0.125	159.6	0.596	43.3	-0.567	101.4	0.014
0.150	146.0	0.460	55.0	-0.450	100.5	0.005

Table 2.1 provides J_{in}, J_{out}, and J_{AVG} as the respective percentages of J_∞ along with the corresponding correction factor, ε, which relates the observed flux to J_∞:

$$J_\infty = \frac{J}{1+\varepsilon} \tag{2.20}$$

The data in Table 2.1 covers a highly transient region, which roughly corresponds to the time frame at which the short-time solutions given by Eqs. (12) and (17) are applicable. It can be noticed that at Fo = 0.100 when the theoretical J_{in} and J_{out} represent 178.4% and 29.3% of J_∞, respectively, J_{AVG} is already within 4% of J_∞. At Fo = 0.15, when J_{AVG} is within

0.4% of J_∞ , J_{in} and J_{out} are still more than 45% away from the steady state value. For J_{in} and J_{out} to be within 0.4% of J_∞, it requires $Fo > 0.6$. In other words, J_{AVG} approaches the steady state value approximately four times faster than the individual J_{in} and J_{out}.

Alternatively, rather than waiting for J_{AVG} to fall within a certain percentage of the steady state value, J_∞ can be estimated from Eq. (2.20) at any early time, provided that the diffusivity of the membrane in known (the latter is necessary for the evaluation of ε). In turn, the diffusivity of the membrane is evaluated using Eq. (2.17) from the downstream pressure data starting at $Fo \simeq 0.05$, i.e. when the gas begins to appear at the downstream side of the membrane. It is important to note that while J_∞ can be evaluated using J_{in}, J_{out}, or J_{AVG}, a given Fo, ε is always lowest for J_{AVG}. Consequently, to minimize the noise in such evaluated J_∞ and thus the permeability coefficient determined from transient permeation data, one should use J_{AVG} rather than J_{in} or J_{out}.

2.3 Experimental

Membrane preparation is identical to that carried out by Lashkari and Kruczek [8,9]. Polyphenylene oxide in 10% trichloroethylene solution is used in a spin coating machine over a silicon wafer. The wafer was coated three times, and yielded a final membrane thickness of 42 μm after solidification. The membrane is heat treated in order to minimize any time-dependent changes in the properties of the cast membranes [10].

The heat treatment was done by placement of the free standing membrane in a vacuum oven initially purged by nitrogen. An operating temperature of 240 ^oC (above its

glass transition temperature) was achieved and maintained for 12 hours. The temperature was the gradually decreased to room temperature over a period of 24 hours prior to removal of the membrane from the oven.

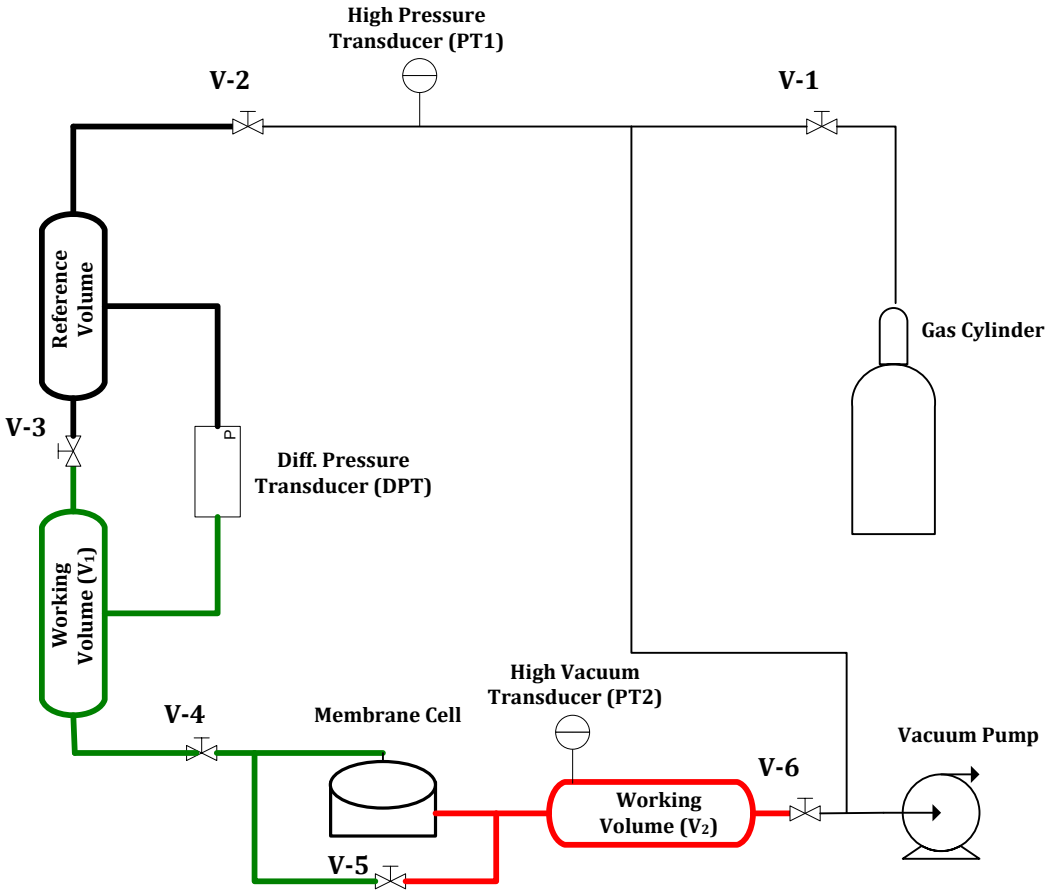

Figure 2.3 Schematic illustrating the experimental setup used to monitor the permeation tests in the upstream/downstream. The design of the upstream part of the system allows very accurate monitoring of the pressure decay in the working volume by comparing the pressure in the working volume with the constant pressure in the reference volume.

The membrane is held in a short, cylindrical-shaped stainless steel separation cell, which consists of an upper and lower section, it is equipped with an O-ring to completely seal it. The feed line from the upstream connects to the lower section, while the permeate

line connects towards the downstream from the upper section of the cell [5]. A schematic of the experimental setup is illustrated in Fig. 2.3. The downstream and upstream reservoirs from the membrane cell exist to monitor the pressure increase and decay during the experiment, respectively.

The downstream section is identical to the low resistance receiver demonstrated by Lashkari and Kruczek (2010) [11]. The receiver is configured to operate at minimum resistance consisting only of 1/2" and 1/4" stainless steel tubing completely sealed from atmosphere. The downstream section is evacuated over a period of 72 hours by means of a Nelson 3 rotary vane pump. Evacuation is carried out by keeping valves V-5 and V-6 open, which are then eventually closed prior of testing. Leak tests are performed by monitoring any pressure rise via the high vacuum transducer, where a rate of 3.7e-8 torr/s appeared to be negligible in the context of this experiment. The high vacuum transducer (PT2, MKS model 627B11TBC1B) operates at a range of 0 to 1 torr, with an accuracy of 0.0001 torr and a maximum error of 0.12% of the read pressure.

The upstream end of the membrane is where the feed pressure decay is monitored. The difficulty with using an absolute pressure transducer to directly measure the pressure decrease is retaining a similar resolution to PT2, while also accommodating for larger pressures. For example, a low operating feed pressure of only 1 psig would require a very high precision transducer of at least 7 significant figures (in torr). Such devices are not only expensive, but also tend to lack in durability.

To overcome the problem with accurate measurement of the pressure decrease in the upstream section of the system, this part contains two connected volumes that can be

separated by a valve (V-3). The concept of a two-tank volume was developed by Arkilic et al. [12] for the flow measurement of gasses flowing out of micro-channels and accumulating at relatively high pressures (e.g. atmospheric pressure). In our two-tank system shown in Fig. 2.3, a gas (nitrogen) from the cylinder is supplied until a desired pressure is achieved as valves V-2 and V-3 are kept open. Prior to starting up the experiment, valves V-2 and V-3 are closed, where the two volumes are compartmentalized as they maintain the same pressure. Measuring the pressure decay is carried out by means of a differential pressure transducer (DPT, MKS model 226A.2TCDCDFB2A1) connected to the two volumes; where one acts as a reference volume, and the other as the working volume. Therefore during startup, pressure decay will be observed on the working volume, while the reference volume remains at constant pressure, and DPT monitors the pressure decrease by measuring the pressure difference between the two volumes. The working volume, V_1, is comprised of the volume between the valves V-3, V-5, the DPT, and the membrane inside the cell. The DPT transducer operates at a full scale of +/-0.2 torr, with an accuracy of 0.00001 torr and a maximum error of 0.3% of the read pressure difference.

Similar to the downstream, the upstream section consists of tubing in its entirety. The tubing is 1/4" in size, stainless steel, and completely sealed from atmosphere. A high pressure transducer PT1 is used to read absolute feed pressure, p_{A0}.

The system is operated at room temperature (22^{o}C). Polyethylene pipe insulation is applied throughout the system to minimize heat losses/gain with the environment. With all valves initially closed except for V-3, experimental startup begins by opening valve V-4, which is immediately followed by closing V-3 to initiate the experiment. The handling of V-

3 in such a manner is to avoid the DPT readings from going off chart, which would be caused by the expansion effect resulting from opening V-4 with V-3 closed. Data acquisition is carried out through the pressure transducers (DPT and PT2, primarily) connected to a PC using LabView. Transient pressure profiles in both the upstream and downstream are simultaneously recorded and saved. Upon completing the experiment, valve V-4 is then closed, and the downstream is re-evacuated by opening valves V-5 and V-6. Additional details on the operating conditions are provided in Table 2.2. All the valves used in the system are high purity bellows-sealed valves supplied by Swagelok Canada.

Table 2.2 Brief summary of experiment operating parameters and conditions.

Membrane surface area, A	12.57 cm^2
Membrane thickness, l	42 μm
Temperature, T	22.1 ^oC
Inflow working volume, V_1	115.1 cm^3
Outflow working volume, V_2	77.6 cm^3

2.4 Results & Discussion

Permeation tests were carried out on the PPO membrane with pure nitrogen gas. The experiments were performed under 3 different pressures. From each experiment four sets of the permeability, diffusivity, and solubility results are obtained and compared.

2.4.1 Correction of upstream pressure profile

A sample of raw data, which includes the upstream and downstream pressure profiles, collected in the experiment carried at p_{A0} = 3.372 psia is shown in Fig. 2.4. The initiation of the experiment is associated with "a compression effect" at the upstream side, which originates from closing of the valve V-3. The valve V-3 has a finite volume and its closure results in a simultaneous compression in the reference volume and the working volume. Since the working volume V_1 is larger the reference volume, V_2, the net effect of the compression in both volumes is an expansion in the working volume. This "compression effect" serves as the primary reason why tests were performed at relatively low pressures. Knowing the exact volume of the valve V-3 and the working volume, the magnitude of the correction due to the compression effect could be evaluated ahead of time for any p_{A0}. However, we used an alternative approach, which is explained next.

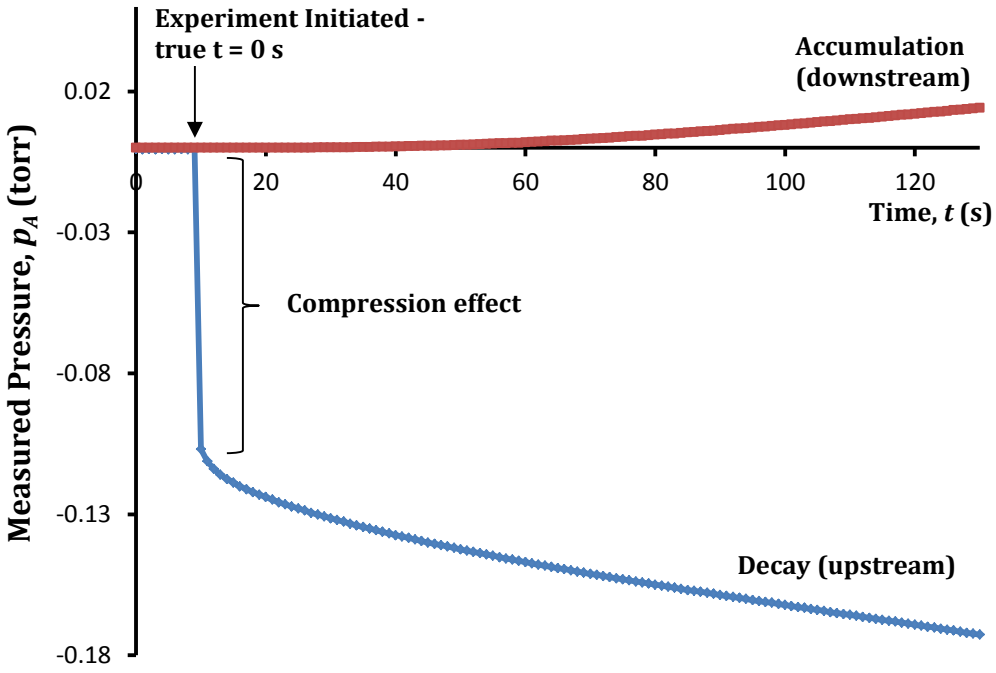

Figure 2.4 Sample of data acquisition carried out by the system at start of the experiment. Pressure accumulation and decay are recorded, alongside the "compression effect" present on the upstream. The compression effect is due to closing valve V-3 (Fig. 2.3). Since the working volume is greater than the reference volume (Table 2.2), the net result of the compression effect is an instantaneous expansion in the working volume.

The theoretical pressure decay in the working volume V_1 is obtained by integrating the inflow flux given by Eq. (2.18) over time, which after rearrangements leads to:

$$p_{A0} - p_A(0,t) = \frac{2p_{A0}S_A RTA_f l}{V_1}\sum_{n=0}^{\infty}\left\{\begin{array}{l} n\cdot erf\left(\dfrac{nl}{\sqrt{D_A t}}\right) + (n+1)\cdot erf\left(\dfrac{(n+1)l}{\sqrt{D_A t}}\right) - 2n - 1 \\ + \dfrac{\sqrt{\pi D_A t}}{l}\left[\exp\left(\dfrac{-l^2(n+1)^2}{D_A t}\right) + \exp\left(\dfrac{-l^2 n^2}{D_A t}\right)\right] \end{array}\right\} \tag{2.21}$$

For very short times, i.e., before the gas emerges from the downstream side of the membrane, the membrane behaves as a semi-infinite solid. An alternative "short-time" equation for the pressure decay in the working volume resulting from the upstream flux into a semi-infinite solid is then given by:

$$p_{A0} - p_A(0,t) = -\frac{2p_{A0}S_A RTA_f\sqrt{D_A}}{V_1\sqrt{\pi}}\sqrt{t} \tag{2.22}$$

Plotting the upstream pressure decay versus $\sqrt{t}$ for very short times should yield a straight line with no intercept and a slope of:

$$m = -\frac{2p_{A0}RTA_f S_A\sqrt{D_A}}{V_1\sqrt{\pi}} \tag{2.23}$$

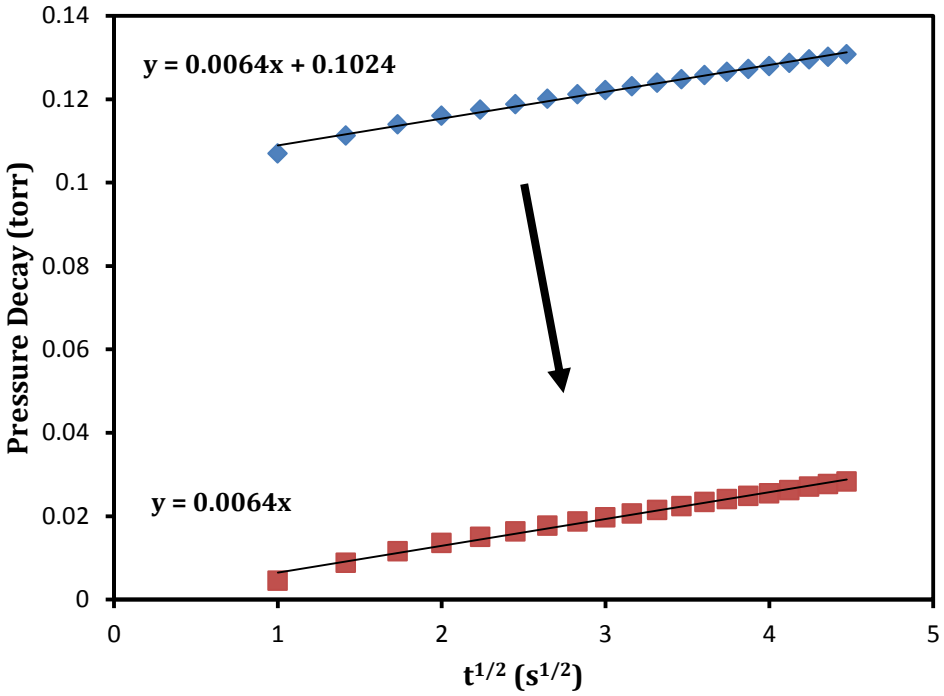

Figure 2.5 Plot demonstrating the correction of the upstream pressure profile due to the compression effect shown in Fig. 2.4. At early times, the upstream pressure decay data substituted into Eq. (2.21) should yield a straight line with no intercept. The upstream pressure data is corrected by subtracting the experimentally determined intercept from the observed upstream pressure data.

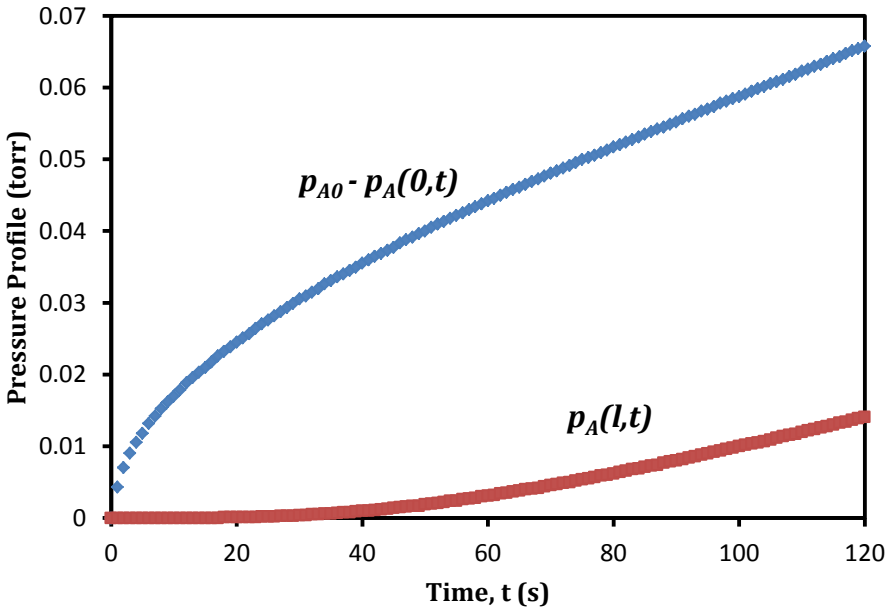

Figure 2.6 Final pressure profiles after correction. To show both pressure profiles on the same scale positive axis, the upstream pressure profile is represented by the absolute values.

The observed pressure decay profile is corrected by subtracting the negative intercept yielded from the short time evaluation of the raw data. This is shown in Fig. 2.5, where a very early set of the data is used in order to ensure the applicability of a semi-infinite model. The corrected upstream pressure profile along with the downstream pressure profile is presented in Fig. 2.6.

2.4.2 Determination of diffusion coefficient from experimental data

The key to the shortcut method for the determination of the permeability, presented in section 2.2, is the simultaneous determination of the diffusivity using the Rogers et al. [7] short-time solution. It is important to emphasize that despite the fact that this solution is available for more a half century, it has been rarely used in practice [13,14]. Typically, the diffusivity is evaluated using the classical time lag approach [2,3].

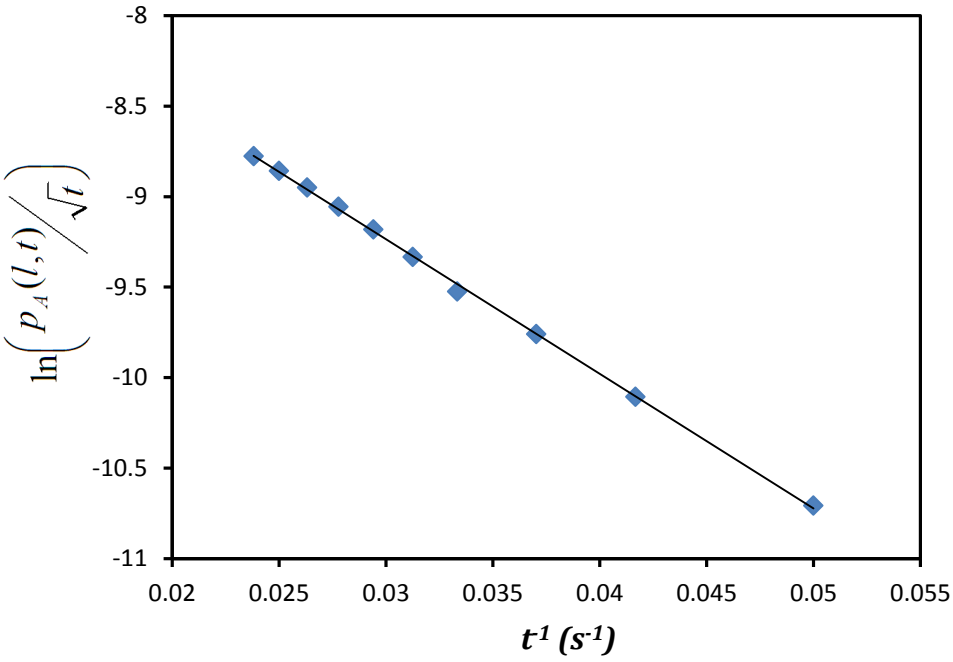

Figure 2.7 A plot demonstrating the application of the downstream short time solution, Eq. (2.17). The diffusivity is determined from the slope obtained by plotting $\ln\left(p_A(l,t)/\sqrt{t}\right)$ vs. t^{-1}. The diffusivity and thickness on the membrane shown in this figure are 4.390 x10^{-8} cm^2/s and 42 μm, respectively. Therefore the time frame from 20 s to 41 s shown in this figure corresponds to Fourier numbers from 0.051 to 0.1.

Fig. 2.7 demonstrates the application of the short-term solution using the downstream pressure data collected in the experiment carried out at p_{A0} = 3.372 psia. It is evident that the plot of $\ln\left(p_A(l,t)/\sqrt{t}\right)$ vs. t^{-1} yields a straight line, which validates the short-time solution model. A diffusion coefficient of D_A = 4.390 x10^{-8} cm^2/s is obtained in this plot, this is from the data collected between 20 and 41 seconds, which corresponds to the range of Fourier numbers between 0.051 and 0.1. Therefore, D_A can be easily determined from an experimental set of data of Fo < 0.1. The diffusion coefficients under different

pressures using the inflow and the outflow time lag methods, and short-time methods and compared in Table 2.3. The estimated diffusivities using these three methods are shown to be reasonably similar to one another. The diffusivities obtained using the upstream time lag method seem to be underestimated, which could be due to some resistance effects [8,9].

The diffusivity calculated using the short time methods tend to exhibit a slightly greater standard deviation with respect to the individual pressure trials. When performing permeation tests in systems with a relatively large receiving volume and/or under low pressure gradient, a pressure transducer may have an inadequate precision, and time-series replicates during the early stages of the permeation test may be observed. This problem is illustrated in Fig. 2.8.

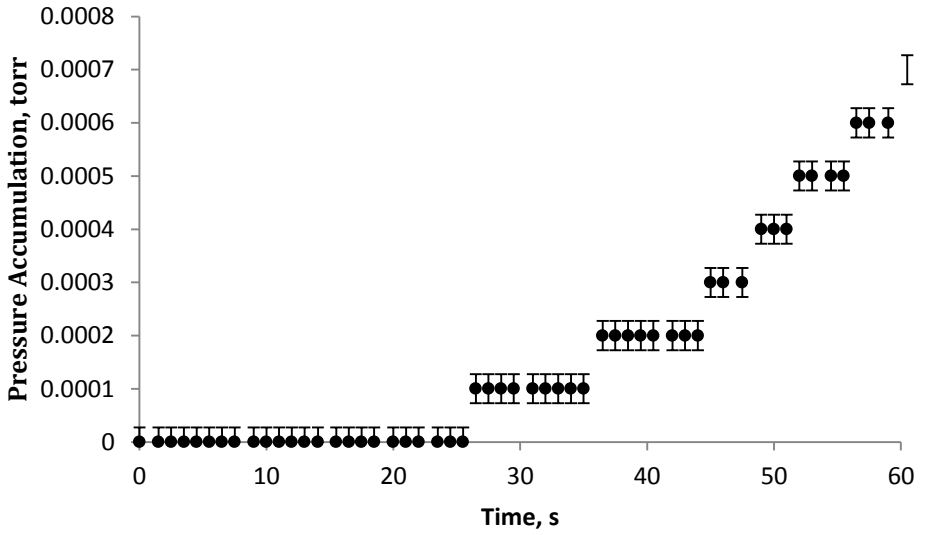

Figure 2.8 Plot showing potential rise of replicates in cases of extreme low permeation rates or imprecise transducers.

Roelanta et al. [15] suggested a nonlinear least square method of preconditioning transient experiments containing time-series replicates based on systems of partial

differential equations such as the one presented in this paper. Alternatively, the time series replicates may be averaged and regressed; this follows important assumptions that the noise is normally distributed amongst the replicates and that the independent time variable has no experimental error associated with it (automated data acquisition is thus recommended).

Table 2.3 Comparison of estimated permeabilities, diffusivities and solubilities using classical downstream and upstream time lag methods, the short time method of Rogers et al. [7], and the short-cut method based on averaging fluxes in and out of membranes for *P* and the short-time method for *D*. Tests performed under different feed pressures.

Pressure	**Classical Time Lag Method (Downstream)**			**Time Lag Method (Upstream)**		
[psig]	D_A [cm^2/s]	P_A [Barrer]	S_A[cm^3(STP)/cm^3 cm Hg]	D_A [cm^2/s]	P_A [Barrer]	S_A [cm^3(STP)/cm^3 cm Hg]
3.372	4.52 x 10^{-8}	3.69	0.00817	3.788 x 10^{-8}	3.70	0.00977
2.546	4.54 x 10^{-8}	3.74	0.00825	3.410 x 10^{-8}	3.69	0.01082
1.514	4.51 x 10^{-8}	3.72	0.00826	3.770 x 10^{-8}	3.77	0.00999
Pressure	**Short Time Solution of Rogers et al. [7]**			**Shortcut method proposed in this work**		
[psig]	D_A [cm^2/s]	P_A [Barrer]	S_A[cm^3(STP)/cm^3 cm Hg]	D_A [cm^2/s]	P_A [Barrer]	S_A [cm^3(STP)/cm^3 cm Hg]
3.372	4.39 x 10^{-8}	0.748	0.00170	4.39 x 10^{-8}	3.71	0.00864
2.546	4.59 x 10^{-8}	0.649	000141	4.59 x 10^{-8}	3.95	0.00815
1.514	4.16 x 10^{-8}	0.540	0.00130	4.16 x 10^{-8}	3.93	0.00964

2.4.3 Determination of permeability coefficient from experimental data

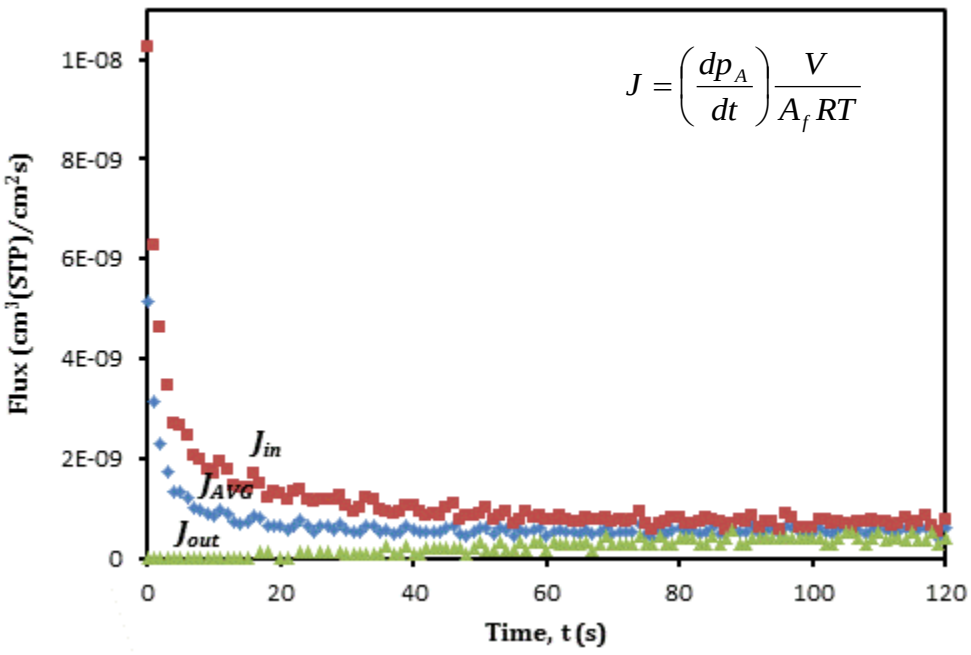

Figure 2.9 Experimental demonstration the concept of the average flux shown in Fig. 2.2. The time interval of 20 s corresponds to Fourier number interval of 0.051.

Fig 2.9 presents the experimental J_{in}, J_{out}, and J_{AVG} as a function of time. The experimental flux profiles show a close resemblance to the theoretical flux profiles shown in Fig. 2.2. However, despite very smooth experimental pressure profiles evident in Fig. 2.6, the experimental fluxes are associated with a significant noise. This is because the individual fluxes are obtained by a numerical differentiation of the pressure data. More specifically, the numerical derivatives were calculated using second order divided difference formulas derived from Taylor series expansions [16]. An obvious shortcoming with numerical differentiation is that it tends to amplify even the smallest errors presented in empirical data.

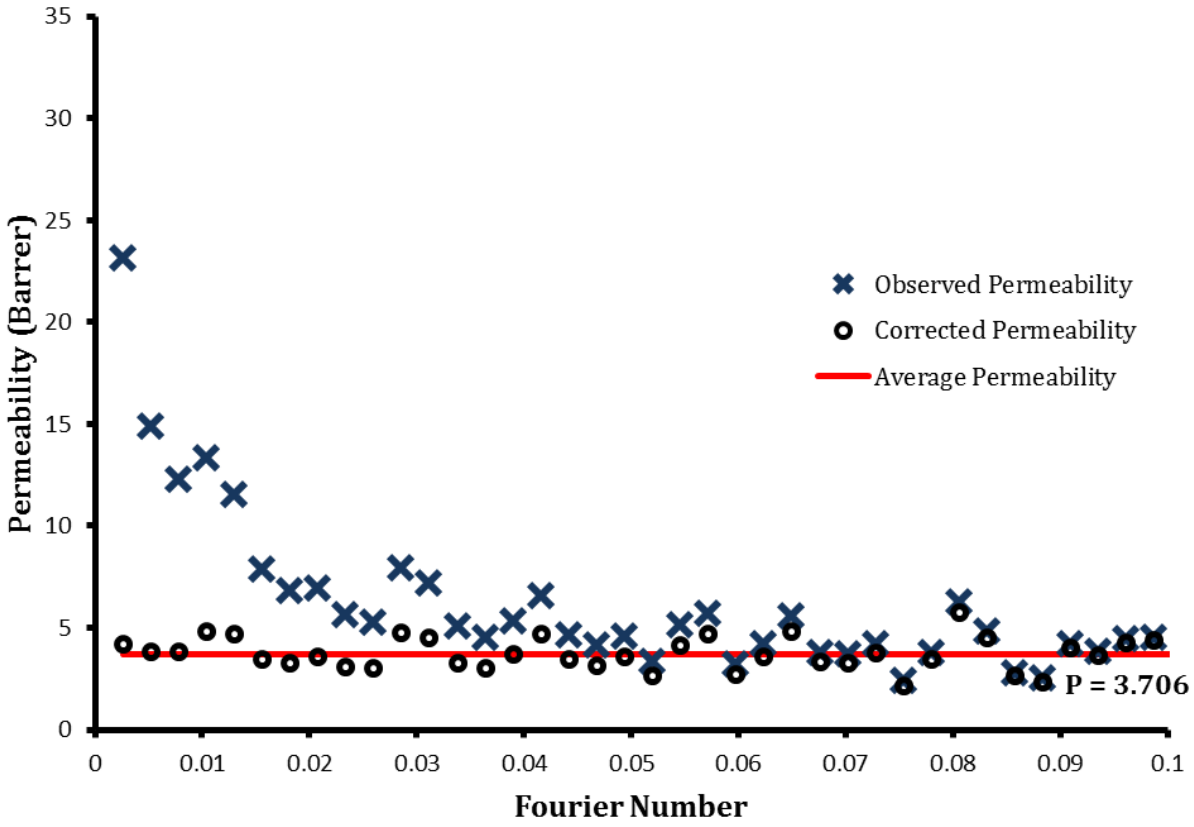

Figure 2.10 Plot revealing the method behind estimating the permeability in the short-time method. The observed permeability values are determined from the average flux (J_{AVG}) data shown in Fig. 2.9, while the corrected permeability values are determined from the steady state flux (J_∞) obtained by correcting J_{AVG} using the Fourier number-dependent correction factors (ε_{AVG}). The average permeability of 3.706 Barrer, which is denoted by a horizontal line, is obtained from the arithmetic average of the corrected permeability values for $Fo < 0.1$.

To alleviate the problem with a noise in the experimental data, least squares fit of pressure decay/accumulation data to differentiable short time models in Eq. (2.16) & (2.22) could be used. However, instead of doing this the steady state flux (J_∞) was evaluated from Eq. (2.20) using the average flux (J_{AVG}) along with the corresponding correction factor

(ε_{AVG}) based on the previously determined diffusivity. Such calculated J_∞ was then used to evaluate the corrected permeability.

Fig. 2.10 presents the plot of the corrected permeability as a function of *Fo*. The corrected permeability values in Fig. 2.10 are compared with the observed permeability values evaluated based on the experimental J_{AVG} shown in Fig. 2.9. It is evident that while the corrected permeability values in Fig. 2.10 are not constant, there is not trend between the corrected permeability and *Fo*. The corrected permeability values randomly oscillate around the average permeability (indicated as a horizontal line in Fig. 2.10), which is determined by taking the arithmetic average of the all corrected permeability values shown in Fig. 2.10. The average permeability in Fig. 2.10 is 3.706 Barrer

The data shown in Fig. 2.10 covers the time up to 40 s from the initiation of the experiment, which corresponds to $Fo < 0.1$. It is evident however, that this the upper limit of *Fo* could easily be lowered without affecting the average permeability. In principle, even using the data in the first 10 s of the experiment ($Fo < 0.025$) would lead to the average permeability very close to the previously reported value of 3.706 Barrer. On the other, the determination of the diffusivity based on the downstream pressure requires the data for $Fo > 0.025$. Therefore, the time frame corresponding to $0.025 < Fo < 0.1$ is sufficient for simultaneous determination of the diffusivity and permeability in the proposed method. Moreover, oscillation of the corrected permeability values around the average permeability over the entire range of *Fo*, including $Fo < 0.025$, as well as linearity of Eq. (2.17) may serve as an indication of the validity of the assumed transport model, which is this case was Fickian diffusion with a constant diffusivity.

In the traditional time lag method the steady state J_{in} and J_{out} are determined using the pressure data from $3\theta_0$ to $4\theta_0$ [6], which correspond to Fo number from 0.50 to 0.67. However, to ensure that the permeation rate had reached steady state, the experiments are typically carried out until at least the time corresponding to Fo = 1. In other words, the short cut method developed in this study allows the determination of the permeability, diffusivity and solubility of the membrane properties in time which is one order of magnitude shorter than the classical time lag method.

In principle, the method based on the short-time solution of Rogers et al [7] offers the same time saving advantage as the method developed in this work. The problem with the former method becomes evident when considering the permeability and solubility coefficients listed in Table 2.3. These coefficients are considerably different from those determined by the other three methods. The short-time solution of Rogers et al [7] relies on the transient pressure data from the outflow volume in a highly transient period right after the gas starts to appear downstream from the membrane. Naturally, the problem with the time-series replicates is most prominent in this early stage of a permeation experiment (Fig. 2.8). Despite this problem, with preconditioning of the transient data suggested by Roelanta et al. [15], one can get an excellent approximation of the slope, which is used for the determination of the diffusivity (Eq. (2.13)). On the other hand, even small variations in the slope may significantly affect the value of the intercept (Fig. 2.7). Moreover, the intercept is the natural logarithm of a term involving the solubility coefficient, thus any error in the intercept is exponentially magnified when recovering the solubility coefficient.

The comparison of the membrane properties determined by the four different methods, i.e. the classical time lag method based on the downstream pressure profile, the time lag method based on the upstream pressure decay, the short-time solution of Rogers et al [7], and the method developed in this work which uses the diffusivity from the short-time solution of Rogers et al [7] and the concept of the corrected averaged flux, is summarized in Table 2.3. It can be noticed that the best agreement between the membrane properties determined using the short cut method, and the outflow and inflow time lag methods occurs at the highest experimental feed pressure. While the permeability, diffusivity and solubility coefficients should be independent of the feed pressure, since the permeation rate is directly proportional to the pressure gradient across the membrane, a noise associated with the data is minimized in the experiments at higher feed pressures. Alternatively, the same effect could be achieved by decreasing the receiver volume and/or the thickness of the membrane. Finally, it is important to emphasize that steady state permeabilites in Table 2.3 are in a good agreement with the documented value of 3.8 Barrer for nitrogen in PPO [17].

2.5 Conclusion

In this paper, an experimental design and approach has been developed for the estimation of diffusion and permeability coefficients in thin polymer films under very short times, considerably before the permeation rate reaches quasi-steady state conditions.

The diffusion coefficient was determined using a short-time solution model developed by Rogers et al. [7]. The permeability coefficient was evaluated using a novel

procedure based on monitoring the transient fluxes in and out of the membrane, which were averaged and corrected using theoretical Fourier number-dependent correction factors. This allowed the determination of the permeability coefficient based on the data collected at $Fo < 0.1$, which represents at most 10% of the time required by the classical time lag method.

To determine the transient flux entering the membrane, the upstream part of the constant volume system consisted of two volumes, the working volume connected to the membrane during the permeation experiment, and the reference volume maintained at constant pressure. The two volumes were connected via a high accuracy differential pressure transducer, which allowed for a very accurate monitoring of the pressure decay in the working volume due to gas permeation. The results obtained appeared to be in good agreement with not only literature data, but also in comparison with the classical time lag method of membrane characterization. While time savings offered by the shortcut method are of critical importance in case of characterization barrier materials, this method also allows a closer adherence of the boundary condition at the downstream surface of the membrane, $C_A(l,t) = 0$, on which the solution of the governing partial differential equation is based.

Acknowledgements

The authors (BK and MA) acknowledge the financial support received from Natural Science and Engineering Research Council of Canada (NSERC) to carry out this project.

Special thanks are expressed to the Ministry of Manpower, Oman for sponsoring MA graduate studies the University of Ottawa.

Nomenclature

A_f: Membrane/film cross-sectional area (cm^2)

C: Concentration of component A (cm^3(STP) cm^{-3})

D: Diffusion coefficient (cm^2/s)

erf: Error Function

Fo: Fourier Number

l: Thickness of membrane/film (cm)

J: Flux (cm^3(STP) cm^{-2} s^{-1})

m: Slope

n: Taylor series integer

p: Partial pressure of component A (torr)

P: Permeability coefficient (Barrer)

R: Ideal gas constant (J mol^{-1} K^{-1})

S: Solubility Coefficient (cm^3 (STP) cm^{-3} $cmHg^{-1}$)

t: Time (s)

T: Absolute Temperature (K)

V: Reservoir Volume (cm^3)

x: Distance from and within membrane/film (cm)

Greek Symbols:

ε: Fourier number-dependent correction factor

θ: Time lag (s)

Δ: Difference

Subscripts:

1: Upstream reservoir

2: Downstream reservoir

A: Component A – permeating species

AVG: Average

$corr$: Corrected

f: Membrane/film

i: Initial

in: Entering

obs: Observed

out: Exiting

0: Upstream (Position $x \leq 0$ of membrane)

l: Downstream (Position $x \geq l$ of membrane)

∞: Steady State

References

[1] M.R. Shah, R.D. Noble, D.E. Clough, Measurement of sorption and diffusion in nonporous membranes by transient permeation experiments, J. Membr. Sci. 287 (2007) 111–118.

[2] H.A. Daynes, The process of diffusion through a rubber membrane, Proc. R. Soc. London Ser. A 97 (685) (1920) 286–307.

[3] R.M. Barrer, Permeation, diffusion and solution of gases in organic polymers, Trans. Farad. Soc., 35 (1939) 628-643.

[4] S.W. Rutherford, D.D. Do, Review of time lag permeation technique as a method for characterization of porous media and membranes, Adsorption 3 (1997) 283.

[5] A. Tabe-Mohammadi, T. Matsuura, S. Sourirajan, Design and construction of gas permeation system for the measurement of low permeation rates and permeate compositions, J. Membr. Sci. 98 (3) (1995) 281–286.

[6] R.C. Jenkins, P.M. Nelson, Calculation of the transient diffusion of a gas through a solid membrane into a finite outflow volume, Trans. Farady Society 66 (1970) 1391-1401.

[7] W.A. Rogers, R.S. Buritz, D. Alpert, Diffusion coefficient, solubility, and permeability for helium in glass, J. Appl. Phys. 257 (1954) 868–875.

[8] S. Lashkari, B. Kruczek, H.L. Frisch, General solution for the time lag of a single tank receiver in the Knudsen flow regime and its implications for the receiver's configuration, J. Membr. Sci. 283 (2006) 88–101.

[9] S. Lashkari, B. Kruczek, Effect of resistance to gas accumulation in multi-tank receivers on membrane characterization by the time lag method. Analytical approach for optimization of the receiver, J. Membr. Sci. 360 (2010) 442–453.

[10] Y. Huan and D.R. Paul, Experimental methods for tracking physical aging of thin glassy polymer films by gas permeation, J. Membr. Sci. 244 (2004) 167-178.

[11] S. Lashkari and B. Kruczek, Reconciliation of membrane properties from the data influenced by resistance to accumulation of gases in constant volume systems, *In Press* Desalination, DOI: 10.1016/j.desal.2011.01.071.

[12] E.B. Arkilic, K.S. Breuer, M.A. Schmidt, Gaseous slip flow in long microchannels, Microelectromechanical Systems 6 (1997) 167-178.

[13] R.M. Barrer, H.T. Chio, Solution and diffusion of gases and vapors in silicone rubber membranes, J. Polym. Sci. Part C, 10 (1965) 111-138.

[14] T.N. Kompaniets, A.A. Kurdyumov, Surface Processes in hydrogen permeation through metal membranes, Prog. Sur. Sci. 17(2) (1984) 75-151.

[15] R. Roelanta, D. Constalesb, R.V. Keerb, G.B. Marina, Second-order statistical regression and conditioning of replicate transient kinetic data, Chem. Eng. Sci. 63 (2008) 1850–1865.

[16] S.C. Chapra, R.P. Canale, Numerical Methods for Engineers, Fifth Edition, McGraw-Hill Publishing, 2007, p. 525.

[17] M. Mulder, Basic Principles of Membrane Technology, Second Edition. Springer, 1996, p. 313.

CHAPTER 3

THEORETICAL EVALUATION ON THE UPSTREAM SHORT TIME SOLUTION – AN OVERVIEW

3.1 Overview: Introduction & Objectives

With the concept of the short time solution being the basis of this project, the specific introduction of the upstream short time solution (Eq. (2.21)) was only briefly touched upon in Chapter 2, despite the crucial role it played in processing upstream data collected. In this chapter, a more comprehensive look into the derivation of the upstream short time solution is carried out, including the inspiration behind it.

More importantly, application of the short time solution will be carried out on the pressure decay data in the case of a two-membrane composite system. This is done by exploiting the "pressure decay vs. square root of time" on the composite membrane system, and assessing how the behaviour relates to the properties of the two membranes. This is a central topic of this chapter, since it serves as a main prerequisite to the analysis performed on the resistance effects witnessed in Chapter 4.

Unlike the downstream short time solution (Eq. (2.17)), the upstream version isn't capable of extracting both diffusion and solubility coefficients independently. In here, we will disclose two alternative, but imprecise ways of approximating the diffusivity. This is mainly to serve as a supplementary understanding of the system, and bring about possible avenues where a more concrete methodology may be established in the future, owed to the findings of this paper.

3.2 Uncovering the Upstream Short Time Solution

The solution for the gas flux entering the membrane, given by Eq. (2.18), is based on the initial/boundary conditions describing the permeation of the current system: initially free of species, the upstream experiences a step change in concentration, while the downstream is under vacuum (fixed boundary conditions). Retaining only the first term of the infinite series given by Eq. (2.18) simplifies to

$$J_A(0,t) = \frac{\sqrt{D_A}C_{A0}}{\sqrt{\pi t}}\left[\exp\left(-\frac{l^2}{D_A t}\right)+1\right] \tag{3.1}$$

It is evident that Eq. (3.1) cannot be linearized, because of the constant (unity) inside the square brackets.

Similarly, the simplified expression for the upstream pressure profile, given by Eq. (3.2), which is obtained by retaining only the first term of the infinite series formula (Eq. (2.20)), cannot be linearized.

$$p_{A0} - p_A(0,t) = \frac{2p_{A0}S_A RTA_f l}{V_1}\left\{erf\left(\frac{l}{\sqrt{D_A t}}\right) - 1 + \frac{\sqrt{\pi D_A t}}{l}\left[\exp\left(\frac{-l^2}{D_A t}\right) + 1\right]\right\} \qquad (3.2)$$

As a result, a solution was brought about by looking at the problem from a different angle. It is assumed that in a slab membrane of thickness *l* with fixed boundary conditions, the concentration profile *at* and *near* the upstream face of the membrane has the tendency of behaving as in a semi-infinite solid at very short early times. Particularly, before a significant quantity of species has already emerged on the other side of the membrane to impact the transient concentration profile.

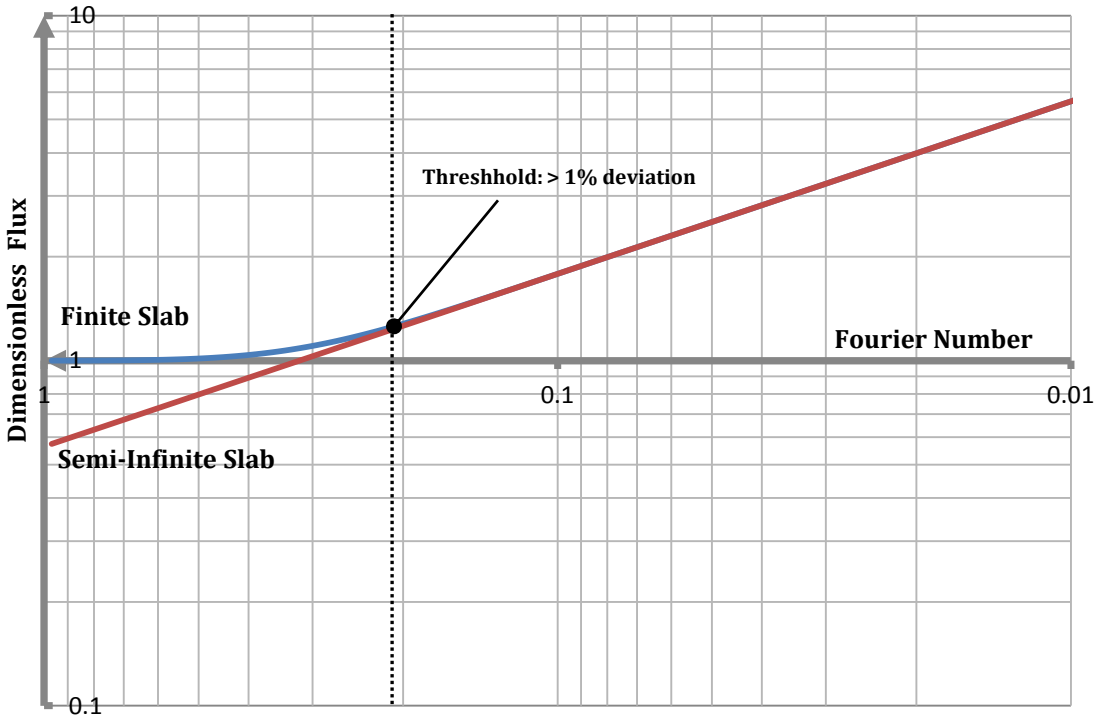

Figure 3.1 Transient dimensionless flux profiles of finite and semi-infinite slabs. Plot presented in logarithmic scale. *x*-axis in reverse direction (←).

When performing a comparison between the upstream flux profiles of the finite and semi-infinite slab in Fig. 3.1 [1], they exhibit identical behaviours at an early time period

not exceeding a Fourier number of 0.2. The Fourier number threshold is based on the system with a finite slab, since the length of a semi-infinite medium is not applicable.

Details of the derivation of the upstream short time solution are disclosed in Appendix A, which reveal the semi-infinite analytical form of the upstream flux profile as

$$J_A(0,t) = C_{Ao}\sqrt{\frac{D_A}{\pi}}\frac{1}{\sqrt{t}} \tag{3.3}$$

where C_{A0} is the upstream concentration experiencing the step change. The pressure is the result of "integral permeation" as the flux is integrated over time 0 → t and multiplied by the membrane cross-sectional area as it is depleted from the upstream reservoir of volume V_u

$$p_{A0} - p_A(0,t) = \frac{2p_{A0}S_A RTA_f\sqrt{D_A}}{V_u\sqrt{\pi}}\sqrt{t} \tag{3.4}$$

As a result, the upstream short time solution is a ***linear*** expression described by Eq. (3.4), where the pressure decay [p_{A0} - $p_A(0,t)$] is plotted against $\sqrt{t}$ to yield a slope and no intercept. The diffusivity (D_A) and solubility (S_A) coefficients are coupled within the slope and may ***not*** be solved for individually. The solution has no intercept; however this serves as a very compelling guideline when handling the experimental data in Chapter 4, and previously in Chapter 2. This type of plot will be referred to as a ***semi-infinite decay plot*** from this point onwards.

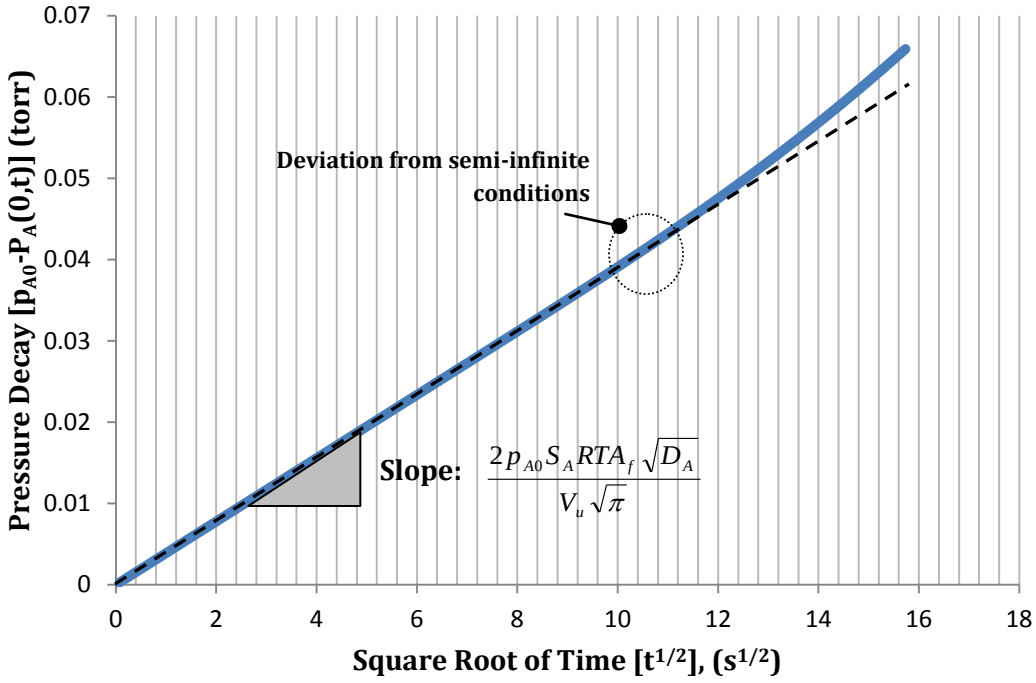

Figure 3.2 Demonstrating the upstream short time solution: [p_{A0} - $p_A(0,t)$] vs. $\sqrt{t}$

Application of the developed short time solution is illustrated in Fig. 3.2. It is based on a simulation carried out with a membrane of similar properties as in Chapter 2, with D_A = 4.5 x 10^{-8} cm^2/s, P_A = 3.8 Barrer, and a thickness l = 0.0042 cm. This time however, deviations are observed at $\sqrt{t}$ =10.4 $s^{-1/2}$, which translates to Fo = 0.276, which is a higher limit than the one set out by the flux profiles. This is expected since the pressure is essentially an integrated form of the flux, which numerically has the tendency of further reducing the 1.0% error criterion set in Fig. 3.1 [2]. The slope contains the product of both S_A and D_A, which unlike the downstream short time solution; can't be acquired independently. What is also evident in the slope is the lack of dependence on the membrane thickness (l), a key property of a semi-infinite medium.

3.3 Attempts to Decouple the Diffusivity and Solubility for the Upstream Short Time Solution

The purpose behind this section is similar to what was unveiled in Section 3.2: Finding a way to decouple D_A and S_A in order to provide a short time scheme using only the pressure decay profiles.

Two methods are disclosed in this section: The least squares approach, and the relative slope method.

3.3.1 Least Squares Method

Since $P = D \cdot S$, the short-time inflow pressure profile solution given by Eq. (3.4) can be presented in terms of permeability instead of solubility

$$p_A(0,t) = p_{A0} - \frac{2 p_{A0} RTA}{V_u \sqrt{\pi}} \left(\frac{P}{\sqrt{D_A}} \right) \sqrt{t} \tag{3.5}$$

Or

$$p_A(0,t) = p_{A0} - m\sqrt{t} \tag{3.6}$$

In which the slope m is given by,

$$m = \frac{2 p_{A0} RTA}{V_u \sqrt{\pi}} \left(\frac{P}{\sqrt{D_A}} \right) \tag{3.7}$$

The early short time behaviour may also be approximated using an alternative expression; this was mentioned earlier in Eq. (3.1) which was deemed useless due to its non-linearity. However, this formula is used, and redefined in terms of the rate of decay:

$$\frac{dp_A(0,t)}{dt} = \frac{p_{A0}RTA}{V_u\sqrt{\pi}}\left(\frac{P}{\sqrt{D_A}}\right)\frac{1}{\sqrt{t}}\left[\exp\left(-\frac{l^2}{D_A t}\right)+1\right] \tag{3.8}$$

Where in terms of the slope *m* of Eq. (3.7), is expressed as

$$\frac{dp_A(0,t)}{dt} = \frac{m}{2\sqrt{t}}\left[\exp\left(-\frac{L^2}{D_A t}\right)+1\right] \tag{3.10}$$

Methodology:

1. Collect transient upstream pressure data
2. Plot pressure profile $p_A(0,t)$ vs. $\sqrt{t}$, obtain slope *m*
3. Create second plot of experimental pressure derivative $\left(\frac{dp_A(0,t)}{dt}\right)$ vs. t
4. Perform a sum of least squares regression fit in the standard time scale with the model in Eq. (3.10) to solve for the applicable diffusivity (D_A) range.
   - Applicable D_A range: 0 to $D_{A,max}$
5. Ideally, the best fit is obtained as $D_A \rightarrow 0$ since it follows the behaviour of a semi-infinite slab at an early stage (Eq. (3.5)). However, it is when D_A exceeds a certain criteria ($D_{A,max}$) that a notable deviation is observed.
6. Find the observable $D_{A,max}$ iteratively. Starting from a large initial guess then moving downhill until no apparent change is observed. This method is best carried out by moving in decade steps (logarithmic steps – factor of 10, e.g. 1 , 10^{-1}, 10^{-2}..etc).

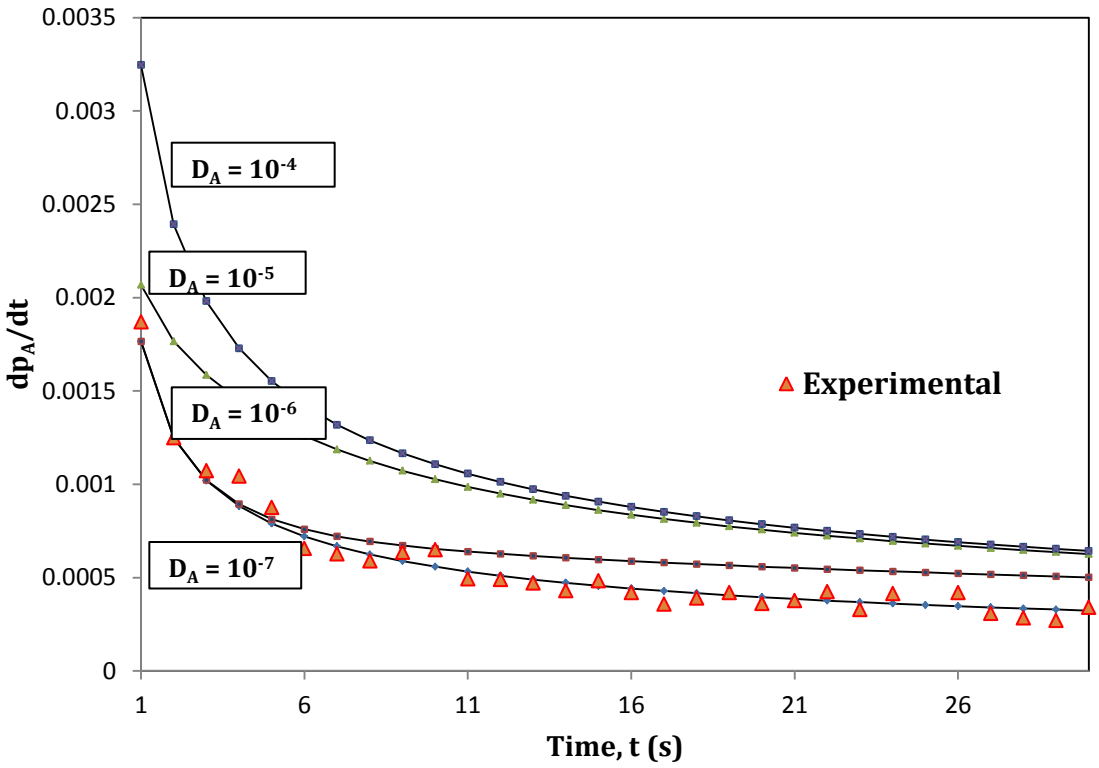

Figure 3.3 Graph illustrating the approach of model in Eq. (3.10) towards experimental data using decade steps

7. Finally, the value of D_A can be further narrowed down by plotting the sum of least squares with respect to decreasing diffusivity until no change is observed. A smaller fixed step size is used for this case.

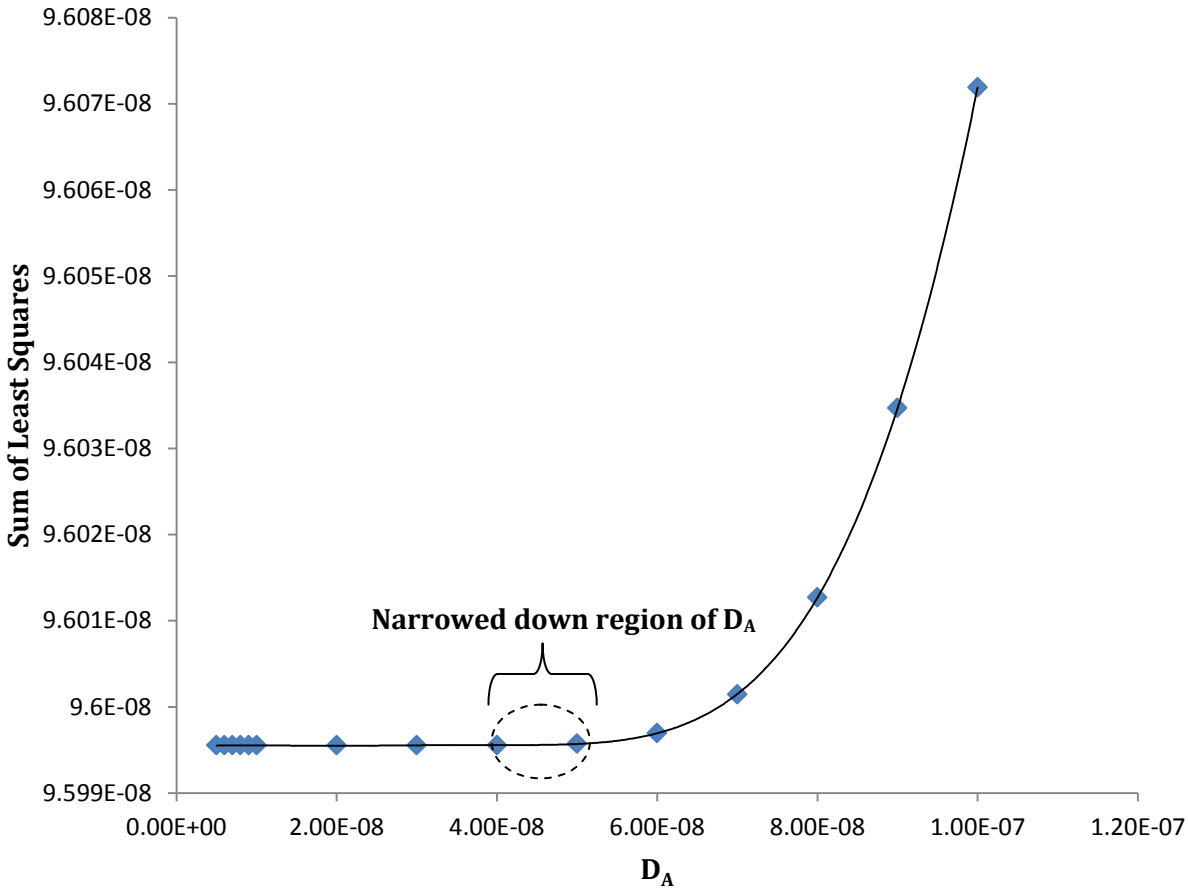

Figure 3.4 Sum of Least squares as a function of inputted D_A (in reversed order). Indicated narrowed down region corresponds to the highest value of D_A when the profile settles off ($D_{A,max}$).

So in conclusion, the region form approximating D_A is obtained by finding the *largest* possible value of D_A that can yield the *best fit for the sum of least squares method*. Similar to the time lag technique, the membrane thickness (l) is the only condition required to perform this procedure. However, unlike the time lag technique, a much lower timeframe

($Fo_{Least\ Squares} = 0.07 << Fo_{,time\ lag} = 0.5$)

Unfortunately, the least squares method described above provides just a vague approximation, where a distinct value for D_A is unobtainable. This serves as a testament to difficulty involved with individually extracting the solubility and diffusivity within the short time decay.

3.3.2 Relative Slope Method

The relative slope method represents another approach for extracting the diffusivity from the short time decay in the upstream. The relative slope is defined as:

$$RS = \frac{\frac{\partial J_{in}}{\partial Fo}}{\frac{J_{in}}{Fo}} \tag{3.11}$$

where J_{in} is the flux at the upstream face of the membrane given by Eq. (2.18).

Eq. (3.11) is redefined in terms of the upstream pressure decay and time, by considering linear proportions of:

$$\begin{aligned} \frac{dp_A(0,t)}{dt} &= f\left(J_{in}\right) \\ Fo &= f\left(t\right) \end{aligned} \tag{3.12}$$

which results in

$$RS = \frac{dp_A^2(0,t)}{dt^2}\frac{t}{\frac{dp_A(0,t)}{dt}} \tag{3.13}$$

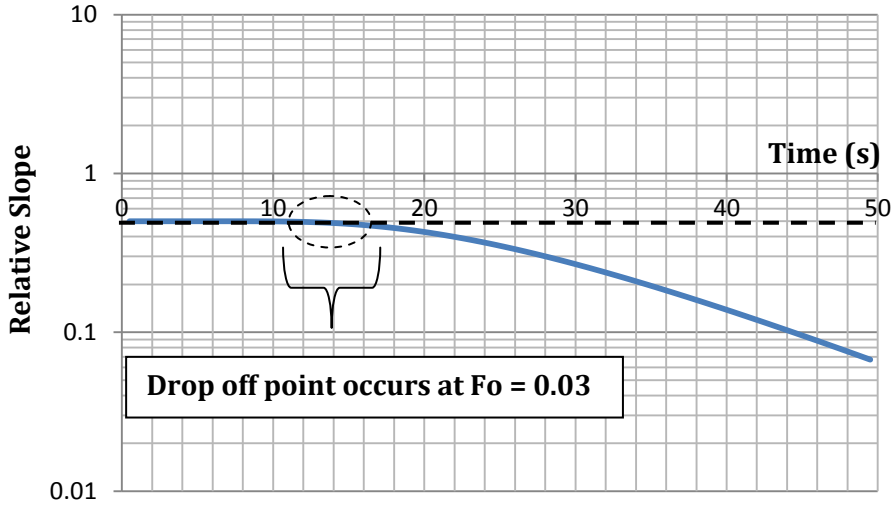

Figure 3.5 The relative slope as a function of time in a semi-log scale.

With Eq. (3.11), the relative slope is plotted as a function of time; a simulation of the behaviour is illustrated in Fig. 3.5. The theoretical profile starts at 0.5, then begins to drop at a Fourier number *Fo* = 0.03. Knowing that the drop is supposed to occur at around *Fo* = 0.03, identifying the time at which the experimental data presented in terms of Eq. (3.13) starts to decrease, would allow an estimate of the diffusivity D_A.

$$D_A = \frac{0.03 \cdot l^2}{t} \tag{3.14}$$

Unfortunately, errors are exceedingly enlarged when calculating the second derivative of the pressure decay, so at the moment, the proposed approach isn't possible unless the smoothness of current decay curves are improved upon. An example of this is shown in Fig. 3.6.

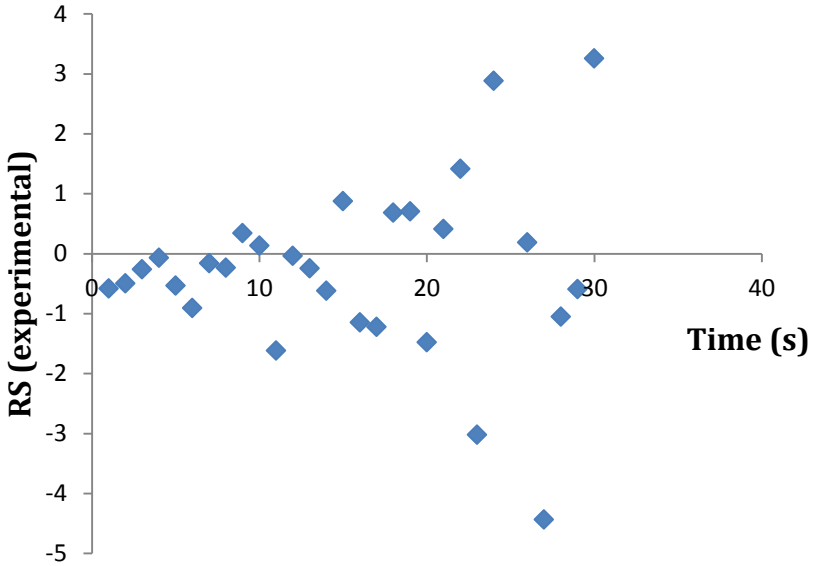

Figure 3.6 Demonstrating the errors associated when evaluating the relative slope of the experimental data

3.4 Short Time Solution in the Case of Composite Slab Membranes

The inspiration behind analyzing composite membrane was another attempt to decouple the diffusivity and solubility from the short time solution. In this approach, a membrane (or laminate) of known properties and thickness is placed on top of the membrane whose properties are being sought. This concept is illustrated in Fig. 3.7.

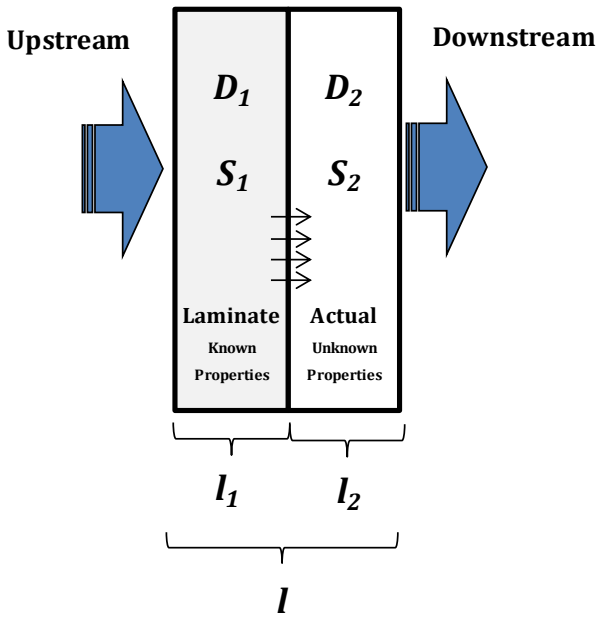

Figure 3.7 Diagram of composite slab system

Analytical expressions for composite slabs have been provided by the likes of Carlsaw [3] and Ash et Al. [4], which focused on the pressure accumulation in the outflow volume. In our case, we focus on the pressure decay in the inflow volume. As a result, a different analysis on the composite slab pressure profile is conducted, which instead provides us with a different perspective of the composite system. Despite the inability to decouple the two properties, this section takes on a different approach to utilize the previously developed short time solution.

To investigate this behaviour, similarly to the upstream short time solution (Eq. (3.4)), a semi-infinite decay plot is again carried out, but this time from a simulation of a pressure decay response curve in a two-membrane composite system. This is done in an attempt to observe the effect that the placement of a different membrane in the upstream face of the original has on the pressure decay response curves. ***A laminate of higher***

permeability and lesser thickness is demonstrated in this case due to the relevance it would eventually have in Chapter 4. The composite slab system was successfully modelled ***numerically*** which is detailed in Chapter 5.

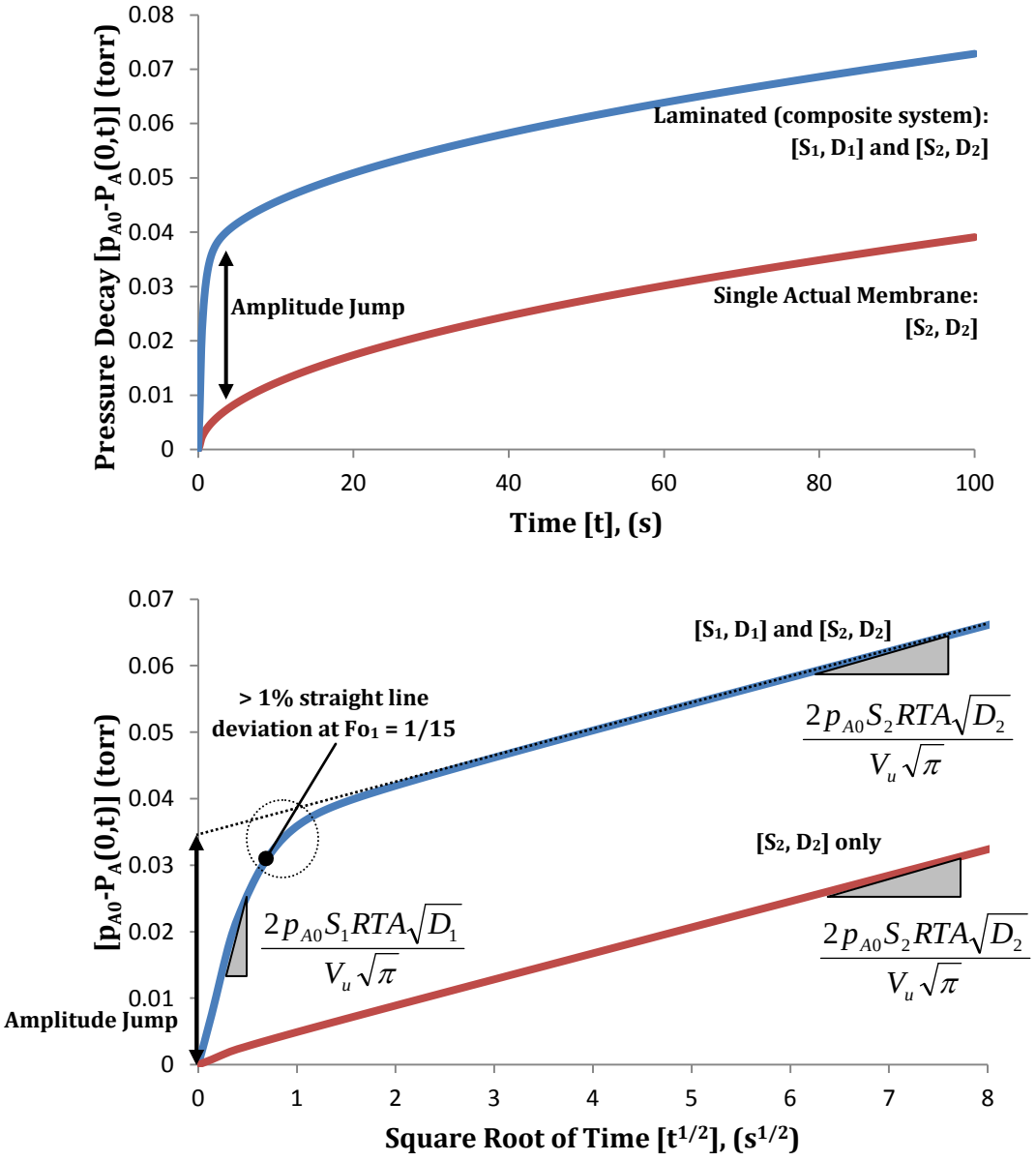

Figure 3.8 Comparison of simulated pressure decay curve of laminated and non-laminated membrane, illustrated in two plots: 1st plot: Standard pressure decay plot, 2nd Plot: Short time semi-infinite decay plot.

With the exact same membrane used in 3.3 (defined as subscript 2), in the composite system, it was laminated (subscript 1) with the following properties: $D_1 = D_2$ x 50, $l_1 = l_2$ x (1/3), $S_1 = S_2$. It is evident that Fig. 3.8 reveals an abundance of very notable observations, which is best conveyed in the following bullet points:

Standard Decay Plot (Fig. 3.8 - Graph #1):

- Addition of the laminate is viewed as an **added layer of resistance**.
- When comparing the two curves, their permeation behaviours are very similar, but the "resistance-added" plot exhibits a notable amplitude-jump at the very start of the permeation process. This results in a much higher overall time lag.
- Considering that membrane 1 has a much lower resistance than membrane 2, the jump, is owed to the significant amount of species instantly absorbed due to its permeability ($S_1 \cdot D_1$). As a result, the upstream time lag becomes much greater than the sum of the individual time lags of the laminate and membrane, respectively.
- This amplitude-jump doesn't occur instantly at t = 0, but over a very early and short period of time. During the short period, a concentration profile develops over membrane 1. Once that is established, the permeation (also decay) is governed by the resistance of membrane 2 as evident by the transition regime. The amplitude-jump depends on the diffusivity and thickness of membrane 1.

Semi-Infinite Decay Plot (Fig. 3.8 - Graph #2):

- The behaviour of the single actual membrane discussed in 3.2 is compared against.

- In the case of a double composite system, the semi-infinite decay plot reveals a profile which employs the short time behaviour of both membranes. The plot displays an initial linear behaviour which corresponds to a short time slope of membrane 1, then transitions to a second linear region corresponding to the short time slope of membrane 2.
- The transition point in time is dependant only on membrane 1, which occurs at a Fourier number of $Fo_1 = 1/15$ (documented as $Fo = 1/16$ in Ref. [5]).
- This is however inconsistent with the transition exhibited in Fig. 3.1 which occurs at $Fo = 0.2$. The reason to that is because a very small flux at the outlet of membrane 1 – which is negligible to what is allowed in the inlet of membrane 1 – is no longer negligible compared to the maximum influx of membrane 2 at an early short time.
- One may easily salvage and predict the individual early/short time behaviour of membrane 2 (actual) from the composite system by extrapolating the linear profile of its (second) region and forcing the intercept to 0. This is indicated by the dotted line, and the amplitude jump which is subtracted.
- Finally, it is important to note that if the permeability of membrane 1 is less than 40 times the permeability of membrane 2, the slope of membrane 2 is impacted by this resistance. Hence, when evaluating the slope of membrane 2 for such a case, it would actually be different than that obtained via a short time test of a single membrane.

To conclude this, it is very important to emphasize that the following points disclosed in this section play a very important role in the analysis and discussion of experimental results in Chapter 4.

3.5 Conclusion

A short time solution was developed using the upstream decay plot based by assuming the upstream face of the membrane behaves as a semi-infinite solid at early short times. However, unlike the downstream solution developed earlier, estimation of the diffusivity and solubility individually was not possible. A degree of freedom was still present since both property variables were within the slope.

The least squares method of estimating D_A - although somewhat successful - was still inadequate because a decisive value of D_A was unobtainable. It is also extremely difficult to salvage anything from the relative slope, since a 2^{nd} derivative of the transient decay data would magnify any errors associated with the system.

A model based on a composite 2-membrane system was attempted in order to examine the possibility of decoupling S_A and D_A. The analysis was unsuccessful; however it was observed that the profile in the semi-infinite decay plot behaved as 2 linear regions incorporating the short time slope of membranes 1 and 2. It is also important to note that if the linear portion of the second membrane was extrapolated, this provides a y-intercept that is dependent on the properties of both membranes. This reveals a potential avenue in the future where S_A and D_A may be decoupled.

So in conclusion, it was impossible at this stage to deduce a short time solution for independently estimating the diffusivity and solubility. However, the analysis performed in this section brings to light many of the key features involved with the transport in the upstream face of the membrane.

Nomenclature

A: Membrane/film cross-sectional area (cm^2)

C: Concentration (cm^3(STP) cm^{-3})

D: Diffusion coefficient (cm^2/s)

erf: Error Function

Fo: Fourier Number

l: Thickness of membrane/film (cm)

J: Flux (cm^3(STP) cm^{-2} s^{-1})

m: Short time solution slope ($torr/s^{1/2}$)

p: Partial pressure(torr)

P: Permeability coefficient (Barrer)

R: Ideal gas constant (J mol^{-1} K^{-1})

RS: Relative Slope

S: Solubility Coefficient (cm^3 (STP) cm^{-3} $cmHg^{-1}$)

t: Time (s)

T: Absolute Temperature (K)

V: Reservoir Volume (cm^3)

x: Distance from and within membrane/film (cm)

Subscripts:

1: Membrane 1 in composite system - laminate (Higher permeability)

2: Membrane 2 in composite system (Actual Membrane)

A: Component A – permeating species

in: Entering

u or *0*: Upstream

References

[1] F.P. Incropera, D.P. DeWitt, T.L. Bergman, A.S. Lavine, Fundamentals of Heat and Mass Transfer, Sixth Edition, Wiley, 2006, p. 291.

[2] S.C. Chapra, R.P. Canale, Numerical Methods for Engineers, Fifth Edition, McGraw-Hill Publishing, 2007, p. 525.

[3] H.S. Carlsaw, J.C. jaeger, Conduction of Heat in Solids, Second Edition, Oxford University Press, 1995, p.382.

[4] R. Ash, R.M. Barrer and J.H. Petropoulos, Diffusion in heterogeneous media: properties of a laminated slab, 14 (1963) 854-862

[5] J. D. Seader and E. J. Henley, Separation Process Principles, 2nd Edition, John Wiley & Sons, 2006, p. 87.

CHAPTER 4

RESERVOIR DESIGN & ASSESSMENT FOR MONITORING THE PRESSURE DECAY

4.1 Overview

4.1.1 Objectives

As assessed in Chapter 2, adoption of the proposed short cut solution is inspired by the use of a custom-built upstream reservoir, which possesses the added feature of monitoring the pressure decay. The current chapter will investigate this system in two parts, firstly is a detailed design and portrayal of the entire two reservoir (upstream/downstream) constant volume (CV) system. Later on, a thorough analysis will be carried out on the mechanisms that govern the way inflow permeation rates are measured, which also includes some issues that coexist with the newly designed system, particularly the "resistance effect". The primary objective of this chapter is to achieve a more levelled understanding for a system that is a little bit more complicated than what was described in Chapter 2, which not only

acts as a review paper to the reader, but also encourages any potential future work where the laid out details to the design may be attributed to.

4.1.2 Introduction

The utilization of Daynes' (1920) [1] classical time lag method, and the proposed short cut method in Chapter 2 are in essence used for the characterization of polymer membranes. This involves the estimation of the diffusivity (D), solubility (S), and permeability (P) coefficients. The application of these available tools is based upon measurements of gas transport through the polymeric films via integral permeation.

Integral permeation is where the single penetrating species permeates through the membrane and into an enclosed reservoir of constant volume, and as a result a transient signal is generated to represent the cumulative mass of the permeating species with respect to time [2]. This accumulation of mass is depicted in the form of pressure, which is recorded as a function of time. Prior to testing, the gas to be examined is held in a reservoir located upstream of the membrane, while the downstream volume and the membrane itself are ensured to being completely relinquished of any species. Therefore, the species will instantly begin permeation due to the pressure gradient established across the membrane.

The traditional time lag method is solely based upon evaluating the pressure accumulation on the downstream. However, the newly developed short cut method employed in this project bestows an alternative and unorthodox approach of monitoring the integral permeation, which is by the measurement of the pressure decay (mass loss) of the gas in the upstream reservoir as a result of the permeation through the membrane. The

monitoring of the pressure decay due to gas permeation serves as the ultimate cornerstone in exploiting the short cut method centered on this thesis.

Unfortunately, measurements of the pressure decay lacks the [relative] simplicity found in recording the downstream pressure profile. This is because the simple placement of an absolute pressure transducer (PT) at the upstream reservoir would require for the device to not only be of high accuracy, but also capable of accommodating a larger range of pressures, considering that the upstream is operated under pressure. This could prove to be especially difficult when dealing with membranes of ultra-low permeability, as the demand of those two constraints further limits the availability and heightens the value of pressure transducers in the market.

Therefore to tackle this issue, a novel design of the upstream reservoir is proposed and discussed at detail in this chapter. The primary improvement this scheme provides is eliminating the need of accommodating high ranges of the operating pressure. Similar to measurements carried out in the downstream (initially at vacuum), pressure profile readings may now begin at 0.0000 torr as opposed to the problematic +100.0000 torr. Generally, this is implemented by having the upstream reservoir split up into two volumes under the same pressure, where one volume serves as a working volume directly connected to the membrane, and the other serves as a buffer known as a reference volume. Upstream permeation rates may therefore by carried out via the placement of a differential pressure transducer connected to the two volumes, as one volume (working volume) experiences a decay in species, while the other volume remains unchanged from its original starting pressure.

As the details of the design are further revealed, the credibility and reproducibility of the experimental results will be presented, alongside the tackling of problems encountered, factors that limit the usability of the current design, and recommendations of design improvements which would be implemented in future iterations of this novel scheme.

4.2 System Design

4.2.1 Basic framework of the two reservoir CV system

As mentioned before, the central operation of the newly modified integral permeation system still functions as a traditional constant volume receiver, particularly like the ones employed by Lashkari and Kruczek (2010) [3,4] which is primarily made up of the membrane cell and the downstream reservoir.

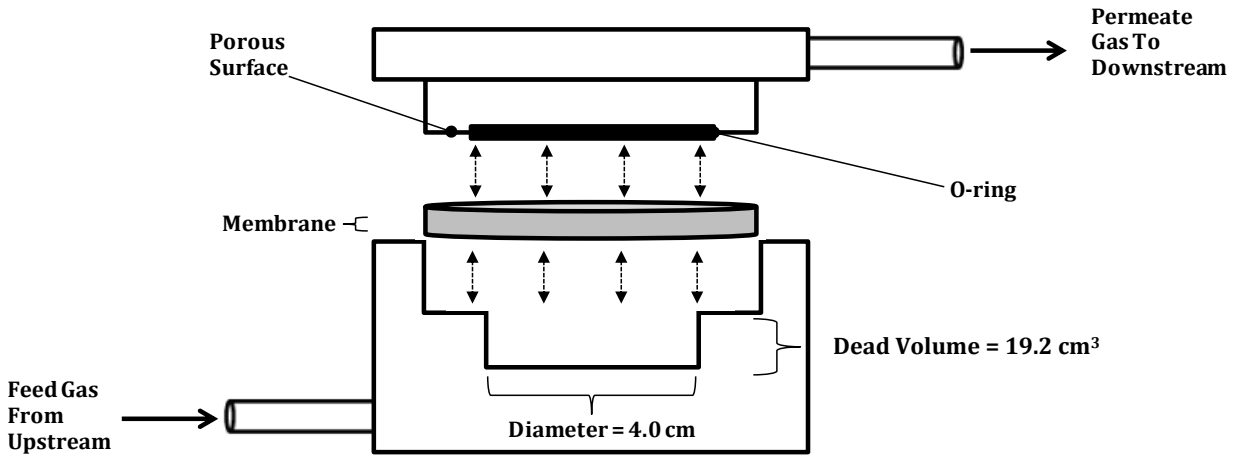

Figure 4.1 Disassembled representation of the membrane cell.

As shown in Fig. 4.1, the membrane is held in a short, cylindrical-shaped stainless steel separation cell, which consists of an upper and lower section. The bottom surface of the upper section is porous (to allow passage of permeate), and encompassed by an O-ring in order to completely seal it. One important element from the cell design (Fig. 4.1) that needs to be accounted for is the presence of a dead volume (V_{dead}) at the lower section after placement of the membrane. This volume not only contributes to the total volume of the upstream reservoir (V_1), but also affects the initially recorded feed pressure (p_{A0}) which will be elaborated upon even further later in this section. The feed line from the upstream connects to the lower section, while the permeate line connects towards the downstream from the upper section of the cell [5].

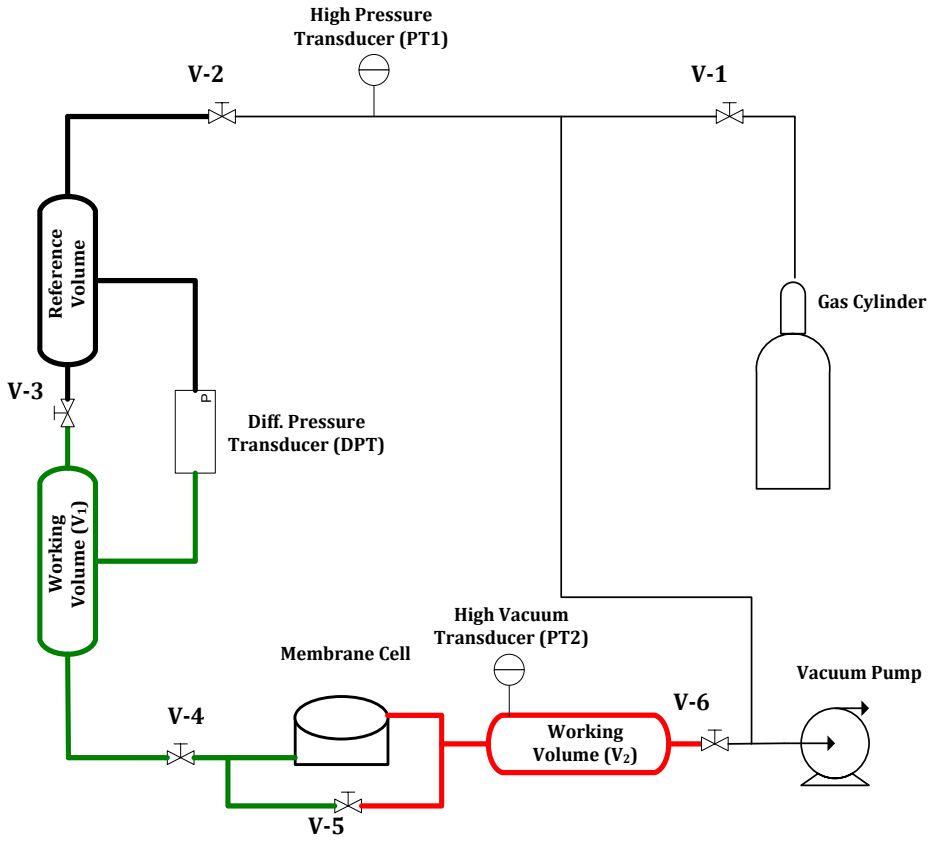

Figure 4.2 Schematic illustrating the experimental setup used to monitor the permeation tests in the upstream/downstream.

A basic schematic of the experimental setup is illustrated in Fig. 4.2. The downstream and upstream reservoirs (indicated as V_2 and V_1) from the membrane cell exist to monitor the pressure increase and decay during the experiment, respectively. An experimental run is achieved via 3 main steps.

Step 1: Evacuation

The downstream reservoir is evacuated over a period of 72 hours by means of a Nelson 3 rotary vane pump. Evacuation is carried out by keeping only valves V-5 and V-6 open, this way both sides of the of the membrane are exposed to the vacuum pump. These valves are eventually closed prior to testing.

Step 2: Start-up

The upstream two-volume reservoir is supplied with the gas (nitrogen) until a desired initial upstream pressure is achieved (p_{A0}) via the high pressure transducer (PT1). This is done by having valves V-1, V-2, and V-3 open, and the remaining valves closed. Once completed, all valves are closed, with only V-3 kept open (which separates the working and reference volumes)

Step 3: Operation

With the downstream completely evacuated of species ($C_A(x,0) = 0$) and the upstream supplied with the gas to be tested, experimentation can now truly begin. The actual operation of the test at time t > 0 is done by: Opening valve V-4, ***immediately*** followed by the closing of valve V-3, ***not*** simultaneously.

It is self-explanatory that the opening of valve V-4 begins the permeation test (boundary condition $C_A\ (0,\ t) = C_{A0} = p_{A0}S$), and that the closing of valve V-3 compartmentalizes the working and reference volumes. However, there is a strategic relevance to the closing of V-3 ***after*** V-4 and ***not before***. The problem with opening it before brings rise to the issue of species expansion present in the working volume due to the exposure to the added volume from membrane cell dead volume (V_{dead}) and the short tubing that follows V-4. This expansion effect would cause the differential pressure transducer readings to go off-chart, and beyond it's available scale, rendering the upstream permeation readings meaningless. The concept of a two-volume system is loosely based on a design by Arkilic et al. [6] for the flow measurement of gasses flowing out of micro-channels and accumulating at relatively high pressures (e.g. atmospheric pressure).

Step 4: Completion and Re-evacuation

After concluding the permeation tests, valve V-4 is closed, and evacuation procedures from *Step 1* are repeated.

4.2.2 Detailed design and configuration of the two reservoir CV system

In this section, a more detailed and comprehensive look into the layout of the two reservoirs is presented. This includes tubing configurations, allocation of tanks and pressure transducers, and their contribution to the reference and working volumes.

We start off with a quick look at the schematic of the downstream reservoir, followed by a heightened emphasis on the design of the upstream reservoir, which is where the focus of this chapter and thesis are based on.

The valves (V-1, V-2…V-6) displayed in Fig. 4.2 are only the ones ***directly*** involved in the operation of the permeation tests. All specific valves involved at downstream (D-1→ D-4) and upstream (U-1 → U-11) reservoirs are also displayed, where the ones which are directly involved would be indicated.

Downstream Reservoir:

Application of the traditional time lag technique in gas permeation tests are carried out by observing the accumulation of permeated gas in a receiver of constant volume (downstream reservoir). A more detailed overview of the constant volume system can be found in section 1.2 Chapter 1.

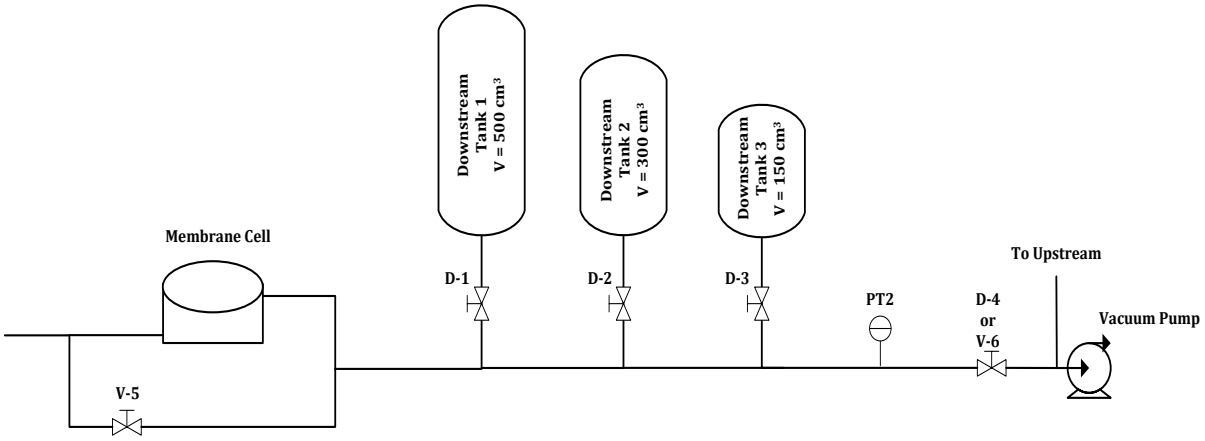

Figure 4.3 Detailed schematic of downstream reservoir

As shown in Fig. 4.3, the downstream reservoir is configured with multiple accumulation tanks separated by valves D-1, D2, and D-3. The concept of the accumulation tanks is similar to the one adapted by Stern et al. [7], which allows a flexibility in altering the reservoir volume without exposure to atmosphere. Adjustment of the volume is done based on the anticipated permeation rate. This is motivated by the need to accommodate for the limitation of the pressure transducer, where larger volumes are used for high permeability membranes, and vice versa.

In a study published by Lashkari & Kruczek [3, 4], it was observed that when the receiver was configured with tanks present, it greatly impacted the measured time lag, and hence the diffusivity. This implication was mainly present in monitoring the *early transient* period of the pressure accumulation response curve, which leads to an inaccurate estimation of the actual membrane properties (P, and especially D). Although details of this study won't be discussed here, the general idea of it is summarized since it plays a critical role in the behaviour of the upstream reservoir which is centered on this thesis. It was concluded that this implication on the decrease of the measured time lag, which is owed to the presence of tanks, is due to the increase in the overall resistance of the downstream reservoir.

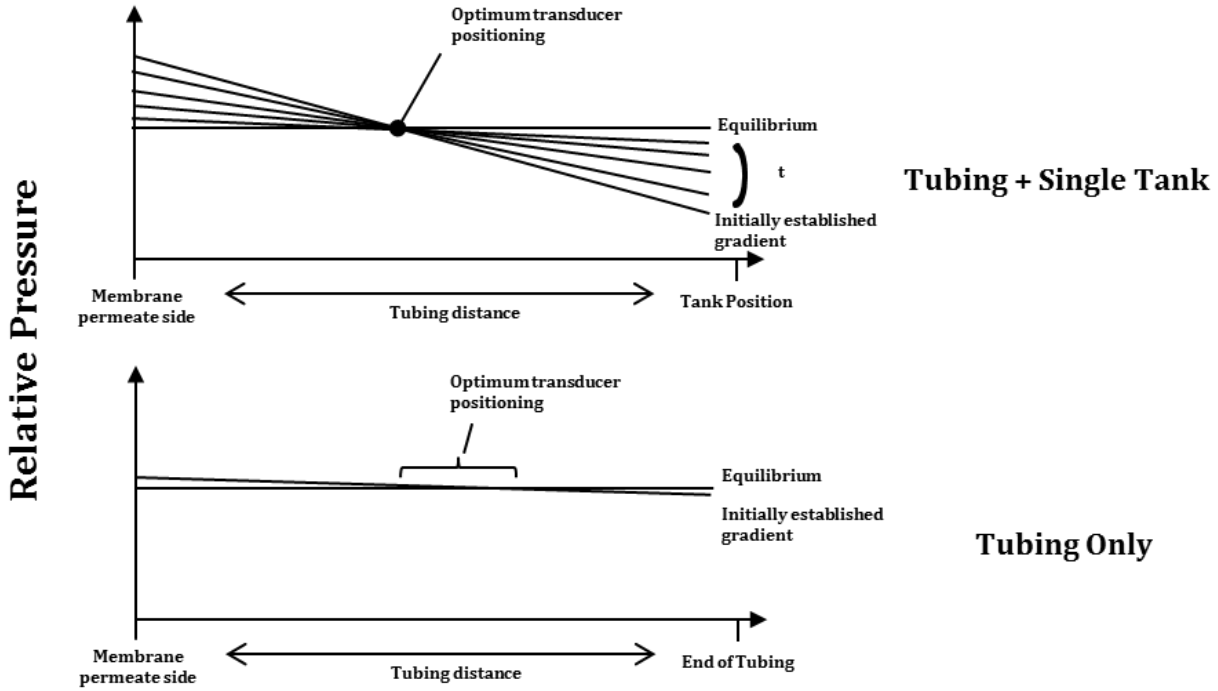

Figure 4.4 Demonstration of the pressure profile between the point of reference (downstream membrane face) and the end point of receiving reservoir, done under two unique CV system configurations. Not only does the tubing-only configuration equilibrate much fast, but also offers a wider range of optimum transducer positioning.

When compared to the actual tubing, an individual tank is considered to have an infinitely higher capacity (much larger diameter), with its resistance to gas flow being inversely proportional and consequently negligible [8]. However, during a permeation test, such a contrast in the two resistances (tube vs. tank) leads to the rise of a non-negligible pressure gradient between the permeate side of the membrane and the tank. This is a far cry from the conditions of classical time lag method, which relies on the assumption that there is no resistance to gas transport across the downstream reservoir at time $t > 0$. The concept of this behaviour is illustrated in Fig 4.4, revealing the pressure gradients, and

their approach to equilibrium for single tank w/tubing and tubing-only configurations. The tubing-only configuration provides the lowest overall resistance, and most accurate representation of the time lag, despite being intrinsically at a higher resistance than a tank. Addition of more tanks in a [high resistance] tank + tubing configuration would decrease its overall resistance since they contribute to reducing the established pressure gradient. Also, the positioning of the pressure transducer also affects the measured time lag, with an optimum position (nearest to final equilibrium pressure) that provides the best estimate of the time lag.

As mentioned before, details on the mechanisms that govern such behaviour are fundamentally explained and proven in the papers by Lashkari and Kruczek [3, 4].

Finally, for arguments sake, separate time lag permeation tests were performed under all possible configurations to further divulge on this resistance effect, results are presented in Table 4.1 below. It is important to emphasise that ***all experiments conducted outside of the ones presented in Table 4.1 are performed using the tubing-only downstream reservoir configuration***.

Table 4.1 Observed downstream time lag under various downstream reservoir configurations. Gas: N_2, membrane: PPO, thickess: 26.7 μm

Configuration	Time Lag [s]	Diffusivity [cm^2/s]
Tubing only	27.0	4.40×10^{-8}
Tubing + Tank 3	26.3	4.52×10^{-8}
Tubing + Tank 2 + Tank 3	25.2	4.71×10^{-8}
Tubing + Tank 2	23.9	4.97×10^{-8}
Tubing + Tank 1 + Tank 3	22.9	5.19×10^{-8}
Tubing + Tank 1 + Tank 2+ Tank 3	22.8	5.21×10^{-8}
Tubing + Tank 1 + Tank 2	22.2	5.35×10^{-8}
Tubing + Tank 1	21.3	5.58×10^{-8}

Upstream Reservoir:

In a nutshell, the newly designed upstream reservoir is in the form of a two volume system, which is collectively supplied with a feed gas and brought up to a desired upstream starting pressure p_{A0}, then separated via valve V-3 (Fig. 4.2). At the start of a permeation experiment, one volume (working) is exposed to the membrane and experiences a decrease in pressure, while the other volume (reference) remains unchanged at p_{A0}. The placement of a differential pressure transducer (DPT) between the two volumes is used for monitoring the pressure decay. The concept of a two-volume system is loosely based on a design by Arkilic et al. [6] for the flow measurement of gasses flowing out of micro-channels and accumulating at relatively high pressures (e.g. atmospheric pressure).

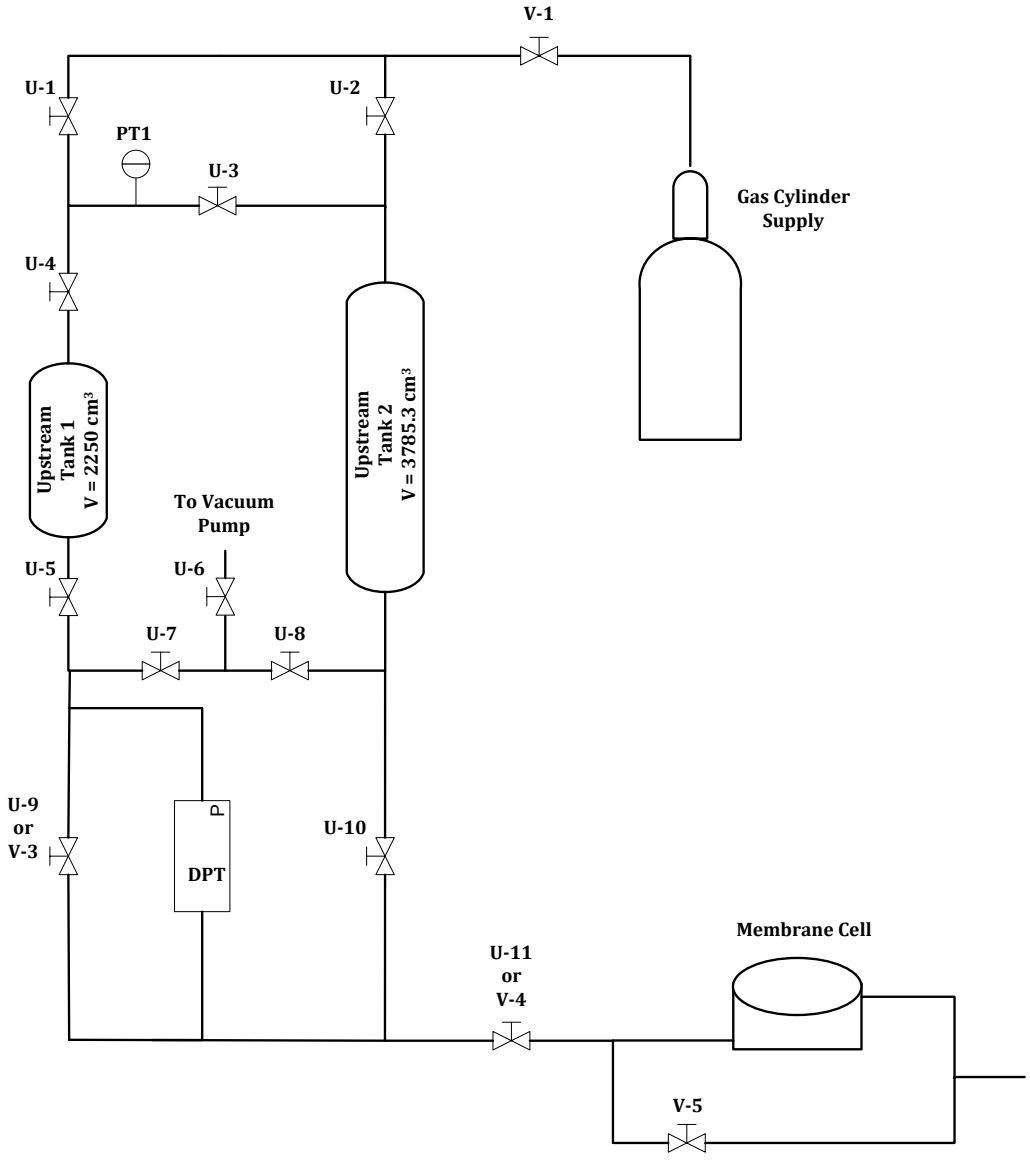

Figure 4.5 Detailed schematic of upstream reservoir

Specifics of the design of the upstream reservoir are exhibited in Fig. 4.5. With a first glance at the schematic, one would instantly conclude that the two tanks present are the ones acting as working and reference volumes. However, the actual functionality of the system is ***far from*** such a trivially drawn out conclusion.

The system presented in Fig. 4.5 is the final (or more recent) iteration from an initially designed concept; which ***did*** in fact operate with the two tanks acting as reference and working volumes. Unfortunately, the pressure decay response curve observed with the initial design yielded exceedingly large estimates of time lag measurements when compared to the more stable and proven downstream time lag (with no tanks). Therefore, as an operator of the system, one is inclined to think that the resistance effect discussed in the downstream section earlier also plays a role in the upstream. Redesign iterations that followed were motivated by configuring the working volume in the form of tubing-only. However, deviations in the upstream time lag persisted until a best estimate was obtained ***when both the working and reference volumes were set as tubing-only***. Experiments performed in Chapter 2 for the short cut method are achieving using the following configuration.

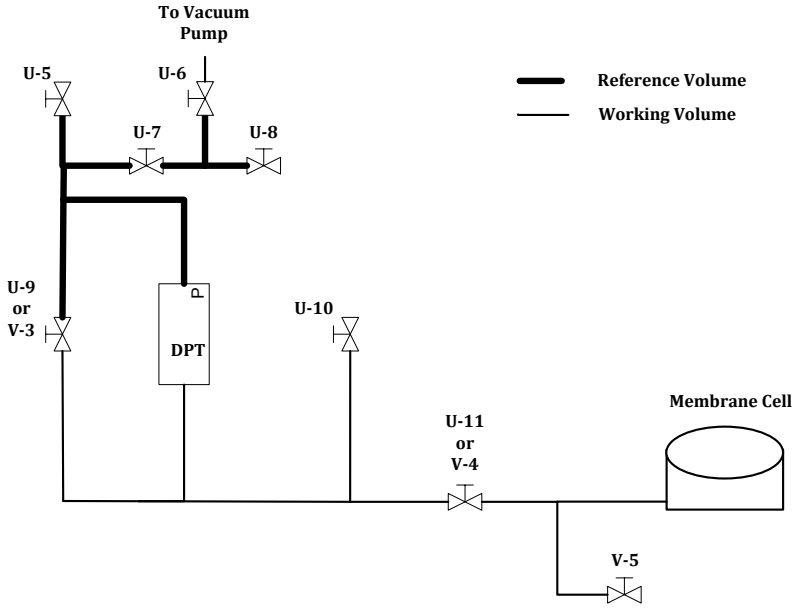

Figure 4.6 Upstream reservoir schematic: Base case configuration #0

The schematic presented in Fig. 4.6 is the best case configuration used to provide the best pressure decay response curve for the estimation of membrane properties. The tubing shown as thick drawn out flow lines represents the reference volume. Initially, and after evacuation of the downstream, the tubing (volume $V_{tube\text{-}exp}$) ahead of valve U-11 (aka V-4 in Fig 4.2) is under vacuum, including the dead volume (volume V_{dead}) present at the base of the membrane cell. At this point, only valves U-7 and U-9 (V-3) are open.

The permeation experiment is initiated as soon as the species are exposed to the upstream surface of the membrane. This occurs when valve V-4 is opened, as the gas initially enclosed between U-5, U-8, and U-11 expands. As stated in section 4.2.1, valve V-3 (shown as U-9) is closed immediately after the expansion process and pressure equalization in the tubing in order to begin recording the pressure decay. ***This permeation recording sequence is exactly what is practiced in all experiments discussed in this thesis***.

It was observed in the earlier version of the upstream design that the presence of tanks in the reference volume also impacted the measured time lag. In the primary and remaining sections of this chapter, an in-depth look will be done on the impact the various configurations have on the pressure decay curves. The other 3 configurations to be evaluated are presented in Fig. 4.7.

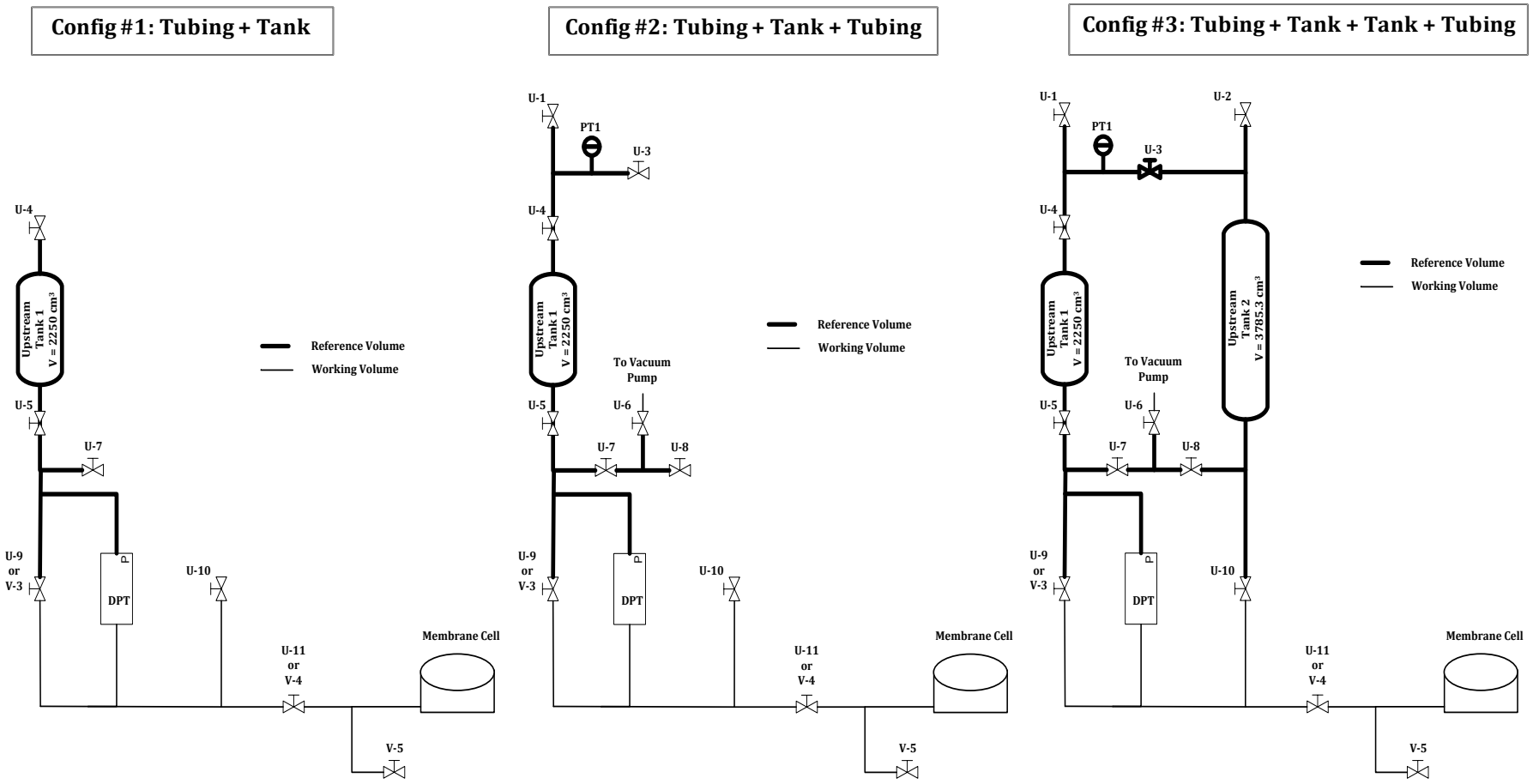

Figure 4.7 Three different configurations of the reference volume in the upstream reservoir are to be analyzed. Configuration #1: Tubing with Tank, Configuration #2: Addition tubing from config 1, Configuration #3: More tubing combined with both available tanks.

Fig. 4.7 shows the three configurations in which the resistance effect will be assessed in this project. Configuration #1 is similar to the base case (Fig. 4.6), but with an added tank and lesser tubing, and valve U-5 kept open during the process. Configuration #2 is a near-replica of configuration #1 but with additional tubing, as valves U-4 and U-7 left open alongside U-5. Configuration #3 involves the usage of both tanks parallel to the direction of DPT, and more tubing. And of course, valves which are kept open are: U-3, U-4, U-5, U-6, and U-8.

During an operation, it is important to highlight the fact that both volumes are at uniform pressure prior to separation with valve V-3. The initial absolute upstream pressure (p_{A0}) drops insignificantly due to:

1- Expansion after opening valve V-4/U-11
2- Minuscule depletion of species at the very short early time lost between opening V-4/U-11 and closing V-3/U-9

Pressure drop due to expansion is neglected in configurations #1 to #3 since their combined working + reference volumes are much larger compared to V_{dead} + $V_{tube\text{-}exp}$, also considering that PT1 does not possess sufficient accuracy to respond to the drop. The initial drop however, is more prominent in configuration #0 since the volumes used are relatively smaller, but PT1 isn't present to in either volume to monitor the drop. Therefore a 17% pressure drop is assumed since it is based on the volume ratios of V_{dead} + $V_{tube\text{-}exp}$ compared to the remaining reservoir volume of configuration #0. A summary of all volumes present in the system, operating conditions, features of the pressure transducers used, and relevant dimensions within the system are summarized through Tables 4.2-4.4.

Table 4.2 Summary of the upstream volumes involved in all configurations

Configuration	V_{ref} [cm^3]		V_1 ($V_{working}$) [cm^3]	Added volume due to expansion (part of V_1)	
	Tanks contribution	Tubing contribution		V_{dead} [cm^3]	$V_{tube-exp}$ [cm^3]
#0 (base case)	0.0	65.36	77.6	19.2	13.5
#1	2250.0	67.42			
#2	2250.0	81.10			
#3	6035.3	98.77			

Table 4.3 Properties of pressure transducers used and size of tubing used.

Tubing sizes used in	***Upstream***	¼" Only
	Downstream	¼" and ½"
Pressure transducer PT1	***Range***	0 to 40 pisa
	Accuracy	10^{-3} psia
Pressure transducer PT2	***Range***	0.0 to 1.0 torr
	Accuracy	10^{-4} torr
Pressure transducer DPT	***Range***	+/- 0.2 torr
	Accuracy	10^{-5} torr

Table 4.4 Summary of tank sizes present in entire system in cm^3

Upstream Tank 1	Upstream Tank 2	Downstream Tank 1	Downstream Tank 2	Downstream Tank 3
2250	3785.3	500	300	150

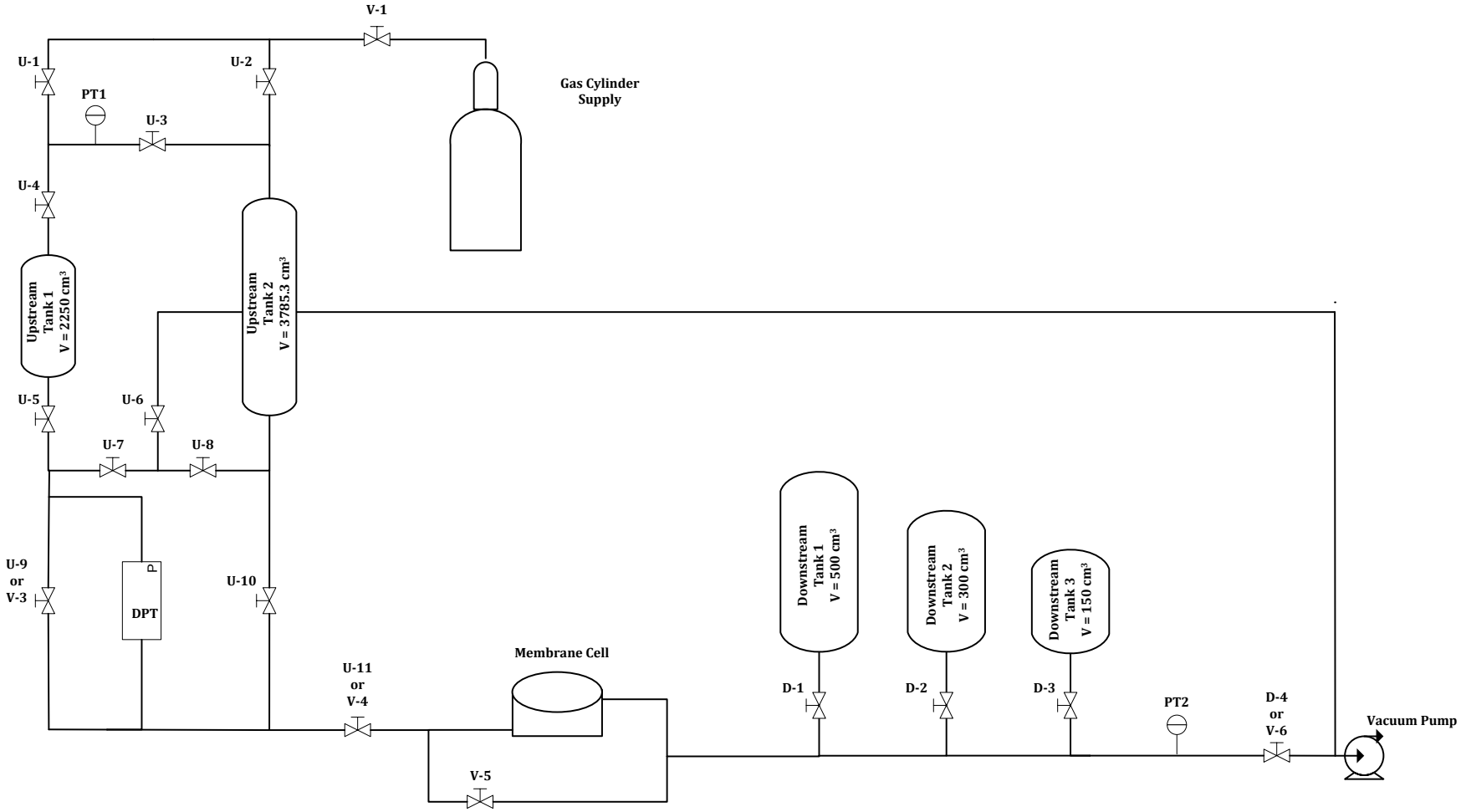

Figure 4.8 Final schematic of the two-reservoir integral permeation system proposed in this project

4.3 Experimental Results & Observations – Base Configuration (0)

4.3.1 Raw Data Acquisition

A sample of the raw data of the pressure decay collected for the base configuration was demonstrated earlier in Chapter 2 (Fig. 2.4). It was witnessed that the data experiences some minor added disturbances due to the design of the upstream reservoir.

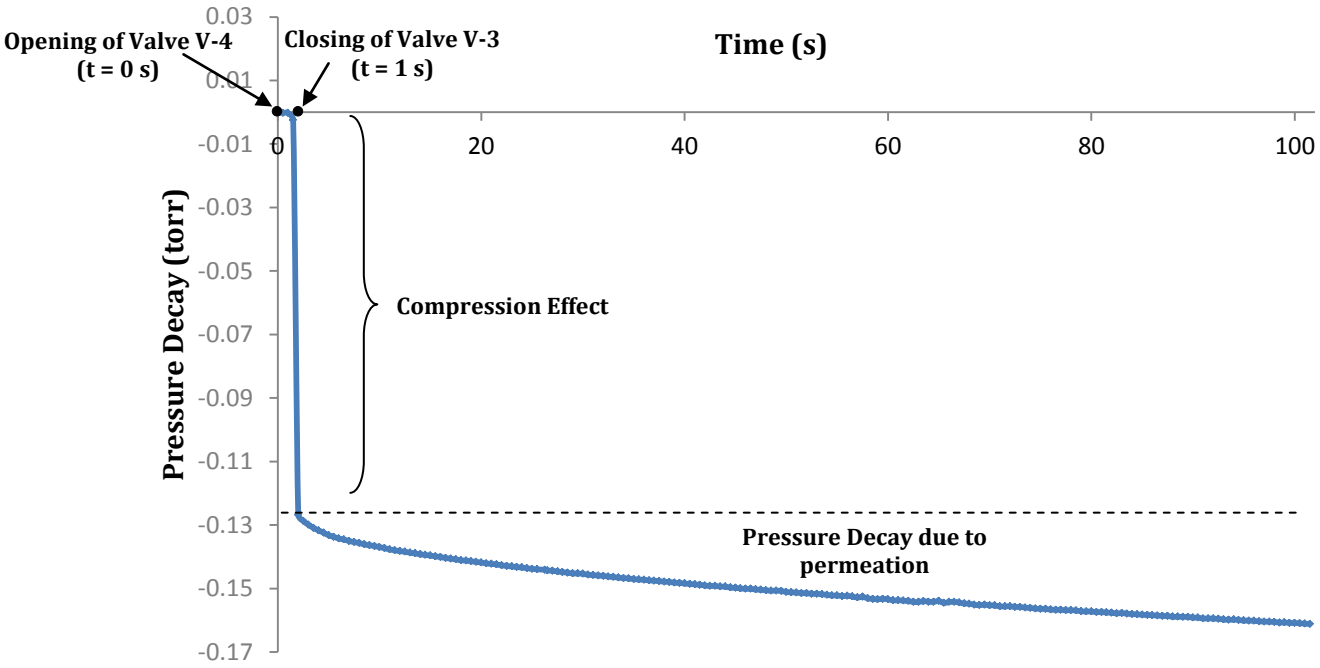

Figure 4.9 Sample of data acquisition of pressure decay at the base configuration. Recordings performed via DPT transducer.

Fig. 4.9 is an example of the raw data originally collected at the base configuration when performing a permeation test. It contains two very notable observations: First of all, there is a very minor "time loss" between opening V-4 and closing V-3. Although it is accounted for that the experiment still truly begins at t = 0 s, data collection however doesn't start until valve V-3 is closed, which is at t > 1 s. The other observation is the

existence of a very significant and instant drop in the measured differential pressure as V-3 was closed. This drop is described as a "compression effect", which is the result of the net-compression bestowed upon the reference and working volumes as valve V-3 is closed. The type of valve adapted in this reservoir design is a bellow-sealed valve, which has the distinct benefit of being employed in pilot-scaled equipment operated under vacuum [9]. A bellow-sealed valve comprises of a stem at the bottom that when closed, would contribute to a slight decrease of the volumes connected to both sides of the membrane, as the stem is viewed to 'press against' the two volumes when closed (hence, compression). Typically, this minor effect owed to the valves is negligible; however it is more prevalent in the current system as it is easily picked up due to the very limited range and extreme high accuracy of DPT (Table 4.3).

It is important to note that since DPT readings are difference-based, pressure changes occurring on the reference side are the opposite of what read in the working side. Therefore, when the minor compression from V-3 is applied, that should result in a positive (p_+) pressure jump from V_1, and a negative (p_-) pressure jump from the reference side V_{ref}. Fig. 4.9 reveals the net effect to being negative, which is indicative of $p_- > p_+$, the reason to this is as follows:

1. Reference volume V_{ref} is less than V_1 in the base case configuration (see Table 4.3)
2. The shape of the valve stem isn't symmetrical, as the side oriented towards the reference volume is larger, hence further contributing to a larger compression on the negative side (p_-)

4.3.2 Correction of Data

In an attempt to correct for the data due to the compression effect imposed on the pressure decay response curve, an elaborate scheme utilizing the upstream short time solution is employed in this section. It is important to keep in mind that a simple way of just 'subtracting' off the compression jump is highly not recommended because this doesn't account for the short and early "time loss" at the start of the experiment, nor does it consider any compression after-effects that follows the jump. Hence the exact amount contributed to the net pressure effect isn't always precisely known since it varies between the tests performed depending on the human error associated with operation of the system (e.g. initial time loss, manner of closing the valves, absolute upstream pressure).

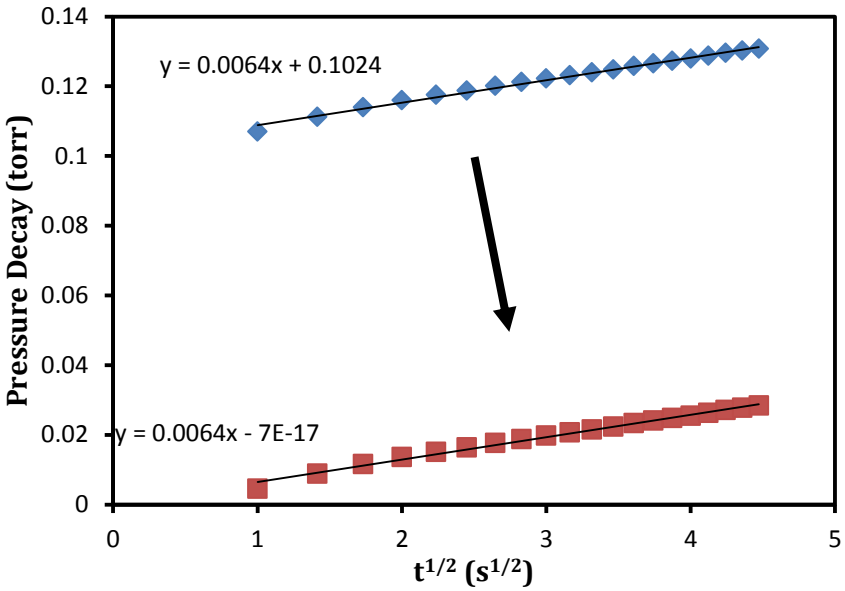

Figure 4.10 Correction of upstream pressure decay curve – A semi-infinite decay plot

Fig. 4.10 illustrates how this is rectified. Since it is known that the pressure decay during the early stages (Fo < 0.2) behaves linearly when plotted against $\sqrt{t}$ (discussed in

Chapter 3, section 3.2), this is therefore carried out on a select range of data points succeeding the compression jump. What is revealed - as displayed in Fig. 4.10 - is a linear profile, but with an intercept present. This intercept therefore corresponds to the best estimate to the actual compression effect. The entire data-set is therefore corrected for by subtracting this intercept, or in other words; forcing the intercept to 0.

This procedure plays a very crucial role in the post-treatment of the collected data, and will be performed in a similar but somewhat altered fashion in section 4.4.

4.4 Experimental Results & Observations – Configurations 1-3

4.4.1 Raw Data Acquisition

As discussed in section 4.3, the collected raw data is analyzed for configurations 1-3. These configurations are grouped together because they exhibit very key common behaviour to one another, and share in the differences they have with the base configuration (0). A quick look into the lone compression effect will firstly be carried out.

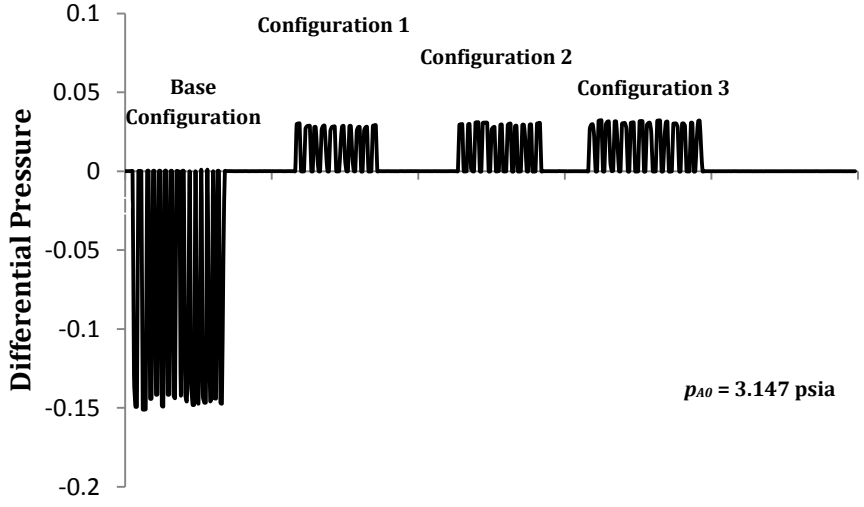

Figure 4.11 An isolated view on compression effect of all 4 configurations (0, 1, 2, and 3)

The compression effect of the various configurations is revealed in Fig 4.11. In the base case, the jump is similar to what was viewed in Fig. 4.9 while the other three show: 1- a smaller jump; 2- Positive net compression; 3 – are equivalent to one another. The reason for this is because the reference volume has now increased dramatically (see Fig. 4.7 and Table 4.2), rendering the compression effect on the reference volume (p_-) negligible. Thus, the compression effects in 1-3 are only equal to p_+ imposed on the working volume.

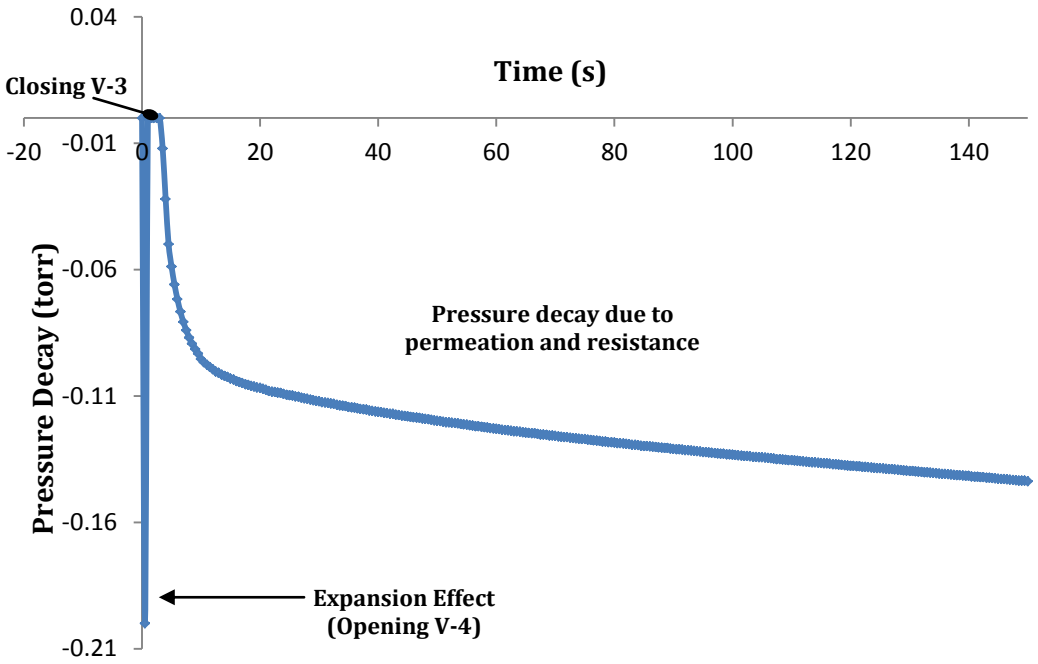

Figure 4.12 Sample of data acquisition of pressure decay at configuration 1. Recordings performed via DPT transducer.

In the case of dealing with the latter 3 configurations, a sample of the pressure response curve obtained is illustrated in Fig. 4.12. The first very notable observation is the massive drop in the pressure reading as soon as valve V-4 was opened at t = 0 (again, before closing V-3). It was determined that this was due to the expansion effect discussed earlier as a result of opening V-4. However, this was never witnessed when operating at

the base configuration, but only in configurations which included the tank in the reference volume (1-3). This is when the resistance effect disclosed in section 4.2.2 come into play. The expansion effect observed in Fig. 4.12 is ***our underlying proof of the existence of a "resistance effect" due to the non-equalization of the pressure gradient across the reservoir volume during experiment start-up***. The drop is basically indicative of the existence of a pressure gradient across V-3, which instantly recovers as the gradient equalizes.

Another piece of evidence to existence of this resistance effect from the pressure gradient is in the actual decay plot following the closure of V-3. Firstly, the compression effect which is supposed to occur towards the positive axis of the pressure scale isn't visible, which indicates that it is being concealed by none other than an instant decay witnessed after closing V-3. However initially, this decay occurs a ***lot more rapidly*** than the standard decay witnessed at the base configuration below the dotted line in Fig. 4.9 (same conditions). This is due to the non-equalization of the pressure gradient in the reference side of the reservoir due to existence of tanks. The contribution to the more rapid decay witnessed in Fig. 4.12 occurs because DPT at the reference end still detects a rise in pressure.

4.4.2 Correction of Data

As performed in section 4.3.2, the data corrections here are also carried out by utilizing the semi-infinite pressure decay plot. Interestingly enough, this lead to an observation comparable to simulations of the pressure decay response of composite membranes in Chapter 3, section 3.3. Before correction, it is important to discuss the actual observation.

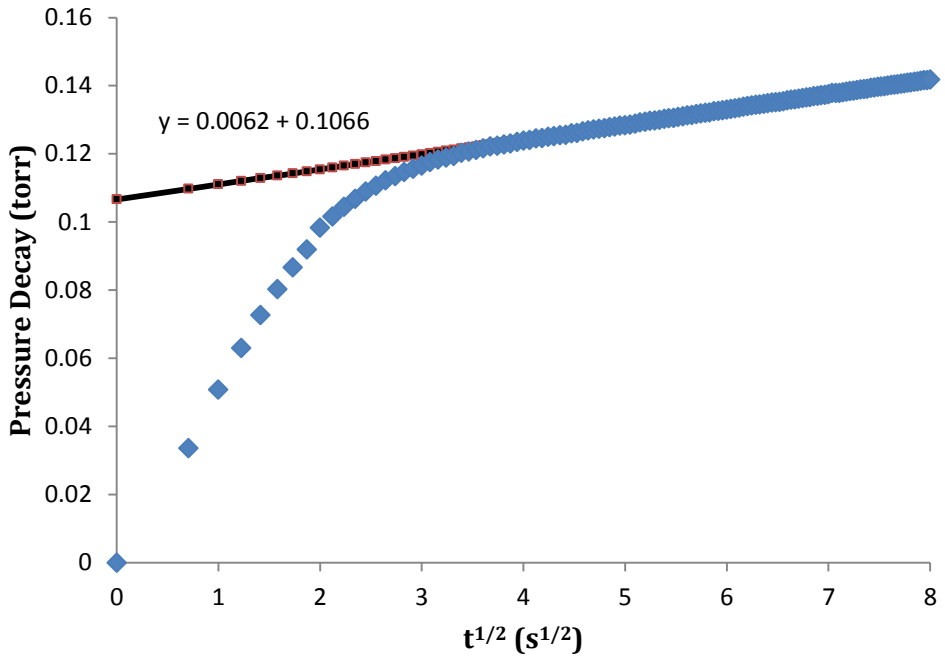

Figure 4.13 Sample of semi-infinite decay plot with tank present in reference volume (after correction)

The behaviour under a semi-infinite decay plot is disclosed in Fig. 4.13 after correction. What's revealed is graph parallel to the graphical representation of a semi-infinite decay plot of a composite membrane system witnessed in Chapter 3. The plot consists of two linear regions, where the latter region represents the short time slope obtained for the actual membrane, ***and the earlier linear region due to the "resistance-effect" is analogous to the presence of a layer of resistance such as a laminate***. It is important to establish that this behaviour is purely coincidental, and by no means describes a concrete way of characterizing the resistance effect. However, it does provide us with an added dimension in terms of quantifying the resistance effect and how it changes under various configurations. This is further analyzed in section 4.5.

As far as corrections are concerned, the intercept of the plot is forced to 0 based on the short time linear slope of the ***initial region*** in the semi-infinite decay plot. The correction this time is negative as opposed to positive for the base case scenario, which is consistent with the *positive* correction applied in the base configuration (Fig. 4.10 & 4.11)

4.5 Discussion

4.5.1 Amplitude and Time Constant of the Resistance Effect

The analysis to be presented is centered on the results obtained in configurations 1-3, since the results obtained in the base configuration (0) have already been disclosed in Chapter 2. It is evident from Fig. 4.13 that the jump contributed by the resistance effect is characterized by two components, which is viewed with respect to approaching the true short time slope of the membrane (region 2). Firstly an amplitude jump ($p_{ref\text{-}0}$) is defined, this corresponds to the maximum pressure difference between the reference and working volumes after separation (resistance based, ***not*** compression). The second component is the time it takes to exhibit a semi-infinite pressure decay of the actual membrane, this is described as a time constant, τ. The two components are calculated by firstly extrapolating the second linear (actual membrane) behaviour in the semi-infinite decay plot to the y-intercept, then calculating the difference between the new linear plot and the observed decay plot. The differences are then plotted as a function of time (not $t^{1/2}$) and fitted to a 1st order exponential function. This is illustrated in Fig. 4.14.

$$p_{ref} = p_{ref-0} \exp\left(-\frac{t}{\tau}\right) \tag{4.1}$$

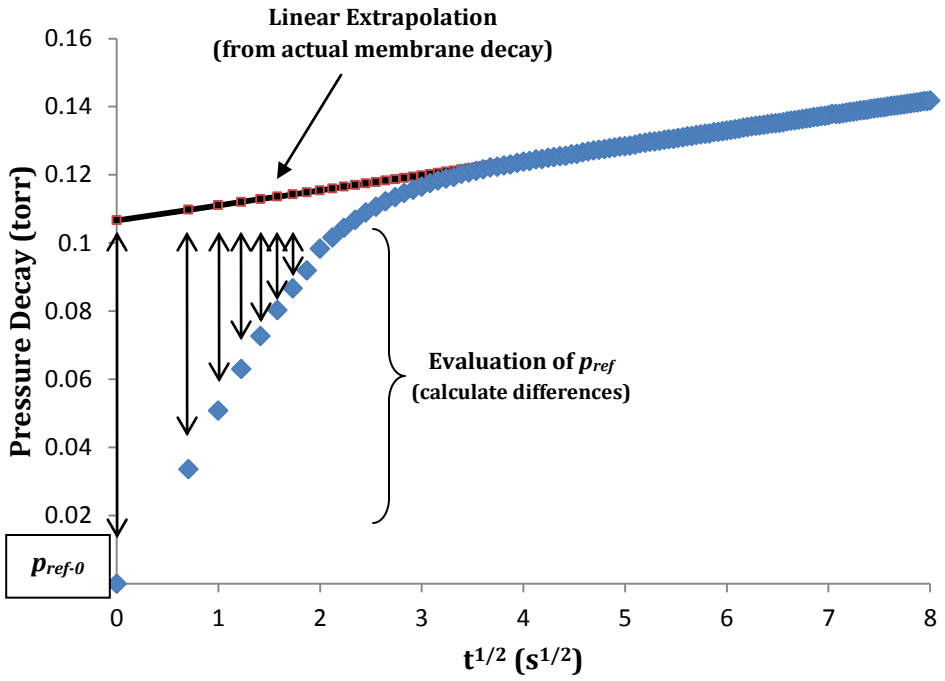

Figure 4.14 Resistance-based semi-infinite decay plots demonstrating how p_{ref} is extracted.

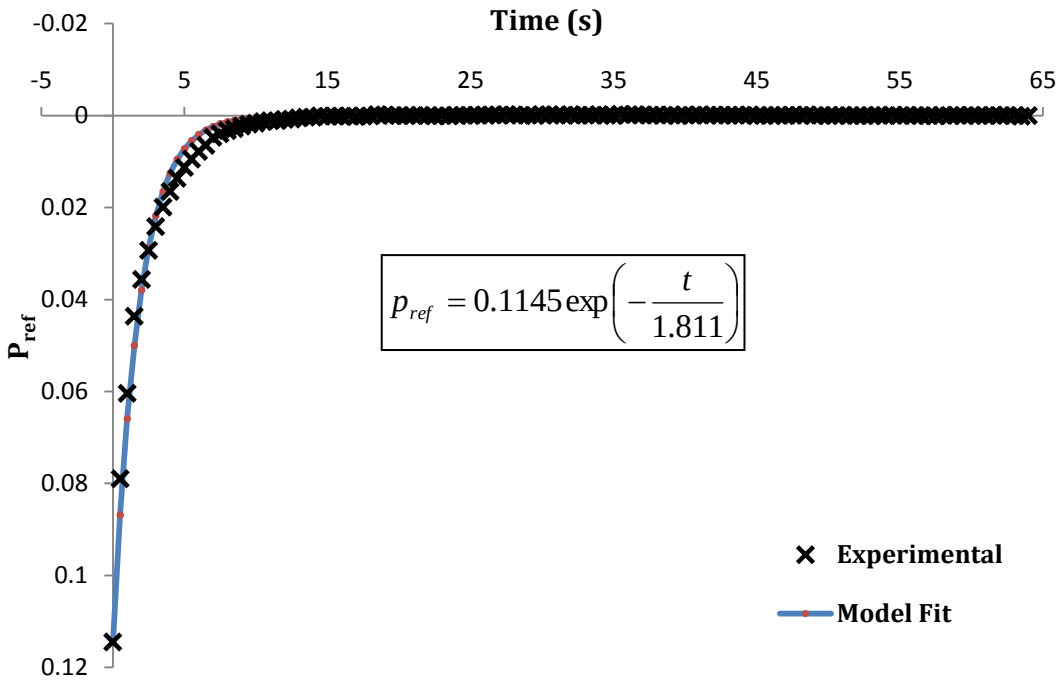

Figure 4.15 Graph presenting the experimental and model based fits for the evaluation of the amplitude (p_{ref}) and time constant (τ)

Acquiring the p_{ref} values with respect to time is visually demonstrated in Fig. 4.14, and then a fit to the exponential model in Eq. 4.1 is done and shown in Fig. 4.15 using the sum of least squares method. This is carried out at an upstream initial pressure of p_{A0} = 3.147 psia, at configurations 1-3. The upstream pressure is fixed, and each configuration is performed 3 times to demonstrate its repeatability. Results are shown in Table 4.5.

Table 4.5 Amplitude (p_{ref}) and time constant (τ) results due to the resistance effect present in the 3 tank-based reference volume configurations.

Configurations	**Eq. (4.1) variables**	**Trial Attempts**		
		First	**Second**	**Third**
Configuration # 1	$\boldsymbol{p_{ref}}$ [torr]	0.1125	0.1112	0.1169
	$\boldsymbol{\tau}$ [s]	1.870	1.848	1.923
Configuration # 2	$\boldsymbol{p_{ref}}$ [torr]	0.1145	0.1166	0.1191
	$\boldsymbol{\tau}$ [s]	1.811	1.826	1.760
Configuration # 3	$\boldsymbol{p_{ref}}$ [torr]	0.0267	0.0233	0.0275
	$\boldsymbol{\tau}$ [s]	2.092	2.138	2.152

An increase in resistance effect is favoured towards a higher p_{ref}, and a lower τ (τ determines the sharpness of the recovery time). In configurations 1 and 2, the amplitude and time constants were very similar to one another. This shows that the placement of the additional tubing with the tank already present configuration 1 yielded an insignificant impact on the resistance. However, when an additional parallel tank was added in configuration 3, the overall resistance was reduced as evident by the lower amplitude and

somewhat higher time constant. This is expected since this gradient originally present in configurations 1 and 2 from the tank towards the direction of the flow was reduced due to the placement of the second tank in-between which contributed to reducing the overall gradient that was established. This is in very good agreement with the analysis performed on the downstream reservoir by Lashkari at al [8].

Firstly, when comparing the individual trials of all configurations, the amplitude and time constants obtained are fairly close to one another, this is a testament to the integrity of the system, and how the observed resistance effects were quite reproducible. The p_{ref} standard deviation in configurations 1 and 2 of σ_1 = 0.00299 and σ_2 = 0.00230, respectively, is slightly higher than the σ_3 = 0.0023 obtained in configuration 3. The reason to this is because the resistance effect was more prominent in configurations 1+2 when compared 3. This is due to the fact that they exhibited a higher initial rate of species decay which is very susceptible to any human errors, and consequently affecting the time loss involved with the "open V-4, close V-3" start-up procedure.

4.5.2 An Approach of Eliminating the Resistance Effect

An enormous degree of errors in the measured upstream time lag was witnessed in configurations 1-3 (θ_u = -300 to -700 s), specifically when compared to well-established downstream time lag (θ_u = 65 s), which severely inconsistent with the expected $\theta_u = -2\theta_d$.

As Illustrated in Fig. 4.13, the actual short time profile of the membrane was revealed in the second linear region of the plot, which was extrapolated to the y-intercept. This section will briefly go through the observations obtained when the extrapolated

section of the plot replaces the actual resistance based behaviour, and having the intercept shifted towards 0 to truly represent the actual short time semi-infinite behaviour of the membrane. The plot is then re-mapped towards the standards pressure decay time scale and the upstream time lag was estimated (θ_u).

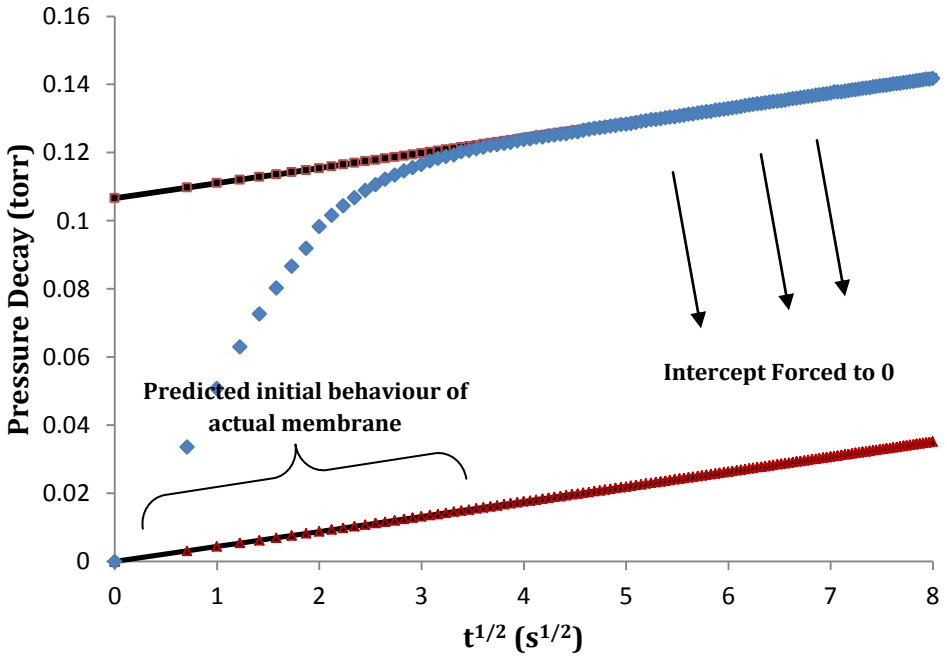

Figure 4.16 Graph presenting the experimental and model based fits for the evaluation of the amplitude (p_{ref}) and time constant (τ)

As mentioned before, the profile is converted back to the standard decay behaviour, and the upstream time lag is subsequently measured. This should considerably reduce the magnitude of the overly-estimated upstream time lags. Results are presented in Table 4.6 below which includes the measured time lag in the downstream reservoir. To serve as a remainder, the upstream time lag should result in double the magnitude of the downstream time lag ($\theta_u = -2\theta_d$). This was revealed in earlier in Chapter 1.

Table 4.6 Measured upstream time lags under the various configurations after eliminating the resistance effect. Downstream time lags are included for comparison purposes

Configurations	Time Lags θ [s]	Trial Attempts		
		First	Second	Third
Configuration # 1	θ_u	-144.2	-138.2	-145.7
	θ_d	65.4	65.4	66.1
Configuration # 2	θ_u	-148.4	-147.3	-156.0
	θ_d	65.8	66.7	65.3
Configuration # 3	θ_u	-133.6	-140.5	-138.1
	θ_d	65.1	65.3	64.9

Table 4.7 Measured upstream and downstream time lags under the base configuration only

Configurations	Time Lags θ [s]	Trial Attempts		
		First	Second	Third
Configuration # 0	θ_u	-145.8	-144.7	-140.5
	θ_d	65.3	66.2	65.3

When comparing the downstream time lags throughout all configurations, results were fairly consistent at around θ_d = 65 s, which is expected since the employed design is and has been fairly reliable in the past [3, 4, 8]. After correction, the upstream time lags (θ_u) in configurations 1-3 are revealed to be slightly higher than the expected $\theta_u = -2\theta_d$.

Interestingly enough, these corrected upstream time lags from the resistance-based configurations (1-3) (Table 4.6) are in very good agreement with the measured time lags associated with the base configuration (0) (Table 4.7) which is assumed to being resistance-free. So in conclusion, based on the current system design, the upstream time lag is in general: slightly over-estimated regardless of the configuration of the reference volume. Note that the issue at hand was briefly discussed in Chapter 2 while operating under the tubing-only (base) configuration.

This perhaps could be attributed to additional resistance effects present in the working volume; which is somewhat affected by the expansion-effect from opening V-4. It could also bring rise to the possibility that the boundary condition at the upstream face of the membrane is not in fact a direct step-change as currently assumed by the predicted models in this project. In a study conducted by Favre et al. [10], the affect of a non-instantaneous step change from the upstream pressure on the permeation of organic vapours in PDMS membranes was performed. The implications it had on downstream time lag was assessed to being subjected to major errors. The design of the upstream reservoir was not disclosed; however the author did recommend considerably reducing the volume of the upstream volume, which could imply that the tanks were possibly involved in their design.

Collectively, the upstream time lags in Tables 4.6 & 4.7 did yield a greater range of errors than their downstream counterparts. This is mainly due to the fact that the constant volume design of downstream is generally well agreed upon, and has been conducted a multitude of times in the past, hence it is well-equipped. On the other hand, the upstream

reservoir is newly-designed and still at its infancy, which is still expected to undergo numerous more iterations before it can provide us with more polished results. Finally, sample trials of the pressure decay on all four configurations are displayed in Fig. 4.17.

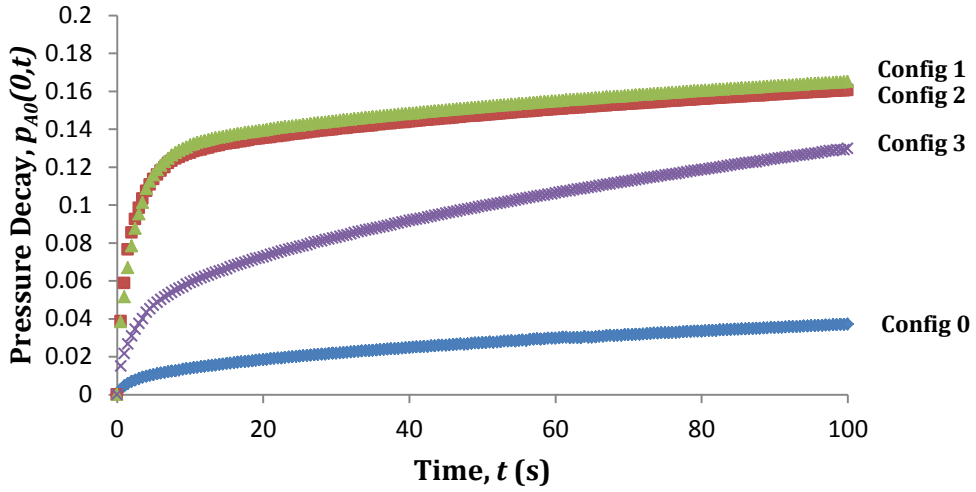

Figure 4.17 Pressure decay plots on configurations 0-4

4.5.3 Quantifying the Resistance effects as an 'Imaginary Membrane'

Section 4.4 previously revealed that the pressure decay of the resistance-based configurations (1-3) in a semi-infinite plot (Fig. 4.13) was very similar to what was exhibited in a composite membrane system if the upstream was laminated with a layer of higher permeability (Chapter 3, section 3.3). This section would attempt to characterize the resistance effect by adopting it as an 'imaginary membrane' of higher normalized permeability (P/l), or in other words; lower resistance. This is done by comparing the two slopes of the semi-infinite decay plot as the resistances transition from one another. Also, the imaginary thickness and permeability of this imaginary laminate is evaluated. Results are revealed in Table 4.8.

Table 4.8 Measured upstream time lags under the various configurations after eliminating the resistance effect. Downstream time lags are included for comparison purposes

Configurations	Trials	Estimated Resistance Parameters					
		m_1	m_2	m_1/m_2	l_1^2/D_1 [s]	l_1 [cm]	D_1 [cm2/s]
Configuration # 1	***Trial #1***	0.0457	0.00392	11.66	1.96	0.0053	1.43×10^{-5}
	Trial #2	0.0472	0.00420	11.24	1.88	0.0047	1.18×10^{-5}
	Trial #3	0.0449	0.00371	12.09	2.13	0.0041	7.89×10^{-5}
Configuration # 2	***Trial #1***	0.0397	0.00336	11.81	2.01	0.0050	1.24×10^{-5}
	Trial #2	0.0404	0.00344	11.75	2.06	0.0055	1.48×10^{-5}
	Trial #3	0.0441	0.00386	11.42	1.92	0.0049	1.25×10^{-5}
Configuration # 3	***Trial #1***	0.0288	0.0129	2.225	1.10	0.0051	2.36×10^{-7}
	Trial #2	0.0216	0.0103	2.107	1.09	0.00049	2.20×10^{-7}
	Trial #3	0.0213	0.0099	2.148	0.93	0.00045	2.18×10^{-7}

The values m_1 and m_2 correspond to the short time slope of the imaginary and actual membranes, respectively, which were evaluated from the semi-infinite decay plot.

$$m = \frac{2 p_{A0} S_A RTA\sqrt{D_A}}{V_u \sqrt{\pi}} \tag{4.2}$$

When comparing the ratio of the two slopes, it can be narrowed down to the following,

$$m_1 / m_2 = \frac{\frac{S_1 A_{img} \sqrt{D_1}}{V_{im}}}{\frac{S_2 A \sqrt{D_2}}{V_{working}}} = \left(\frac{A}{V_{working}} \right) \left(\frac{A_{im}}{V_{im}} \right) \frac{\sqrt{D_1}}{S_2 \sqrt{D_2}} \tag{4.3}$$

In the slope due to the resistance effect (m_1), the full extent of the contribution from the membrane area (A) and reservoir volumes (V_u) is unknown. To a certain degree, it may include volumes of both working and reference compartments, the area may also account for the tubing cross-sectional. Therefore, the ratio may not hold much of a practical meaning as far as permeation properties are concerned, but it serves as a useful tool for examining the repeatability in the obtained decay plots between the membrane and resistance effects.

In configuration 3, the actual slope of actual membrane (m_2) however is higher than what was evaluated in configurations 1-3. This could be attributed to that fact that the short time ratio of the two resistances (m_1/m_2) is significantly lower, and hence impacted the short time slope of the actual membrane. Although it's difficult to justify the reason from such behaviour, this does however confirm what was witnessed in the case of a

simulated composite membrane (low permeability ratios). This is referenced in the end of section 3.3, Chapter 3.

Resistances are quantified as l^2/D. The values in Table 4.8 are obtained via a data-fitting procedure with a composite membrane simulator constructed in Chapter 5. For ease of the operation, l_2^2/D_2 from the known membrane is inputted with actual known values of l_2 = 0.0042 cm and D_2 = 4.5E-8 cm^2/s, hence l_2^2/D_2 = 392 s. A sensitivity analysis was performed on simulator to provide us with a semi-empirical formula for estimating the upstream time lag in a two membrane composite system.

$$\theta_{(u)12} = \frac{\left(l_1^2 + l_2^2\right)\left(\frac{l_1}{D_1^2} + \frac{l_2}{D_2^2}\right)}{\frac{3}{2}\left(\frac{l_1}{D_1} + \frac{l_2}{D_2}\right)} \tag{4.4}$$

Eq. (4.4) is only applicable for cases where D_1, l_1, D_2, $l_2 > 0$.

As expected, the resistances from the imaginary membrane shown in Table 4.8 are considerably lower than that of the actual membrane (l_2^2/D_2 = 392 s), with the value being considerably repeatable since data fitting procedures are generally less error-prone [11]. Configuration 3 exhibited lesser resistance, which is in accordance with the observations done in section 4.51.

4.6 Improvements

Considering what was discussed thus far, it is obvious that the current design is far from perfect, with many notable complications such as the expansion/compression effects and effect from the closure of valve V-3.

The largest issue contributing to the problems in the system lies within the limitations of the differential pressure transducer DPT, since the compression and expansion effects directly influence the readings obtained from it. This is easily tackled by swapping the transducer with one of a lower accuracy and higher pressure range. This would assist in the operation of the system by significantly relaxing the numerous constraints it currently persists. For instance, in the case of operating under the base configuration for the permeation of N_2 in PPO membranes, we are unable to progress to steady state conditions beyond p_{A0} = 3.4 psia because higher pressures would: 1- Amplify the compression effect, hence further limiting the remaining time frame for measuring the pressure decay before making it to -0.2 torr (Fig. 4.9); 2- Higher pressures would also increase the rate of pressure decay, further limiting the range of operation. Therefore, increasing the range of operation in exchange for a lower accuracy (0.00001 torr → 0.0001 torr) is a very reasonable trade-off, as the impact imposed from the compression effect is condensed.

Another desirable improvement from the system design would be eliminating the "open V-4, close V-3" procedure, as it would be preferable to execute the start-up by simply opening V-4 with V-3 initially left close. To do this, the expansion effect would need to be absorbed in order to continue the decay measurements without exceeding the transducer

range. This is carried out by reducing the $(V_{dead}+V_{tube\text{-}exp})/V_1$ ratio, a suggested scheme to this is:

1. Reduce the $(V_{tube\text{-}exp} + V_{dead})$ volume by either reducing the length of tubing after V-4. Another way is decreasing the dead volume with the placement of a 'filler volume' to occupy the base of the membrane cell. The filler volume material will need to be stainless steel so that it doesn't absorb the species being tested.
2. Increase the V_1 volume. In order to achieve a noteworthy impact in this regard, the volume will need to increase considerably, this is best achieved with the placement of a tank (as an added volume) as close as possible to V-4. However, it was discussed earlier that the presence of the tank would bring rise to the resistance effect, but it's also important to note that the positioning of the tank and transducer *also* plays a role towards the impact of the resistance effect. An optimization of these two variables will therefore need to be carried out to yield the best results.

However, most of recommended improvements have their set of issues that co-exist. For instance, increasing the volume V_1 or utilizing a lower accuracy transducer would compromise the sensitivity of decay measurements. Also, reducing the $(V_{tube\text{-}exp} + V_{dead})$ would realistically have little impact on the expansion effect. This is because its volume will need to be reduced by such a large extent for it to be observed on the pressure transducer. The ratio described below (Eq. (4.5)) is the minimum that needs to be achieved in order to salvage at least a few seconds of the pressure decay, not accounting for achieving steady state conditions. So in conclusion, the recommendations provided, although useful in some ways, also have their own limitations.

$$\frac{\left(V_{tube-\exp}+V_{dead}\right)}{V_1-\left(V_{tube-\exp}+V_{dead}\right)} < \frac{\Delta p_{\max}}{p_{A0}} \quad (4.5)$$

where Δp_{max} is the maximum range of the differential pressure transducer.

It is very important to establish that ***the driving force to the resistance effect is the expansion process resulted in opening V-4***. With this issue primarily tackled, not only does it provide an ease to the operation of the system, but also helps eliminate the various problems that are conducive to its existence.

4.7 Conclusion

The thesis at hand is centered on the utilization of a novel scheme for the faster determination of membrane properties; this was disclosed earlier in Chapter 2. A chief component of this scheme involves the design of the upstream reservoir for the measurement of the pressure decay due to permeation.

The current chapter embarked on an in-depth analysis behind the construction of the reservoir. The backdrop behind its operation employs a concept of a two volume reservoir, which are simultaneously supplied by the tested gas at uniform pressure. After separating the two volumes, the decay is then measured by monitoring the pressure between them as one volume is exposed to the membrane during permeation.

For the purposes of measuring the pressure decay, the concept behind the design of the upstream is new, unconventional, and most importantly unpolished. During data

collection, a few problems were encountered such as the expansion effect, compression effect, and more notably the 'resistance effect'. Application of conventional methods for measuring the diffusivity (time lag) is based on the assumption that pressure accumulation is uniform throughout the downstream volume. In previous publications [3, 4, 8], it was revealed that a non-uniform accumulation lead to major errors in estimating the diffusivity. This is encouraged by the combined used of tubes and tanks in the downstream reservoir.

Such errors on pressure response curves were exactly witnessed when the upstream reservoir was also configured in such a manner, hence the 'resistance effect'. To analyze this effect, the architecture of the reservoir was varied into four different configurations. A "base" configuration which involves a tubing-only design resulted in the best depiction of the pressure decay; this was in good agreement with the resistance-based behaviour previously analyzed in the downstream [3]. Alternating between the other three configurations also yielded a trend conducive to the expected magnitude of the resistance effects. On the semi-infinite pressure decay plot, the resistance effect was coincidentally witnessed to mimic the behaviour of the membrane if it were laminated (lower resistance) in the upstream face. The resistance effect was therefore quantified as a layer of added resistance in series with the membrane, basically acting as an 'imaginary membrane'. The imaginary membrane was characterized, and yielded resistance properties that were in trend with the actual impact of the resistance effect.

Finally, all tests were performed multiple times at the same pressure. Results revealed that the pressure decay response curves and the resistance effects were fairly

reproducible. This is a testament to the credibility of the early design of the system, and reveals the potential it possesses for any future improvements.

Nomenclature

D_1:	Diffusivity of imaginary membrane contributing to resistance (cm^2/s)
D_2:	Diffusivity of actual working membrane (cm^2/s)
l_1:	Thickness of imaginary membrane contributing to resistance (cm)
l_2:	Thickness of actual working membrane (cm)
m_1:	Short time slope of imaginary membrane from resistance ($torr/s^{1/2}$)
m_2:	Short time slope of actual working membrane ($torr/s^{1/2}$)
p_{A0}:	Initial upstream feed pressure (psia)
p_{ref}:	Reference volume pressure difference due to gradient (torr)
p_{ref-0}:	Starting reference volume pressure difference due to gradient (torr)
t:	Time (s)
τ:	Time constant of resistance effect (s)
θ_u:	Upstream time lag (s)
$\theta_{(u12)}$:	Upstream time lag of composite membrane system(s)

θ_d: Downstream time lag (s)

V_1: Upstream working volume (cm^3)

V_{dead}: Membrane cell base chamber volume (cm^3)

V_{ref}: Upstream reference volume (cm^3)

$V_{tube\text{-}exp}$: Tubing volume enclosed between V-4, V-5, and membrane cell (cm^3)

$V_{working}$: Upstream working volume (cm^3)

References

[1] H.A. Daynes, The process of diffusion through a rubber membrane, Proc. R. Soc. London Ser. A 97 (685) (1920) 286–307.

[2] T. Al-Ati, J. Garza, J.H. Hotchkiss, Simple Universal Permeation Apparatus, Packag. Technol. Sci. 16 (2003) 249–257

[3] S. Lashkari, B. Kruczek, H.L. Frisch, General solution for the time lag of a single tank receiver in the Knudsen flow regime and its implications for the receiver's configuration, J. Membr. Sci. 283 (2006) 88–101.

[4] S. Lashkari, B. Kruczek, Effect of resistance to gas accumulation in multi-tank receivers on membrane characterization by the time lag method. Analytical approach for optimization of the receiver, J. Membr. Sci. 360 (2010) 442–453.

[5] A. Tabe-Mohammadi, T. Matsuura, S. Sourirajan, Design and construction of gas permeation system for the measurement of low permeation rates and permeate compositions, J. Membr. Sci. 98 (3) (1995) 281–286.

[6] E.B. Arkilic, K.S. Breuer, M.A. Schmidt, Gaseous slip flow in long microchannels, Microelectromechanical Systems 6 (1997) 167-178.

[7] S.A. Stern, P.J. Gareis, T.F. Sinclair, P.H. Mohr, Performance of a versatile variable-volume permeability cell. Comparison of gas permeability measurements by variable-volume and variable-pressure methods, J. Appl. Polym. Sci. 7 (1963) 2035-2051

[8] B. Kruczek, F. Shemshaki, S. Lashkari, R. Chapanian, H.L. Frisch, Effect of a resistance-free tank on the resistance to gas transport in high vacuum tube, J. Mem. Sci. 280 (2006) 29-36

[9] J.M. Slaughter, W.P. Pratt, P.A. Schroeder, Fabrication of layered metallic systems for perpendicular resistance measurements, R. Sci. Instr. , 60 (1989) 127-131

[10] E. Favre, N. Morliere, D. Riozard, Experimental evidence and implications of an imperfect upstream pressure step for the time-lag technique, J. Mem. Sci., 207 (2002) 59-72

[11] M. H. Montgomer, D. Odonoghue, A derivation of the errors for least squares fitting to time series data, Del. Sc. St. News., 13 (1999) 28-32

CHAPTER 5

NUMERICAL MODELLING OF A TWO RESERVOIR GAS MEMBRANE PERMEATION SYSTEM

When observing the transient permeation rates in thin polymer films, it is useful to be able to replicate that behaviour using its mathematical models. In Chapters 2 and 3, a set of reliable analytical formulas derived from first principles were used to simulate the permeation rates, and acted as a prerequisite for the development of the short cut method.

Unfortunately, the capabilities of analytical formulas are limited to specific predefined boundary conditions and flow geometry. Derivation of formulas in the cases of non-constant diffusion coefficient and composite slab formations is rather difficult to accomplish. For instance, as presented in Chapter 3, the resistance behaviour observed in the pressure decay profile closely mimics the case of a composite membrane system. Hence, it is useful to be able to restore that behaviour computationally.

The primary objective of this chapter is to serve as a guide for constructing an alternative numerical model for the gas permeation system. The foundations of the model will be presented, which would serve as a base case for a general type of constant volume system, and can easily be subjected to any modification of geometry, boundary conditions, or penetrant-polymer interactions. Also, a compatibility analysis will be performed to analyse the model's agreement with experimental results.

5.1 Model Construction

5.1.1 Introduction

This section covers the key aspects and steps when it comes to numerically modelling the basics of gas permeation behaviour; this is based on the CV system centered on this thesis.

The backbone of evaluating the permeation rates in a constant volume system lies in defining the behaviour of the permeating species within the polymer membranes. This is carried out by calculating the concentration profile using the finite-differences (FD) numerical method. This is done by discretizing a continuous problem domain defined by partial differential equations, into a finite-difference mesh.

Having defined the FD behaviour, key features such as monitoring the transient flux and pressure profiles are discussed. Also, additional considerations such diffusivities exhibiting concentration dependence and composite membrane systems are brought to light.

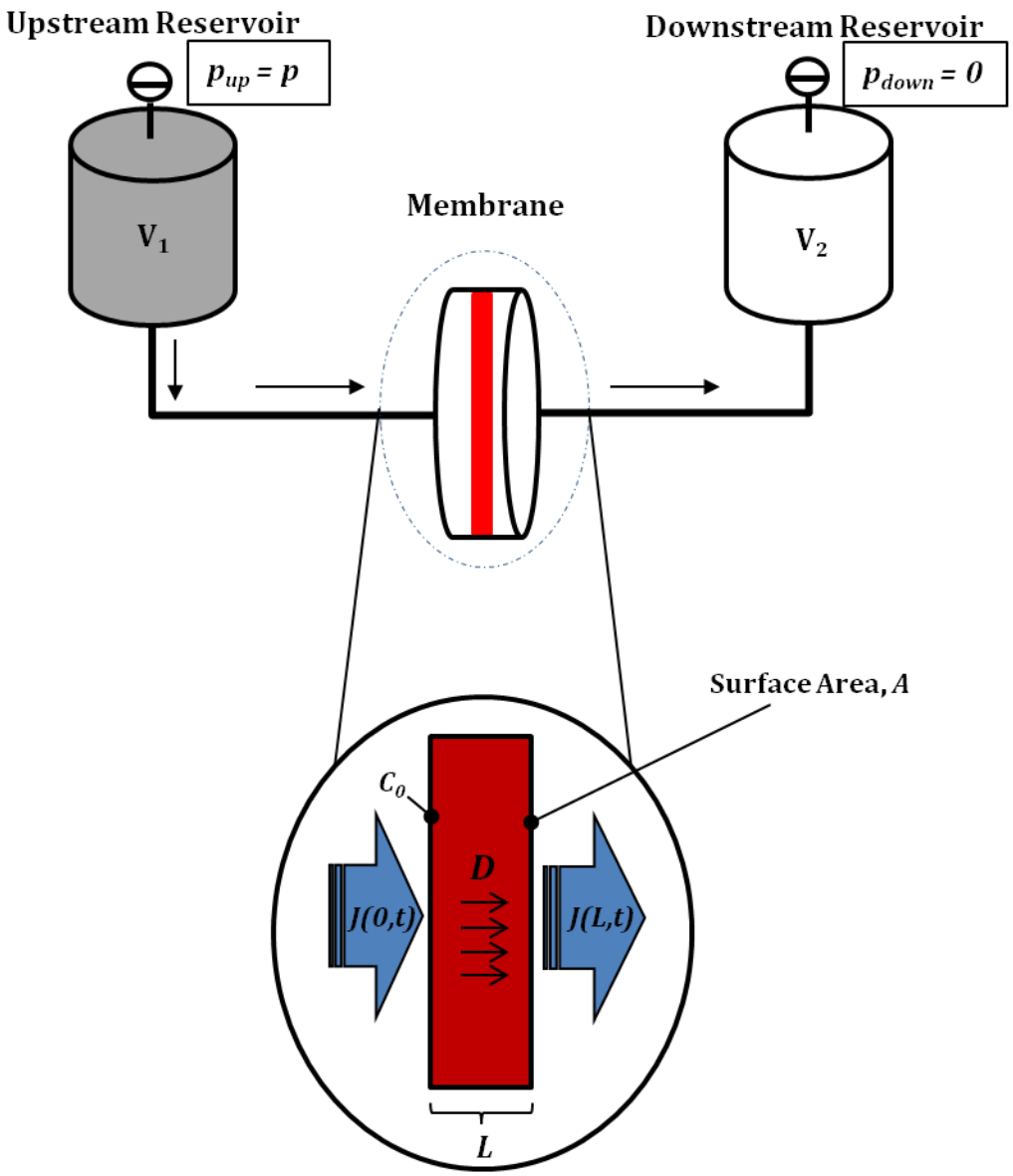

Figure 5.1 General representation of a two-reservoir constant volume system for testing the permeation rates.

Assumptions:

I. 1-D diffusion

II. Isothermal operation

III. Negligible resistance of gas diffusion within reservoir volumes

IV. Pressure accumulation on the downstream end is negligible in comparison to the absolute pressure on the upstream reservoir

V. Negligible leak rates on both upstream/downstream reservoirs

5.1.2 Finite Differences

The space-time transport behaviour in a membrane is governed by Fick's 2nd Law of diffusion.

$$\frac{\partial C}{\partial t} = D\frac{\partial^2 C}{\partial x^2} \tag{5.1}$$

This therefore predicts how the diffusion (D) causes the concentration (C) to change with time (t) and space (x). In a nutshell, finite-differences (FD) is used to numerically solve parabolic partial differential equations by treating the entirety of the space-time domain as a multi-dimensional grid of discrete points. By applying a Taylor's series expansion for the 2nd derivative in space, a discretized form by a centered finite-divided difference is revealed

$$D\frac{\partial^2 C}{\partial x^2} \approx D\frac{C_{i-1}^t - 2C_i^t + C_{i+1}^t}{\Delta x^2} \tag{5.2}$$

The entire space is defined by a membrane thickness (L), where it is divided into multiple k regions of size Δx, and 'i' governs its positioning in space.

Similarly, a forward finite-divided difference is used to approximate the time derivative.

$$\frac{\partial C}{\partial t} = \frac{C_i^t - C_i^{t-1}}{\Delta t} \tag{5.3}$$

Where simulations would be carried out over a defined time period (Γ), also divided into multiple *n* time blocks of size Δt. The *subscript 't'* defines the position of the discrete point in the time domain.

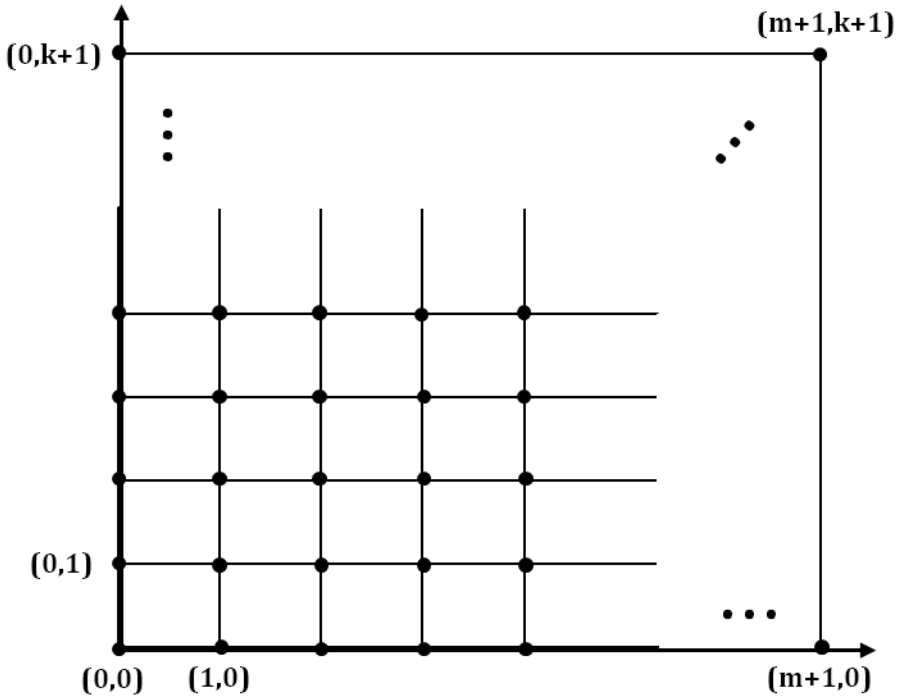

Figure 5.2 Illustration of the finite differences cmesh. The x-axis is progression in the time domain, while the y-axis is for the space domain.

A visual representation of the space-time grid is shown in Fig. 5.2 [1], where each finitely divided region is defined by its corresponding node. As mentioned earlier,

subscripts and superscripts are used to indicate a selected node based on its space and time, respectively.

By performing a mass balance across each interior node, the discretized form from Eq. (5.2) and (5.3) yields the following.

$$\frac{C_i^t - C_i^{t-1}}{\Delta t} = D\frac{C_{i-1}^t - 2C_i^t + C_{i+1}^t}{\Delta x^2} \tag{5.4}$$

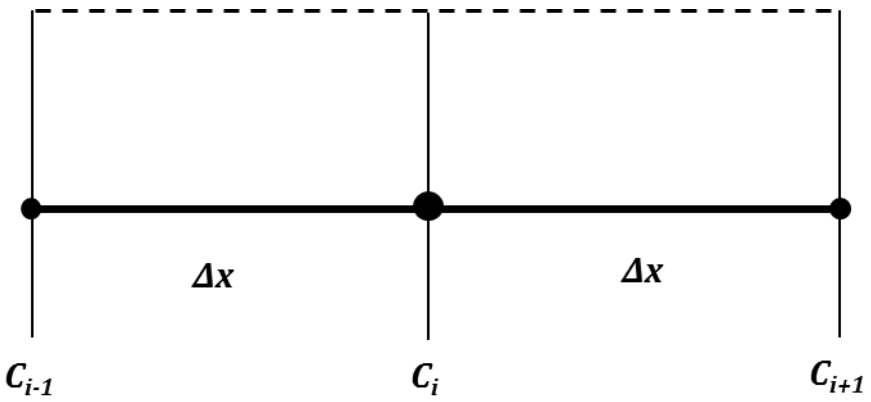

The membrane boundary conditions in a CV system are as follows,

$$\begin{aligned} C(x,0) &= C_{Ai} \approx 0 \\ C(0,t) &= C_{A0} \\ C(L,t) &= C_{AL} \approx 0 \end{aligned} \tag{5.5}$$

Which are accounted for in the exterior nodes of the finite difference domain:

$$C_i^0 = 0 \qquad \forall x \tag{5.6}$$

$$C_0^t = C_{A0} \qquad \forall t \tag{5.7}$$

$$C_{k+1}^t = 0 \qquad \forall t \tag{5.8}$$

The system in modelled by simultaneously solving a linear set of equations (Eq. (5.4)) based on each node. The resulting is a tri-diagonal matrix which may be solved for using the Thomas Algorithm or classical Gaussian Elimination. In dealing with parabolic PDEs, one must consider changes in time. The result is a FD grid that is temporarily open-ended, since not all relevant dimensions (for this case - time), is explicitly bounded. Solutions to these equations brings rise to a number of issues, notably stability [2]. This is also evident in cases of non-constant diffusion coefficient (*D(C)*). In systems of non-constant diffusivity, stability is maintained provided that

$$\frac{D\Delta t}{\Delta x^2} \leq 0.5$$

In systems of reasonable stability, an explicit form of the FD equation is defined as:

$$C_i^t\left(1+\frac{2D\Delta t}{\Delta x^2}\right)-\frac{D\Delta t}{\Delta x^2}C_{i-1}^t+\frac{D\Delta t}{\Delta x^2}C_{i+1}^t=C_i^{t-1} \tag{5.9}$$

In unstable systems, an implicit form is defined

$$C_i^{t+1}\left(1+\frac{2D\Delta t}{\Delta x^2}\right)-\frac{D\Delta t}{\Delta x^2}C_{i-1}^{t+1}+\frac{D\Delta t}{\Delta x^2}C_{i+1}^{t+1}=C_i^t \tag{5.10}$$

Patankar (1978)[3] has proposed a scheme which combines the advantages of both methods and shares the disadvantages of neither, known as the exponential scheme, which happens to be partially implicit. He stated that for every transient parabolic system, there exists a value for *f* which yields an exact solution.

$$f=\left(1-\exp\left(\frac{-D\Delta t}{\Delta x^2}\right)\right)^2-\frac{\Delta x^2}{D\Delta t} \tag{5.11}$$

In terms of the generalized form of the FD equation, the result is

$$C_i^{t+1}\left(1+\frac{2D\Delta t}{\Delta x^2}\right)-\frac{D\Delta t}{\Delta x^2}C_{i-1}^{t+1}+\frac{D\Delta t}{\Delta x^2}C_{i+1}^{t+1}=\left(\frac{1-f}{f}\right)\left(-C_i^t\left(1+\frac{2D\Delta t}{\Delta x^2}\right)+\frac{D\Delta t}{\Delta x^2}C_{i-1}^t-\frac{D\Delta t}{\Delta x^2}C_{i+1}^t\right) \quad (5.12)$$

5.1.3 Concentration Dependant Diffusion Coefficient

When it comes to diffusion through polymer films, there exist cases when diffusivity exhibits a strong dependence to the concentration of the penetrating species. An example is a swelling-induced "plasticization effect" where the penetrating species causes molecules present in the polymer media to re-arrange towards a more glassy state [4]. A more common case is the existence of a Dual Mode diffusion of the penetrant in glassy polymer membranes.

When the diffusivity is concentration dependant, Fick's 2nd law of diffusion is re-expressed as follows

$$\frac{\partial C}{\partial t}=\frac{\partial}{\partial x}\left(D\frac{\partial C}{\partial x}\right) \quad (5.13)$$

In form of the modified FD equation provided by Patankar:

$$\frac{C_i^t-C_i^{t-1}}{\Delta t}=\frac{D\left(C_{i-1}^t\right)C_{i-1}^t-2D\left(C_i^t\right)C_i^t+D\left(C_{i+1}^t\right)C_{i+1}^t}{\Delta x^2} \quad (5.14)$$

When writing a computer program to account for non-constant diffusivity, a unique approach to filling the space-time grid is being carried out. An iterative algorithm has been suggested by Patankar (1980) [5], where the system is solved for with an initial value of the

diffusion coefficient. After obtaining the concentration at various points, the system is solved for again based on the newly calculated diffusion coefficient evaluated from the concentrations in the previous run. This is done until convergence is met.

5.1.4 Modelling Dual Mode Diffusion

In the diffusion through glassy polymer membranes, there exist cases of non-linear sorption of the penetrating species in the polymer matrix. As a result, the solubility deviates from the linear behaviour described by Henry's Law (Eq. (5.15)) under higher pressures as it approaches condensability. Dual mode sorption is used to describe such a behaviour, which suggests the presence of 2 sorption sites within the polymer matrix: Henry sites, and Langmuir sites [6]

$$C = S \cdot p \tag{5.15}$$

Where S is the constant solubility - also known as Henry's law constant, and p is the absolute upstream pressure. The concentration is therefore re-defined as the sum produced by the two modes

$$C = C_D + C_H \tag{5.16}$$

$$C = Sp + \frac{C'_H\, bp}{1 + bp} = C_D\left(1 + \frac{K}{1 + (b/S)C_D}\right) \tag{5.17}$$

Where C_H is the Langmuir sites contribution to the total concentration, while b and C'_H are Langmuir sorption parameters. Langmuir sorption is synonymous with the

presence of semi-permanent gaps (defects) within the stiff chains of the polymer matrix, known as Langmuir sites [7]. The diffusivity also works in pairs, where the total flux accounts for the transport contribution of both Henry (D_D) and Langmuir (D_H) sites

$$J = -D_D \frac{dC_D}{dx} - D_H \frac{dC_H}{dx} \tag{5.18}$$

Usually, the mobility of the penetrants within the Langmuir sites is relatively lower than that of the Henry sites. The fraction F is used to describe the ratio of the two diffusivities. So in cases of dual mode sorption with C_H of zero mobility, $F = 0$.

$$F = \frac{D_H}{D_D} \tag{5.19}$$

To postulate the dual mode sorption behaviour in the model, modifications have been applied to the FD equations as suggested by Toi et al (1992) [8]. Fick's 2nd Law is rewritten as

$$\frac{\partial C}{\partial t} = D \frac{\partial^2 C}{\partial x^2} \left[\frac{1 + FK / 1 + ((b/S)C_D)^2}{1 + K / 1 + ((b/S)C_D)^2} \right] \tag{5.20}$$

This serves to modify the form of the diffusion coefficient as concentration dependant.

$$D(C) = D^* \cdot \left[\frac{1 + FK / 1 + ((b/S)C_D)^2}{1 + K / 1 + ((b/S)C_D)^2} \right] \tag{5.21}$$

This consists of a base diffusivity (D^*), and the remainder which acts as a modifier.

It is important to note that the proposed models for dual mode sorption provide a satisfactory dependence of concentration to the solubility coefficients. Unfortunately, recent developments on the phenomenological model do not provide an explicit description of the combined presence of Henry and Langmuir sites [7]. Section 5.2 further elaborates on this matter.

5.1.5 Inflow/Outflow Permeate Flux

Once the entire FD grid is solved for, the flux may be estimated. Like concentration, the permeate flux is also a function of space and time, which is defined using Fick's 1st Law of diffusion

$$J = -D\frac{dC}{dx} \tag{5.22}$$

Consequently, numerical differentiation is generally carried across a single Δx slice in the space domain as shown Fig. 5.3

$$J_{i-1}^{t} = D\frac{C_{i-1}^{t} - C_{i}^{t}}{\Delta x} \tag{5.23}$$

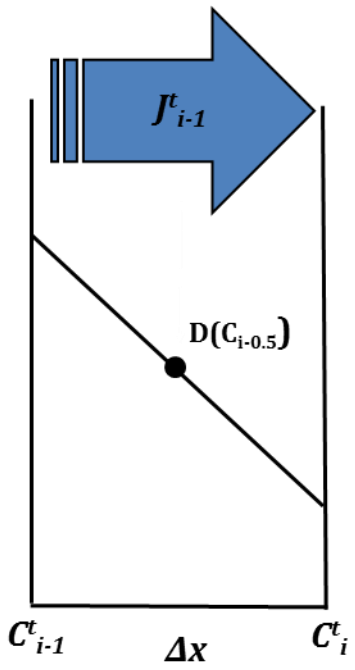

Figure 5.3 Diagram shows a linear concentration profile within a slice of the FD mesh in the space domain. In the case on non-constant diffusivity, *D* is interpolated at the center-point where it acts as an average diffusivity.

In the case of a concentration dependant diffusion coefficient, *D(C)* is estimated as a function of the concentration at the center point of the mesh slice. This based on the assumption that *Δx* is small enough to assume a linear concentration profile, and hence its arithmetic mean is used to predict the average diffusivity.

$$C^t_{i-0.5} = \frac{C^t_{i-1} + C^t_i}{2} \tag{5.24}$$

$$J^t_{i-1} = D\left(C^t_{i-0.5}\right)\frac{C^t_{i-1} - C^t_i}{\Delta x} \tag{5.25}$$

When dealing with dual mode diffusion, which happens to be a function of concentration in the Henry sites, the center point C_D is obtained with the use of Eq. (5.17)

$$J_{i-1}^{t} = D^{*} \cdot \left[\frac{1 + FK \Big/ 1 + \left((b/S) C_{D,i-0.5} \right)^2}{1 + K \Big/ 1 + \left((b/S) C_{D,i-0.5} \right)^2} \right] \frac{C_{i-1}^{t} - C_{i}^{t}}{\Delta x} \tag{5.26}$$

Where $$C_{D,i-0.5} = \frac{1}{2}\left(C_{i-1}^{t} + C_{i}^{t} - \frac{2C'_{H}\, bp}{1+bp} \right) \tag{5.27}$$

At the start of an experiment, the upstream face of the membrane is subjected to a massive step change in concentration. This suggests a high level of continuous activity in the early stages of the upstream face of the membrane. Also, despite the fact that reducing *Δx* segment sizes would serve to reduce any numerical errors, one must consider any computational round-off errors the system may be subjected to as a result of extremely small segment sizes [2]. Such issues may compromise the estimate of the diffusivity when using a simple a first order derivative calculation (Eq. (5.25)). Therefore, a higher accuracy form of the differentiation formula is suggested. This is carried out by retaining more of the earlier terms used in the Taylor series expansion of continuous zero-limit differentiation to a selected order of *m*

$$f'(x_i) = \frac{f(x_{i+1}) - f(x_i)}{\Delta x} - \frac{f''(x_i)\Delta x}{2} + \frac{f'''(x_i)\Delta x^2}{6} - \ldots \frac{f^{m}(x_i)\Delta x^{m-1}}{!m} + O(h^{m}) \tag{5.28}$$

For this case, a 4th order differentiation formula is used to predict the flux on the upstream face of the membrane. Its general form is as follows

$$J_{i-1}^{t} = D(C)\left\{\begin{array}{l} \dfrac{C_{i-1}^{t} - C_{i}^{t}}{\Delta x} - \dfrac{C_{i+1}^{t} - 2C_{i}^{t} + C_{i-1}^{t}}{2\Delta x} \\ + \dfrac{C_{i+2}^{t} - 3C_{i+1}^{t} + 3C_{i}^{t} - C_{i-1}^{t}}{6\Delta x} \\ - \dfrac{C_{i+3}^{t} - 4C_{i+2}^{t} + 6C_{i+1}^{t} - 4C_{i}^{t} + C_{i-1}^{t}}{24\Delta x} \end{array}\right\} \tag{5.29}$$

In an attempt to handle concentration dependency, the format presented in Eq. (5.15) is best applied when dealing with the higher order differentiation formulas within the series. Lastly, due to the slow level of activity occurring on the downstream face of the membrane, a simple first order differentiation formula is used to estimate the flux *J(L,t)*

$$J(L,t) = J_{k}^{t} = D\frac{C_{k}^{t} - C_{k+1}^{t}}{\Delta x} \tag{5.30}$$

5.1.6 Reservoir Pressure Decay and Accumulation

With the ability to model the transient flux behaviour in the upstream/downstream face of the membrane, one is able to estimate the pressure depletion/increase based on the cumulative amount of species transferred across the membrane, over a period of time *t* [9]

$$p(t) = \frac{pSRTA}{C \cdot V}\int_{0}^{t} J(t)dt \tag{5.31}$$

Eq. (5.31) is applicable when dealing with non-porous membranes, where *V* is a reservoir volume, *A* is the membrane surface area, *T* is the operating temperature, and *R* is the ideal gas constant. Numerically, the upstream/downstream transient flux is available as discrete values, where based on position '*i*',

$$J_i(t):\left\{J_i^0, J_i^1, J_i^2, \ldots J_i^n\right\} \tag{5.32}$$

For this case, Eq. (5.32) will be applied using Simpson's Rule of numerical integration [2],

$$\int_a^b f(x)dx = \frac{h}{3}\left[f(x_0) + 2\sum_{j=1}^{n/2-1} f(x_{2j}) + 4\sum_{j=1}^{n/2} f(x_{2j-1}) + f(x_n) \right] \tag{5.33}$$

Although an odd number of finite points serves as a prerequisite in utilizing Simpson's Rule, this may easily be tackled by creating additional values of flux. In a system with *n* number of *Δt* subintervals, and *n+1* number of time points, it is necessary to have *n+1* as an odd number for Simpson's Rule to be applicable. By adding an *n* number of points to the original n+1 number of points (2n+1), one may guarantee an odd total number of points to perform Simpson's Rule of integration. The newly added n values of flux are estimated as arithmetic mean mid-point values within each time interval.

This is carried out in a similar manner as concentration in Eq. (24), by assuming that *Δt* is small enough that the flux profile across it behaves in a linear manner.

$$p(t) = \frac{pSRTA}{C \cdot V}\left(\frac{\Delta t}{6}\right)\left[J_i^0 + 2\left(J_i^{0.5}\right) + 4\left(J_i^1\right) + 2\left(J_i^{1.5}\right) + \ldots + J_i^n\right] \tag{5.34}$$

$$J_i^{i+0.5} = \frac{J_i^i + J_i^{i+1}}{2} \tag{5.35}$$

When applying the pressure estimate in Eq. (34), '*i*' is restricted to positions *0* or *k* only, since it is only applicable adjacent faces of the membrane. Consequently the pressure decay/accumulation is estimated numerically as follows

$$p_{up}(t) = p - \frac{pSRTA}{C \cdot V_1}\left(\frac{\Delta t}{6}\right)\left[J_0^0 + 2\left(J_0^{0.5}\right) + 4\left(J_0^1\right) + 2\left(J_0^{1.5}\right) + \ldots + J_0^n\right] \quad (5.36)$$

$$p_{down}(t) = \frac{pSRTA}{C \cdot V_2}\left(\frac{\Delta t}{6}\right)\left[J_k^0 + 2\left(J_k^{0.5}\right) + 4\left(J_k^1\right) + 2\left(J_k^{1.5}\right) + \ldots + J_k^n\right] \quad (5.37)$$

5.1.7 Modelling a 2 Membrane Composite System

It's useful for the model to be capable of predicting changes in the transient permeation behaviour - when for instance, dealing with laminated membranes. Generally, the following boundary condition is implied within the membrane interface

$$-D_1 \frac{dC}{dx} = -D_2 \frac{dC}{dx} \quad (5.38)$$

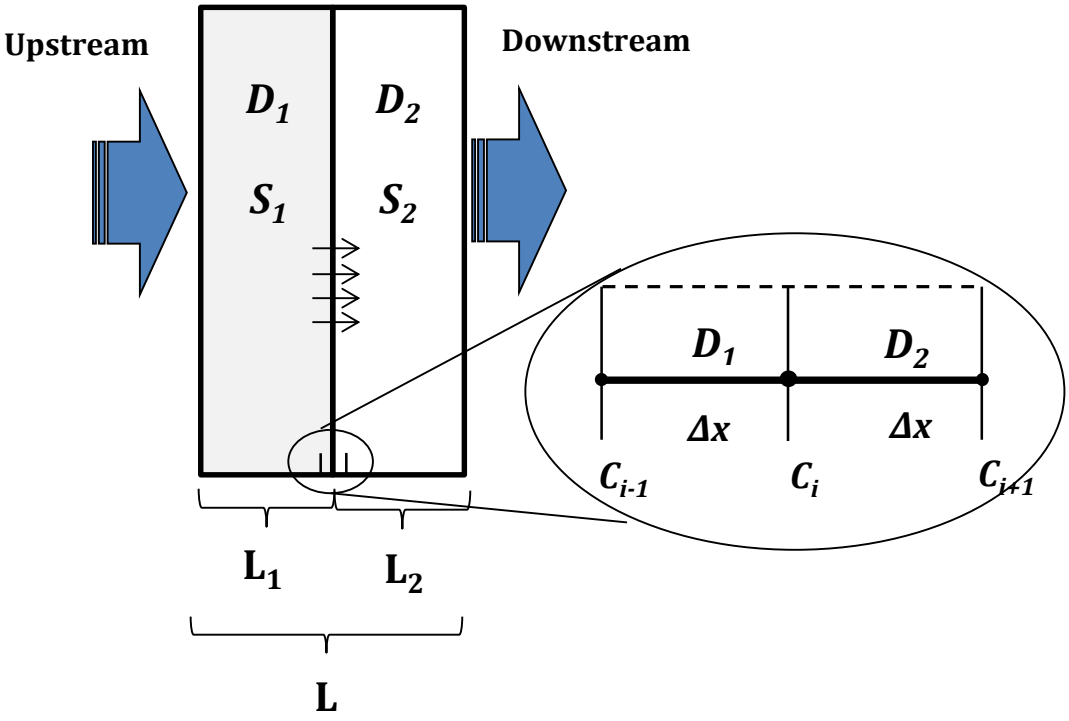

Figure 5.4 Composite slab system of varying properties. The primary modification from the base case of a single membrane is at the interface of the two membranes.

This leads to a slight modification in the FD equation, where the expression remains the same at its core, and only the placement of the corresponding diffusion coefficient is affected. The discretized form of the FD equation across the interface present within two Δx slices is described in Eq. (39), based on the illustration of Fig. 5.4

$$D_1 \frac{C_{i-1}^t - C_i^t}{\Delta x} = D_2 \frac{C_i^t - C_{i+1}^t}{\Delta x} \tag{5.39}$$

Via the code, the program is aware of the presence of the interface ($\Delta x \cdot i \leq L_1$), and the diffusivity is adjusted accordingly each time as it continues to march across the space domain [1].

Recommendations:

For convenience purposes, it's best to design the composite membrane model as a single membrane, which contains the combined individual membrane lengths $L_1 + L_2 = L$. The filling of the FD in the space domain occurs initially using D_1, and when achieving $\Delta x \cdot i > L_1$, the diffusivity in the remaining length (which should correspond to L_2) is modified,

$$D_2 = D_1 \left(\frac{D_2}{D_1} \right) \left(\frac{S_2}{S_1} \right) \tag{5.40}$$

Where S_1 and S_2 are the respective solubilities of membranes 1 and 2, assuming they aren't equivalent. However it is important to note that when applying Eq. (36 & 37) for computing the pressures responses, the solubilities used are based on the membranes exposed to their equivalent reservoir. Therefore, S_1 is used for upstream pressure decay $p_{up}(t)$ and S_2 is used for the downstream pressure accumulation, $p_{down}(t)$.

5.2 Model Validation

With the foundations of the model currently established, this current section will focus on validating its credibility by performing comparisons with some of its main aspects. In detail, a base case (constant *D*) conformity with the provided analytical models for single and composite membranes will be carried out.

As implied at the end of section 5.1.4, concrete methods of validating the dual mode sorption theory may not be entirely possible. The numerical modelling procedure presented in 5.1.4 is based on the paper by Toi et al (1992) [8]. While there exists slightly different forms of the numerical model provided by Kumazawa (1996) [10] and Brolly et al (1996) [11], the preference of Toi's method is due to the fact that it provides the best middle ground in terms of complexity of the model (Kumazawa, 1996), agreement with experimental results, and abidance with our experimental conditions and model assumptions (Brolly at al, 1996). Therefore, validating the dual mode sorption theory won't be attempted in this dissertation.

5.2.1 Base Validation in the Case of Constant Diffusivity

With the use of analytical models developed for estimating the flux and pressure profile in the 2 faces of the membrane (Chapter 2 and Appendix A), they will be compared with the results obtained numerically. This of course goes by the key assumption that *D* and *S* are independent on concentration. The model parameters are as follows:

Table 5.1 Summary of Model Parameters for the Analytical and Numerical Simulations

Analytical and Numerical Parameters	
Run Time, $\boldsymbol{\Gamma}$ [s]	250
Membrane Thickness, $\boldsymbol{L}$ [cm]	0.0042
Operating Pressure, $\boldsymbol{p}$ [psia]	3.372
Operating Temperature, $\boldsymbol{T}$ [K]	298
Membrane Area, $\boldsymbol{A}$ [cm^2]	12.57
Upstream Volume, $\boldsymbol{V_1}$ [cm^3]	77.6
Downstream Volume, $\boldsymbol{V_2}$ [cm^3]	115.1
Diffusion Coefficient, $\boldsymbol{D}$ [cm^2/s]	4.5×10^{-8}
Solubility Coefficient, $\boldsymbol{S}$ [cm^3 (STP) cm^{-3} $cmHg^{-1}$]	0.008444
Numerical Parameters Only	
Number of intervals in the Time Domain, *n*	500
Number of intervals in the Space Domain, *k*	500

Observation of the flux profiles:

The transient flux profiles at both faces of the membrane are calculated numerically, and compared to the solutions obtained using Laplace transforms (Eq. (5.41) & (5.42)),

$$J_A(0,t) = \frac{\sqrt{D}pS}{\sqrt{\pi t}} \sum_{n=0}^{\infty} \left[\exp\left(-\frac{(n+1)^2 L^2}{Dt} \right) + \exp\left(-\frac{L^2 n^2}{Dt} \right) \right] \qquad (5.41)$$

$$J_A(L,t) = \frac{2\sqrt{D}pS}{\sqrt{\pi t}} \sum_{n=0}^{\infty} \exp\left(\frac{-(2n+1)^2 L^2}{4Dt}\right) \tag{5.42}$$

A graphical representation of the 2 profiles under both conditions is illustrated in Fig. 5.5, with the comparisons performed up to a Fourier number of 0.4 where the highest level of transient activity is present. The results show that not only are they in excellent agreement with each other, but the data points yielded an average deviation of 2.4E-6%.

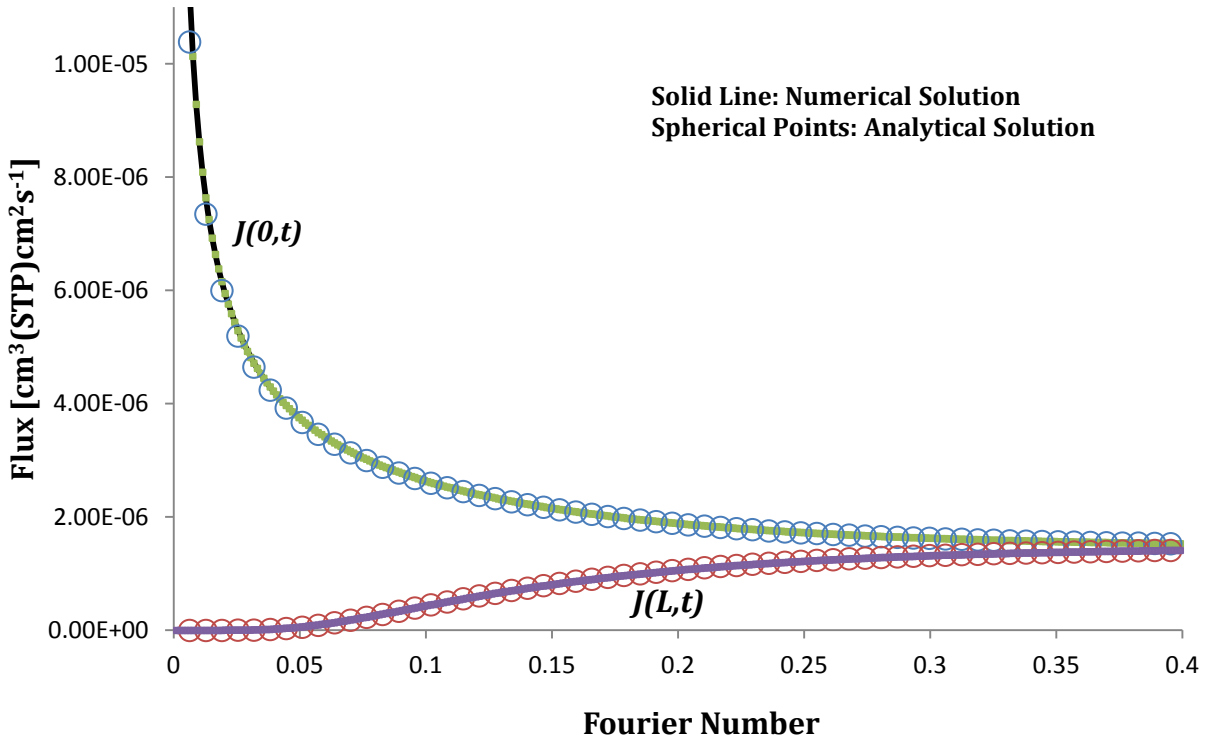

Figure 5.5 Plots illustrating the pair of inflow and outflow flux simulated analytically, and numerically. Used for comparison purposes

Observation of the pressure profiles:

The analytical forms of the pressure profiles upstream and downstream side of the membrane are as follows

$$p_{up} = p - \frac{2pSRTAL}{V_1} \sum_{n=0}^{\infty} \left\{ \begin{array}{l} n \cdot erf\left(\frac{nL}{\sqrt{Dt}}\right) + (n+1) \cdot erf\left(\frac{(n+1)L}{\sqrt{Dt}}\right) - 2n - 1 \\ + \frac{\sqrt{\pi Dt}}{L}\left[\exp\left(\frac{-L^2(n+1)^2}{Dt}\right) + \exp\left(\frac{-L^2 n^2}{Dt}\right)\right] \end{array} \right\} \tag{5.43}$$

$$p_{down} = \frac{2pSRTA\sqrt{D}}{V_2\sqrt{\pi}} \sum_{n=0}^{\infty} \left\{ \begin{array}{l} \left(\frac{(2n+1)\sqrt{\pi}L}{\sqrt{D}}\right) \cdot \left[erf\left(\frac{(2n+1)L}{2\sqrt{Dt}}\right) - 1\right] \\ + 2\sqrt{t}\exp\left(\frac{-(2n+1)^2 L^2}{4Dt}\right) \end{array} \right\} \tag{5.44}$$

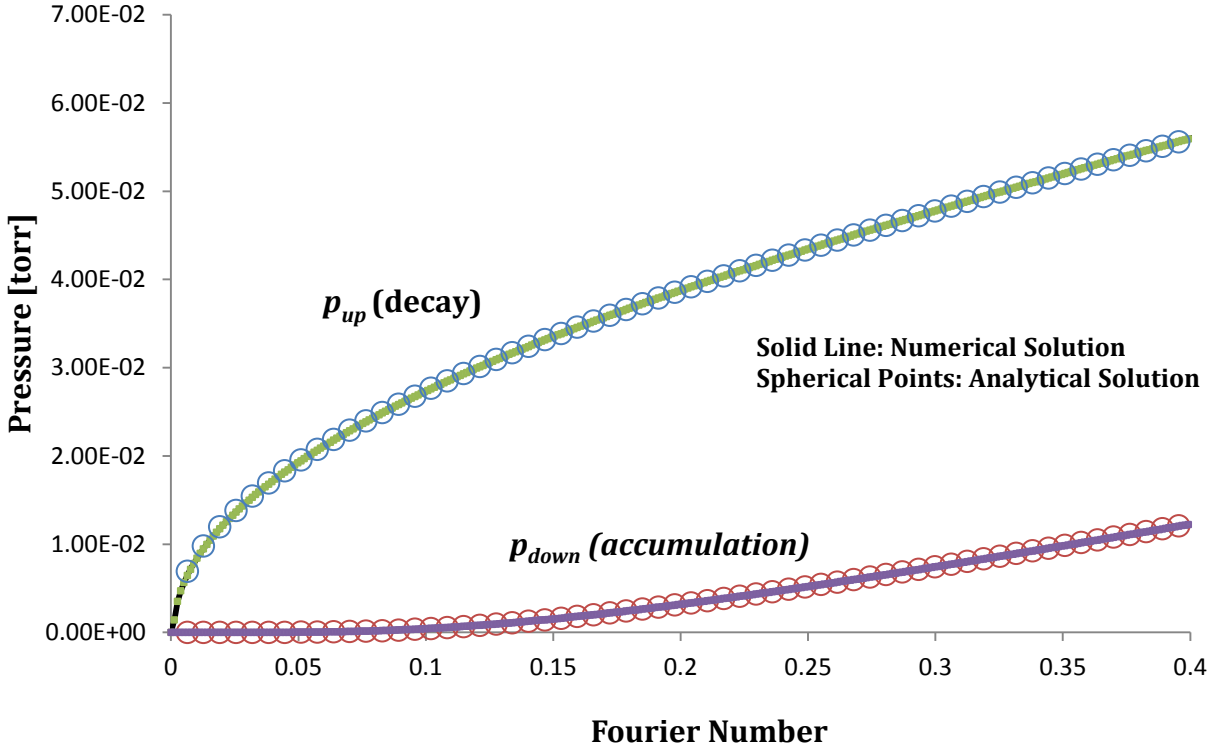

Figure 5.6 Plots illustrating the pair of pressure decay and accumulation simulated analytically, and numerically. Used for comparison purposes

The profiles are again compared graphically in Fig. 5.6, the diffusivities and permeabilities of the numerical solution are recalculated again using the classical time lag

method provided by Daynes (1920) [12], and compared to the actual solution. The actual D and S values are from Table 5.1, while the permeability P is obtained using the solution-diffusion model

$$P = D \cdot S \tag{5.45}$$

Table 5.2 Comparison of actual inputted membrane properties (D and P) to the values extracted using Daynes' time lag method on the numerical solution

	Actual Parameters	**Time Lag Method (Upstream)**	**Time Lag Method (Downstream)**
D [cm^2/s]	4.5×10^{-8}	4.5005×10^{-8}	4.4999×10^{-8}
P [Barrer]	3.198	3.1999	3.1999

The results presented in Table 5.2 and Fig. 5.6 show that the numerical solution is at an excellent agreement with well established analytical formulas for estimating permeation behaviour in the upstream and downstream faces of the membrane.

5.2.2 Time Lag Analysis of Composite Membrane System

In 1963, Ash et al. [13] developed an analytical model for estimating the downstream time lag of a composite membrane system of m layers of unique lengths ($L_1, L_2,...L_m$) and diffusion ($D_1, D_2, ...D_m$) and solubility ($S_1, S_2, ...S_m$) coefficients. For the case of a dual composite system, the proposed time lag formula [14] is

$$\theta_{12} = \frac{\frac{L_1^2}{D_1}\left(\frac{L_1}{6D_1S_1} + \frac{L_2}{2D_2S_2}\right) + \frac{L_2^2}{D_2}\left(\frac{L_2}{6D_2S_2} + \frac{L_1}{2D_1S_1}\right)}{\frac{L_1}{D_1S_1} + \frac{L_2}{D_2S_2}} \tag{5.46}$$

Table 5.3 Arbitrary properties of the composite membrane system for the validation of the numerical solution

	Layer 1	**Layer 2**
D [cm^2/s]	6.0×10^{-7}	4.5×10^{-8}
S [cm^3 (STP) cm^{-3} $cmHg^{-1}$]	0.003877	0.008444
L [cm]	0.0021	0.0042

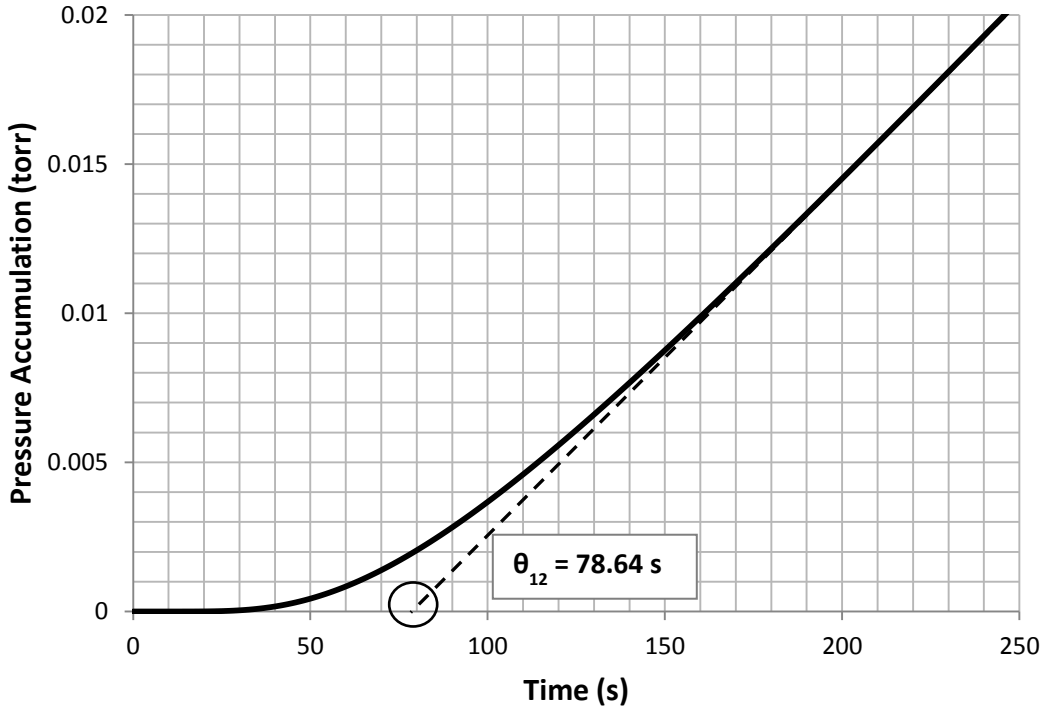

Figure 5.7 Numerical simulation of the pressure accumulation in a composite membrane system from Table 5.3

Estimation of the time lag using Eq. (5.46) from the parameters of Table 5.3 yields a value of θ_{12} = 78.68. The numerical solution is validated by extrapolating the linear asymptote of the downstream pressure profile using the classical time lag method. A near-exact time lag of θ_{12} = 78.64 is obtained; this is illustrated in Fig 5.7.

5.3 Comparison with Experimental Pressure Response Curves

The main purpose of this section is to *further* investigate the integrity of the 2 reservoir gas membrane permeation system constructed for this project, which was discussed in greater detail at Chapters 2 and 3. The compatibility of the developed model with the experimental results is carried in this section, where Daynes' classical time lag method and the short time solution (Chapter 2) are used as a reference point for this analysis.

The experiment is carried at a feed pressure of $p = 3.372$ *psia*, and an ambient temperature of $T = 295.2$ *K*. As detailed in the earlier chapters, a 10% PPO membrane is used, with both reservoir volumes configured as tubing only at minimum resistance to gas flow.

Reference: Classical <u>Downstream</u> Time Lag Method

Firstly, a complete test is performed where steady state permeation is achieved. The properties are obtained using time lag method on the downstream pressure profile.

$$D = \frac{L^2}{6\theta_{down}} \tag{5.47}$$

$$S = \left.\frac{dp}{dt}\right|_{\infty} \frac{L \cdot V}{A \cdot \Delta p \cdot R \cdot T \cdot D} \tag{5.48}$$

After extracting *D* and *S* using Eq. (5.47 & 5.48), they are used as input parameters for the numerical model.

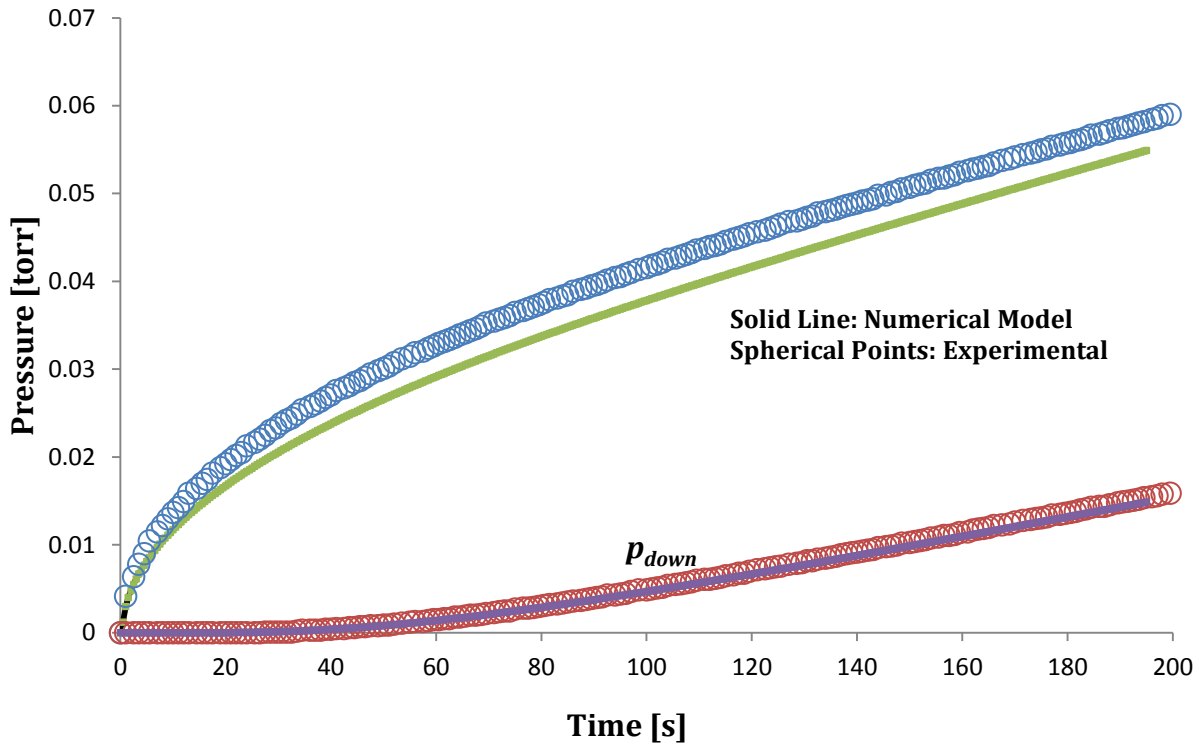

Figure 5.8 Experimental and modelled pressure profiles based on the membrane properties extracted from downstream time lag method

Fig. 5.8 illustrates the recorded pressure profiles, and the respective simulation results. The figure shows is excellent compliance between the downstream of pressure profiles, which further acts as a testament to the well-established design of the downstream reservoir previously employed by Lashkari and Kruczek [15][16]. The simulated upstream pressure profile is however slightly overestimated (higher

permeation), this is due to the 'resistance' present with the flow of species within the tubing of the upstream reservoir. This causes the plot to slightly 'jump' upwards. However, the shape of the two upstream plots is very identical, especially when observing the steady state slope.

Reference: Classical <u>Upstream</u> Time Lag Method

Carried out in a similar manner as the downstream, only this time by observing the pressure decay on the upstream reservoir, where

$$D = -\frac{L^2}{3\theta_{up}} \tag{5.49}$$

The obtained value of D is $3.788 \times 10^{-8}\ cm^2/s$, while $S = 0.009768\ cm^3\ (STP)\ cm^{-3}\ cmHg^{-1}$. Similarly to Fig. 5.8, a comparison between the experimental and modelled pressure profile is carried out

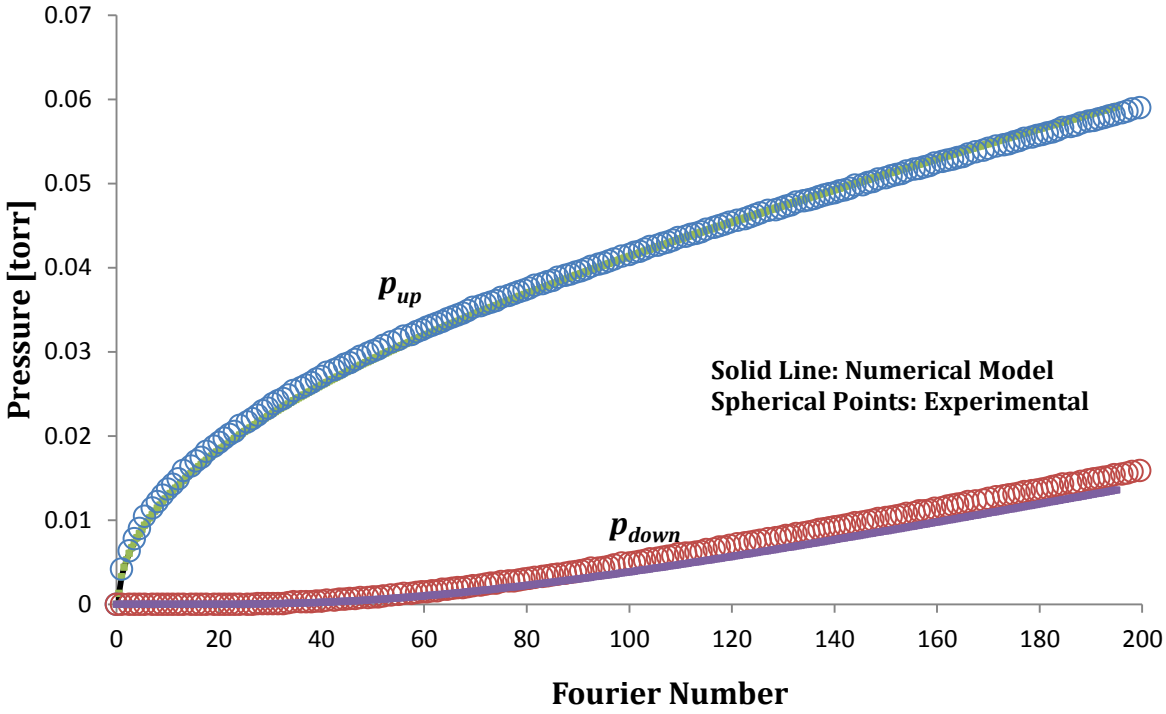

Figure 5.9 Experimental and modelled pressure profiles based on the membrane properties extracted from upstream time lag method

Surprisingly enough, Fig. 5.9 shows that the simulation results exhibited an improved compliance with the experimental data when compared to extracting the properties using the downstream time lag method. This is owed to the improved estimation of the permeability using the upstream time lag method (*P = 3.6 Barrer*) as opposed to the downstream (*P = 3.7 Barrer*) time lag method. As expected, this time the downstream profiles are more offset as opposed to the upstream which was evident previous (Fig. 5.8).

Reference: Short Cut Method Developed in Chapter 2

Using the tools proposed for the short time determination of membrane properties, an attempt is made to predict the entirety of the pressure profiles using a small set recorded data during the very early stages of the permeation test. Again, the predicted values of D and S from the short cut solution would act as inputs for the numerical model. To recap the short cut methods, the diffusivity is obtained from the slope of the linearized plot of $\ln\left(p_{down}/\sqrt{t}\right)$ vs. t^{-1}, where

$$slope = -\frac{L^2}{4D} \tag{5.50}$$

While the estimate of the permeability is discussed in greater detail in Chapter 2

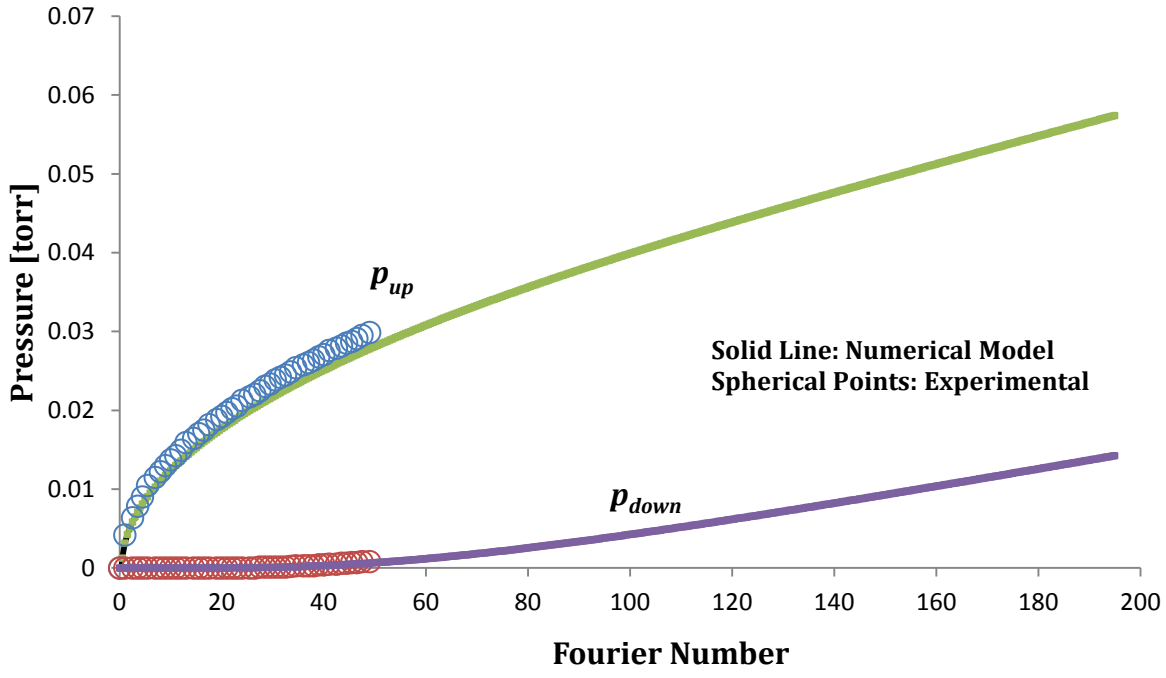

Figure 5.10 Experimental and predicted modelled pressure profiles based on the membrane properties extracted using the newly developed short cut method

As shown in Fig. 5.10, the predicted sets of the pressure profile using the collected data at early short times using this method are also in exceptional agreement with each other. This further affirms the compatibility between the design of the experimental set, the developed tools for the short cut method, and the current numerical model.

5.4 Model Summary

Modified form of the finite differences (FD) equations	$C_i^{t+1}\left(1+\frac{2D\Delta t}{\Delta x^2}\right)-\frac{D\Delta t}{\Delta x^2}C_{i-1}^{t+1}+\frac{D\Delta t}{\Delta x^2}C_{i+1}^{t+1}=\left(\frac{1-f}{f}\right)\left(-C_i^t\left(1+\frac{2D\Delta t}{\Delta x^2}\right)+\frac{D\Delta t}{\Delta x^2}C_{i-1}^t-\frac{D\Delta t}{\Delta x^2}C_{i+1}^t\right)$ $f=\left(1-\exp\left(\frac{-D\Delta t}{\Delta x^2}\right)\right)^2-\frac{\Delta x^2}{D\Delta t}$
Diffusion coefficient estimate for dual mode diffusion	$D(C)=D^*\cdot\left[\frac{1+FK\big/1+((b/S)C_D)^2}{1+K\big/1+((b/S)C_D)^2}\right]$ Where $C_{D,i-0.5}=\frac{1}{2}\left(C_{i-1}^t+C_i^t-\frac{2C'_H\,bp}{1+bp}\right)$
Permeate Flux	Upstream: $J(0,t)=D(C)\left\{\begin{array}{l}\frac{C_0^t-C_1^t}{\Delta x}-\frac{C_2^t-2C_1^t+C_0^t}{2\Delta x}+\frac{C_3^t-3C_2^t+3C_1^t-C_0^t}{6\Delta x}\\ -\frac{C_4^t-4C_3^t+6C_2^t-4C_1^t+C_0^t}{24\Delta x}\end{array}\right\}$ Downstream: $J(L,t)=D\frac{C_k^t-C_{k+1}^t}{\Delta x}$
Pressure	Upstream: $p_{up}(t)=p-\frac{pSRTA}{C\cdot V_1}\left(\frac{\Delta t}{6}\right)\left[J_0^0+2\left(J_0^{0.5}\right)+4\left(J_0^1\right)+2\left(J_0^{1.5}\right)+\ldots+J_0^n\right]$ Downstream: $p_{down}(t)=\frac{pSRTA}{C\cdot V_2}\left(\frac{\Delta t}{6}\right)\left[J_k^0+2\left(J_k^{0.5}\right)+4\left(J_k^1\right)+2\left(J_k^{1.5}\right)+\ldots+J_k^n\right]$
Finite difference equation at interface of composite membrane	$\frac{C_i^t-C_i^{t-1}}{\Delta t}=\frac{D_1C_{i-1}^t-\left(D_1+D_1\left(\frac{D_2}{D_1}\right)\left(\frac{S_2}{S_1}\right)\right)C_i^t+D_1\left(\frac{D_2}{D_1}\right)\left(\frac{S_2}{S_1}\right)C_{i+1}^t}{\Delta x^2}$

Nomenclature:

A: Membrane/film cross-sectional area

b: Hole affinity constant

C: Concentration

C'_H: Hole saturation constant

D: Diffusion coefficient

erf: Error Function

L: Thickness of membrane/film

J: Flux

k: Number of slices in the FD space domain

n: Number of slices in the FD time domain

p: Absolute feed pressure

P: Permeability coefficient

R: Ideal gas constant

S: Solubility coefficient

t: Time

T: Absolute temperature (K)

V: Reservoir Volume

x: Distance within membrane film

C'_H: Hole saturation constant

Greek Symbols:

θ: Time lag (s)

Δ: Difference

Γ: Total run time

Subscripts:

up: Upstream reservoir

down: Downstream reservoir

i: Node positioning in space domain

A: Component A

1: Composite membrane 1 (for D, S, and L)

2: Composite membrane 2 (for D, S, and L)

1: Upstream (for V)

2: Downstream (for V)

∞: Steady State

D: Henry Sites

H: Langmuir Sites

Subscripts:

t: Node positioning in time domain

References

[1] D.A. Anderson, J.C. Tannehill, Computational Fluid Mechanics and Heat Transfer, Second Edition, Taylor & Francis, 1984, p. 127.

[2] S.C. Chapra, R.P. Canale, Numerical Methods for Engineers, Fifth Edition, McGraw-Hill Publishing, 2007, p. 525.

[3] S.V. Patankar, B.R. Baliga, A New Finite Difference Scheme for Parabolic Differential Equations, Num. Heat Transfer Part A: App. 1 (1978) 27-37.

[4] J. Crank, J.S. Park, Diffusion in Polymers, Academic Press Inc. (London), 1968, p. 156.

[5] S.V. Patankar, Numerical Heat Transfer and Fluid Flow, Hemisphere Publishing Corporation, New York, 1980, p. 54-56.

[6] M. Mulder, Basic Principles of Membrane Technology, Second Edition. Springer, 1996, p. 313.

[7] S.A. Stern, S. Zhou, Evidence of Dual-Mode Diffusion of Small Molecules in Glassy Poly(1-Trimethylsilyl-1-Propyne) from Fluorescence Photobleaching Recovery, J. Poly Sci Part c: Poly Letters 27 (1989) 427-431.

[8] K. Toi, K. Saito, Y. Suganuma, T. Ito, I. Ikemoto, Numerical Examination of the Dual-Mode Model for Permeation, Sorption, and Desorption Rate Curves, J Appl Polym Sci 46 (1992) 1939-1944.

[9] S.W. Rutherford, D.D. Do, Review of time lag permeation technique as a method for characterization of porous media and membranes, Adsorption 3 (1997) 283.

[10] H. Kumazawa, S.-Y. Bae, Sorption and Permeation Behavior for a Gas in Glassy Polymer Membrane Near the Glass Transition Temperature, 60 (1996) 115-121.

[11] J.B. Brolly, D.I. Bower, I.M. Ward, Finite Difference Modeling of the Gas Transport Process in Glassy Polymers, J. Poly Sci Part c: Poly Physics 34 (1996) 761-768.

[12] H.A. Daynes, The process of diffusion through a rubber membrane, Proc. R. Soc. London Ser. A 97 (685) (1920) 286–307.

[13] R. Ash, R.M. Barrer and J.H. Petropoulos, Diffusion in heterogeneous media: properties of a laminated slab, 14 (1963) 854-862

[14] J.A. Barrie, J.D. Levine, A.S. Michaels, P. Wong, Diffusion and Solution of Gases in Composite Rubber Membranes, Trans. Faraday Soc. 59 (1963) 869-878.

[15] S. Lashkari, B. Kruczek, H.L. Frisch, General solution for the time lag of a single tank receiver in the Knudsen flow regime and its implications for the receiver's configuration, J. Membr. Sci. 283 (2006) 88–101.

[16] S. Lashkari, B. Kruczek, Effect of resistance to gas accumulation in multi-tank receivers on membrane characterization by the time lag method. Analytical approach for optimization of the receiver, J. Membr. Sci. 360 (2010) 442–453.

CHAPTER 6

CONCLUSIONS, RECOMMENDATIONS, AND CONTRIBUTIONS

As an epilogue to the research conducted in this dissertation, the current chapter will provide concluding remarks on the studies encompassing the proposed novel scheme. Its contribution to the field of membrane science and technology is reported, alongside recommendations that may extend and improve upon what was already investigated

6.1 Conclusions & Recommendations

The theme of the current thesis is based on developing a faster method of characterizing gas transport in non porous polymeric membranes. Following a brief introduction, a comprehensive look into the mathematical and practical aspects of monitoring and predicting the pressure decay due to permeation is carried out. A summary of the most significant finds in this study are as follows:

- When inspecting of the average rate of pressure change (flux) in the upstream and downstream reservoirs of the membrane, a novel scheme is proposed to for the faster estimation of the ***permeability*** at only a $1/10^{th}$ of the time it takes to achieve steady state conditions.
- For estimating the ***diffusivity***, an alternative form to the downstream short time solution by Rogers et al [1] is conceived, which involves a more convenient way of directly inputting the pressure accumulation data points; instead of the error-prone 'rate of pressure accumulation' (flux).
- Short time results are in good agreement with the properties obtained using the standard time lag method. Accuracy of results, especially in the downstream, is improved with the use of a smaller receiving volume, membrane of lesser thickness, or a higher accuracy pressure transducer.
- The novel design of the upstream reservoir for measuring the pressure decay due to permeation was successful. However, the early design did reveal some problems such as the compression/expansion effects, and the resistance effect.
- The compression/expansions effects are difficult to eliminate. However, they may be minimized with the use of a lower accuracy/higher range pressure transducer, or by reducing the added volume due to the start-up of the permeation test.
- The resistance effect was coincidentally observed to behave as a layer of resistance to the membrane, e.g. a laminate, despite the fact that in reality it is due to the non-instantaneous equalization of pressure in the reference volume. This is loosely based on the concept addressed by Lashkari and Kruczek [2], and it is best tackled by configuring the reservoir (working and reference) as only tubing, or performing

an optimization on the location of the pressure transducer which yields the least amount of errors.

- For the many concepts disclosed in this thesis, a guide is provided for constructing a numerical model which simulates a depiction of the current experimental set-up. The model was validated in many aspects, and yielded a good agreement with the experimental data.

6.2 Contributions

When it comes to performing gas permeation tests in ideal systems, this thesis contributes to the field of membrane science and technology in the following ways:

- From a very early set of the transient pressure decay/accumulation data, a novel scheme is developed for not only the estimation of permeation properties, but also a prediction of the approach to steady state prior to achieving it.
- Unlike the classical time lag method, not only does it eliminate the requirement of achieving steady state, but it also imposes a better compliance with the boundary conditions set by the time lag method.
- A partial method for estimation of the membrane properties from only the short time pressure decay is carried out. The method may not be as concrete as the ones previously presented, but solid foundations to its derivation are laid out to bring about the possibility of more established formulas in the future.
- A detailed design and construction of the upstream reservoir or the measurement of the pressure decay of low permeability materials at relatively high pressures.

- A methodology for developing a numerical model for simulating the two reservoir gas permeation system is provided.

References

[1] W.A. Rogers, R.S. Buritz, D. Alpert, Diffusion coefficient, solubility, and permeability for helium in glass, J. Appl. Phys. 257 (1954) 868–875.

[2] S. Lashkari, B. Kruczek, Effect of resistance to gas accumulation in multi-tank receivers on membrane characterization by the time lag method. Analytical approach for optimization of the receiver, J. Membr. Sci. 360 (2010) 442–453.

Appendix A

Mathematical Derivation of the Short Time Solution

A.1 General Solution:

A.1.1 Fick's 2nd Law of Diffusion: Analytical Solution [Finite Slab]

$$\frac{\partial C_A}{\partial t} = D_A \frac{\partial^2 C_A}{\partial x^2}$$

Boundary Conditions: $\begin{cases} C_A(x,0) = C_{Ai} \\ C_A(0,t) = C_{Ao} \\ C_A(L,t) = C_{AL} \end{cases}$

This is used to define the changes in concentration over space (x) and time (t) under a known diffusion coefficient (species A) within a membrane with a thickness L.

Define variables in dimensionless form:

Space: $X = \frac{x}{L}$

Time: $\tau = \frac{Dt}{L}$

Concentration: $\theta = \frac{C_{Ai} - C_A}{C_{AL} - C_{Ao}}$

$\frac{\partial C_A}{\partial t} = D\frac{\partial^2 C_A}{\partial x^2} \rightarrow \frac{\partial \theta}{\partial \tau} = \frac{\partial^2 \theta}{\partial X^2}$ Dimensionless Boundary Conditions: $\begin{cases} \theta(X,0) = 0 \\ \theta(0,\tau) = 1 \\ \theta(1,\tau) = 0 \end{cases}$

Solution performed using Laplace Transforms:

LHS: $L\left[\frac{\partial \theta}{\partial \tau}\right] = s\bar{\theta}(s) - \overbrace{\theta_{\tau=0}}^{\theta=0}$ RHS: $L\left[\frac{\partial^2 \theta}{\partial X^2}\right] = \frac{\partial^2 \bar{\theta}}{\partial X^2} = \bar{\theta}''(s)$

Therefore: $s\bar{\theta}(s) = \bar{\theta}''(s)$

After integration of the equation above: $\theta = A\exp\left(-\sqrt{s}X\right) + B\exp\left(\sqrt{s}X\right)$

(A.1)

Apply 3rd dimensionless boundary condition:

$$\begin{aligned} &A\exp\left(-\sqrt{s}X\right) + B\exp\left(\sqrt{s}X\right) = 0 \\ &A\exp\left(-\sqrt{s}X\right) = -B\exp\left(\sqrt{s}X\right) \\ &A = -B\exp\left(2\sqrt{s}X\right) \end{aligned} \quad \text{(A.2)}$$

Apply 2nd dimensionless boundary condition:

$$A + B = \frac{1}{s} \quad \text{(A.3)}$$

Substitute Eq. (A.2) into Eq. (A.3):

$$-B\exp\left(2\sqrt{s}\right)+B=\frac{1}{s}\quad\rightarrow\quad B=\frac{1}{s\left(1-\exp\left(2\sqrt{s}\right)\right)} \tag{A.4}$$

Reminder:

$A=-B\exp\left(2\sqrt{s}X\right)$ (From Eq. (A.2))

Therefore, using Eq. (A.4)

$$A=-\frac{\exp\left(2\sqrt{s}\right)}{s\left(1-\exp\left(2\sqrt{s}\right)\right)} \tag{A.5}$$

Substitute equations (A.4) and (A.5) (A and B constants) into (A.1)

$$\theta=-\frac{\exp\left(2\sqrt{s}\right)\exp\left(-\sqrt{s}X\right)}{s\left(1-\exp\left(2\sqrt{s}\right)\right)}+\frac{\exp\left(\sqrt{s}X\right)}{s\left(1-\exp\left(2\sqrt{s}\right)\right)}$$

Multiply both terms in RHS by $\left(\frac{\exp\left(-2\sqrt{s}\right)}{\exp\left(-2\sqrt{s}\right)}\right)$:

$$\theta=-\frac{\exp\left(-\sqrt{s}X\right)}{s\left(\exp\left(-2\sqrt{s}\right)-1\right)}+\frac{\exp\left(\sqrt{s}X\right)\exp\left(-2\sqrt{s}\right)}{s\left(\exp\left(-2\sqrt{s}\right)-1\right)}$$

$$\theta=\frac{\exp\left(\sqrt{s}\left(X-2\right)\right)-\exp\left(-\sqrt{s}X\right)}{s\left(1-\exp\left(-2\sqrt{s}\right)\right)} \tag{1.1.6}$$

Taylor series approximation of $\frac{1}{1-\exp\left(-2\sqrt{s}\right)}$:

$$\frac{1}{1-\exp\left(-2\sqrt{s}\right)} = 1+\exp\left(-2\sqrt{s}\right)+\exp\left(-4\sqrt{s}\right)+\exp\left(-6\sqrt{s}\right)+\ldots = \sum_{n=0}^{\infty}\exp\left(-2n\sqrt{s}\right)$$

Apply the series to Eq. (A.6):

$$\theta = \frac{1}{s}\sum_{n=0}^{\infty}\exp\left(\sqrt{s}\left(2n+X\right)\right)-\frac{1}{s}\sum_{n=0}^{\infty}\exp\left(\sqrt{s}\left(-2n+2-X\right)\right) \tag{A.7}$$

Now, invert equation (A.7) back to time domain:

$$L^{-1}\left[\frac{\exp\left(-a\sqrt{s}\right)}{s}\right] = erfc\left(\frac{a}{2\sqrt{\tau}}\right)$$

Profile in dimensionless form:

$$\theta = \sum_{n=0}^{\infty}erfc\left(\frac{2n+X}{2\sqrt{\tau}}\right)-\sum_{n=0}^{\infty}erfc\left(\frac{2n+2-X}{2\sqrt{\tau}}\right) \tag{A.8}$$

Finally, revert back to dimensional form:

$$C_A(x,t) = C_{Ai}-\left(C_{AL}-C_{A0}\right)\sum_{n=0}^{\infty}\left[erfc\left(\frac{2L^{3/2}n+\sqrt{L}x}{2L\sqrt{D_A t}}\right)-erfc\left(\frac{2L^{3/2}\left(N+1\right)+\sqrt{L}x}{2L\sqrt{D_A t}}\right)\right] \tag{A.9}$$

In cases where $C_{Ai} = C_{AL} = 0$

$$C_A(x,t) = C_{A0}\sum_{n=0}^{\infty}\left[erfc\left(\frac{2L^{3/2}n+\sqrt{L}x}{2L\sqrt{D_A t}}\right)-erfc\left(\frac{2L^{3/2}\left(n+1\right)+\sqrt{L}x}{2L\sqrt{D_A t}}\right)\right]$$

A.1.2 Flux Profile:

Fick's 1st law of diffusion:

$$J_A(x,t) = -D_A \frac{\partial C_A}{\partial x}$$

$$J_A(x,t) = -D_A \frac{\partial}{\partial x}\left\{ C_{Ai} - \left(C_{AL} - C_{A0}\right)\sum_{n=0}^{\infty}\left[erfc\left(\frac{2L^{3/2}n + \sqrt{L}x}{2L\sqrt{D_A t}} \right) - erfc\left(\frac{2L^{3/2}(n+1) + \sqrt{L}x}{2L\sqrt{D_A t}} \right)\right]\right\}$$

After obtaining the derivative of the concentration profile:

$$J_A(x,t) = D_A\left\{ C_{Ai} - \frac{\left(C_{AL} - C_{A0}\right)}{\sqrt{\pi D_A t}}\sum_{n=0}^{\infty}\left[\begin{array}{l} \exp\left(-\dfrac{x^2 - 4L(n+1)x + 4L^2(n+1)^2}{4D_A t} \right) \\ + \exp\left(-\dfrac{x^2 - 4Lnx + 4L^2 n^2}{4D_A t} \right) \end{array}\right]\right\} \quad \text{(A.10)}$$

During cases where $C_{Ai} = C_{AL} = 0$

$$J_A(x,t) = \frac{\sqrt{D_A}C_{A0}}{\sqrt{\pi t}}\sum_{n=0}^{\infty}\left[\begin{array}{l} \exp\left(-\dfrac{x^2 - 4L(n+1)x + 4L^2(n+1)^2}{4D_A t} \right) \\ + \exp\left(-\dfrac{x^2 - 4Lnx + 4L^2 n^2}{4D_A t} \right) \end{array}\right] \quad \text{(A.11)}$$

A.2 Downstream of Membrane

A.2.1 Flux Profile at the outflow (x = L):

$$J_A(L,t)=\frac{\sqrt{D_A}C_{A0}}{\sqrt{\pi t}}\sum_{n=0}^{\infty}\left[\exp\left(-\frac{L^2\left(1-4(n+1)+4(n+1)^2\right)}{4D_At}\right)+\exp\left(-\frac{L^2\left(1+4n+4n^2\right)}{4D_At}\right)\right] \qquad \text{(A.12)}$$

Equation (A.12) above will be rearranged to match the form given in Rutherford at. Al (1996):

$$J_A(L,t)=\frac{\sqrt{D_A}C_{A0}}{\sqrt{\pi t}}\exp\left(-\frac{L^2}{4Dt}\right)\sum_{n=0}^{\infty}\left[\begin{array}{l}\exp\left(\frac{L^2(n+1)}{D_At}\right)\exp\left(\frac{-L^2(n+1)^2}{D_At}\right)\\+\exp\left(\frac{-L^2n}{D_At}\right)\exp\left(\frac{-L^2n^2}{D_At}\right)\end{array}\right]$$

$$J_A(L,t)=\frac{\sqrt{D_A}C_{A0}}{\sqrt{\pi t}}\exp\left(-\frac{L^2}{4Dt}\right)\sum_{n=0}^{\infty}\left[\begin{array}{l}\exp\left(\frac{L^2n+L^2}{D_At}\right)\exp\left(\frac{-L^2n^2-2L^2n-L^2}{D_At}\right)\\+\exp\left(\frac{-L^2n}{D_At}\right)\exp\left(\frac{-L^2n^2}{D_At}\right)\end{array}\right]$$

$$J_A(L,t)=\frac{\sqrt{D_A}C_{A0}}{\sqrt{\pi t}}\exp\left(-\frac{L^2}{4Dt}\right)\sum_{n=0}^{\infty}\left[\begin{array}{l}\exp\left(\frac{L^2n}{D_At}\right)\exp\left(\frac{L^2}{D_At}\right)\exp\left(\frac{-L^2n^2}{D_At}\right)\exp\left(\frac{-2L^2n}{D_At}\right)\exp\left(\frac{-L^2}{D_At}\right)\\+\exp\left(\frac{-L^2n}{D_At}\right)\exp\left(\frac{-L^2n^2}{D_At}\right)\end{array}\right]$$

This simplifies to:

$$J_A(L,t)=\frac{\sqrt{D_A}C_{A0}}{\sqrt{\pi t}}\exp\left(-\frac{L^2}{4Dt}\right)\sum_{n=0}^{\infty}\left[\exp\left(\frac{-L^2n^2}{D_At}\right)\exp\left(\frac{-L^2n}{D_At}\right)+\exp\left(\frac{-L^2n}{D_At}\right)\exp\left(\frac{-L^2n^2}{D_At}\right)\right]$$

$$J_A(L,t) = \frac{2\sqrt{D_A}C_{A0}}{\sqrt{\pi t}} \exp\left(-\frac{L^2}{4Dt}\right)\sum_{n=0}^{\infty}\exp\left(\frac{-L^2n^2 - L^2n}{D_A t}\right)$$

$$\underbrace{J_A(L,t) = \frac{2\sqrt{D_A}C_{A0}}{\sqrt{\pi t}} \sum_{n=0}^{\infty}\exp\left(\frac{-4L^2n^2 - 4L^2n - L^2}{4D_A t}\right)}$$

$$\Downarrow$$

$$J_A(L,t) = \frac{2\sqrt{D_A}C_{A0}}{\sqrt{\pi t}} \sum_{n=0}^{\infty}\exp\left(\frac{-(2n+1)^2L^2}{4D_A t}\right) \tag{A.13}$$

Eq. (A.13) above will be used to obtain the short time solution for the outflow

A.2.2 Pressure profile at the outflow (x = L):

The Flux profile from Eq. (A.13) is transformed to provide the pressure profile instead.

$$p_A(L,t) = \frac{p_{A0}SRTA}{C_{A0}V}\int_0^t J_A(L,t)dt \tag{A.14}$$

$$p_A(L,t) = \frac{p_{A0}SRTA}{C_{A0}V}\int_0^t \frac{2\sqrt{D_A}C_{A0}}{\sqrt{\pi t}} \sum_{n=0}^{\infty}\exp\left(\frac{-(2n+1)^2L^2}{4D_A t}\right)dt \tag{A.15}$$

$$p_A(L,t) = \frac{2p_{A0}SRTA\sqrt{D_A}}{V\sqrt{\pi}}\int_0^t \frac{1}{\sqrt{t}} \sum_{n=0}^{\infty}\exp\left(\frac{-(2n+1)^2L^2}{4D_A t}\right)dt \tag{A.16}$$

$$p_A(L,t) = \frac{2p_{A0}SRTA\sqrt{D_A}}{V\sqrt{\pi}} \sum_{n=0}^{\infty}\left[2\sqrt{\pi}\left(\frac{(2n+1)L}{2\sqrt{D_A}}\right)\cdot erf\left(\frac{(2n+1)L}{2\sqrt{D_A t}}\right) + 2\sqrt{t}\exp\left(\frac{-(2n+1)^2L^2}{4D_A t}\right)\right]_0^t$$

$$p_A(L,t)=\frac{2p_{A0}SRTA\sqrt{D_A}}{V\sqrt{\pi}}\sum_{n=0}^{\infty}\left\{\begin{array}{l}\left(\frac{(2n+1)\sqrt{\pi}L}{\sqrt{D_A}}\right)\cdot\left[erf\left(\frac{(2n+1)L}{2\sqrt{D_At}}\right)-1\right]\\+2\sqrt{t}\exp\left(\frac{-(2n+1)^2L^2}{4D_At}\right)\end{array}\right\} \quad \text{(A.17)}$$

A.2.3 "Short Time" solution at the outflow (x = L):

For a Fourier number $\left(Fo=\frac{Dt}{L^2}\right)$ < 0.1 at short times, the latter terms (n>0) present in the series of Eq. (A.13) are negligible. Therefore they would be dropped, and only the first term (n=0) will be included. The result is Eq. (A.18) below:

$$J_A(L,t)=\frac{2\sqrt{D_A}C_{A0}}{\sqrt{\pi t}}\exp\left(-\frac{L^2}{4D_At}\right) \quad \text{(A.18)}$$

Attempt to linearize Eq. (A.18) by taking the natural logarithm of both sides

$$\ln\left(J_A(L,t)\sqrt{t}\right)=\ln\left(\frac{2\sqrt{D_A}C_{A0}}{\sqrt{\pi}}\right)-\frac{L^2}{4D_At} \quad \text{(A.19)}$$

Where the $\ln\left(J_A(L,t)\sqrt{t}\right)$ will be plotted vs. t^{-1}

- Slope $=-\frac{L^2}{4D_A}$
- Intercept $=\ln\left(\frac{2\sqrt{D_A}C_{A0}}{\sqrt{\pi}}\right)$

A.2.4 Outflow "Short Time" solution using pressure profiles:

Starting off with the actual outflow pressure profile from Equation (A.17):

$$p_A(L,t) = \frac{2p_{A0}SRTA\sqrt{D_A}}{V\sqrt{\pi}} \sum_{n=0}^{\infty} \left\{ \begin{array}{l} \left(\frac{(2n+1)\sqrt{\pi}L}{\sqrt{D_A}} \right) \cdot \left[erf\left(\frac{(2n+1)L}{2\sqrt{D_A t}} \right) - 1 \right] \\ + 2\sqrt{t} \exp\left(\frac{-(2n+1)^2 L^2}{4D_A t} \right) \end{array} \right\} \qquad \text{(A.17)}$$

It can be assumed that the latter parts of the series ($n > 0$) are of negligible magnitude, this results in the following:

$$p_A(L,t) = \frac{2p_{A0}SRTA\sqrt{D_A}}{V\sqrt{\pi}} \left\{ \left(\frac{\sqrt{\pi}L}{\sqrt{D_A}} \right) \cdot \left[erf\left(\frac{L}{2\sqrt{D_A t}} \right) - 1 \right] + 2\sqrt{t} \exp\left(\frac{-L^2}{4D_A t} \right) \right\} \qquad \text{(A.20)}$$

It could also be noted that while operating under short times and where the Fourier number is also maintained below 0.1, the error function from Eq. (A.20) can be approximated to 1.0, resulting in the following:

$$p_A(L,t) = \frac{4p_{A0}SRTA\sqrt{D_A t}}{V\sqrt{\pi}} \exp\left(\frac{-L^2}{4D_A t} \right) \qquad \text{(A.21)}$$

Linearize Eq. (A.21) by dividing off $\sqrt{t}$ and taking the natural logarithm on each side:

$$\ln\left[\frac{p_A(L,t)}{\sqrt{t}} \right] = \ln\left[\frac{4p_{A0}SRTA\sqrt{D_A}}{V\sqrt{\pi}} \right] - \frac{L^2}{4D_A} \frac{1}{t}$$

(A.22)

Where the $\ln\left(p_A(L,t) \big/ \sqrt{t} \right)$ will be plotted vs. t^{-1}

- Slope $= -\dfrac{L^2}{4D_A}$

- Intercept $= \ln\left[\dfrac{4p_{A0}SRTA\sqrt{D_A}}{V\sqrt{\pi}}\right]$

A.3 Upstream of Membrane

A.3.1 Flux Profile at the inflow (x = 0):

$$J_A(0,t) = \frac{\sqrt{D_A}C_{A0}}{\sqrt{\pi t}}\sum_{n=0}^{\infty}\left[\exp\left(-\frac{(n+1)^2L^2}{D_A t}\right)+\exp\left(-\frac{L^2n^2}{D_A t}\right)\right] \tag{A.23}$$

A.3.2 Pressure Profile at the inflow (x = 0):

$$p_A(0,t) = p_{A0} - \frac{p_{A0}SRTA}{C_{A0}V}\int_0^t J_A(0,t)dt \tag{A.24}$$

Where Equation (3.1.2) will be used to represent the influx: $J_A(0,t)$

$$p_A(0,t) = p_{A0} - \frac{p_{A0}SRTA}{C_{A0}V}\int_0^t \frac{\sqrt{D_A}C_{A0}}{\sqrt{\pi t}}\sum_{n=0}^{\infty}\left[\exp\left(-\frac{L^2\left(n^2+2n+1\right)}{D_A t}\right)+\exp\left(-\frac{L^2n^2}{D_A t}\right)\right]dt$$

$$p_A(0,t) = p_{A0} - \frac{p_{A0}SRTA\sqrt{D_A}}{V\sqrt{\pi}}\int_0^t \frac{1}{\sqrt{t}}\sum_{n=0}^{\infty}\left[\exp\left(-\frac{L^2(n+1)^2}{D_A t}\right)+\exp\left(-\frac{L^2n^2}{D_A t}\right)\right]dt$$

$$p_A(0,t) = p_{A0} - \frac{p_{A0}SRTA\sqrt{D_A}}{V\sqrt{\pi}}\int_0^t \frac{1}{\sqrt{t}}\sum_{n=0}^{\infty}\left[\exp\left(-\frac{L^2(n+1)^2}{D_A t}\right)+\exp\left(-\frac{L^2n^2}{D_A t}\right)\right]dt$$

Using Wolfram Mathematica's online integrator, the following is the result

$$P_A(0,t) = P_{A0} - \frac{P_{A0} SRTA\sqrt{D_A}}{V\sqrt{\pi}} \sum_{n=0}^{\infty} \left[\frac{2\exp\left(-\frac{L^2\left(2n^2+2n+1\right)}{D_A t}\right)}{\sqrt{D_A}} \right] \left\{ \begin{array}{l} \sqrt{\pi} nL \exp\left(\frac{L^2\left(2n^2+2n+1\right)}{D_A t}\right) erf\left(\frac{nL}{\sqrt{D_A t}}\right) \\ + \sqrt{\pi}(n+1)L \exp\left(\frac{L^2\left(2n^2+2n+1\right)}{D_A t}\right) erf\left(\frac{(n+1)L}{\sqrt{D_A t}}\right) \\ + \sqrt{D_A t}\left[\exp\left(\frac{L^2(n+1)^2}{D_A t}\right) + \exp\left(\frac{L^2 n^2}{D_A t}\right) \right] \end{array} \right\}_0^t$$

Simplified as follows...

$$P_A(0,t) = P_{A0} - \frac{2P_{A0} SRTA}{V\sqrt{\pi}} \sum_{n=0}^{\infty} \left\{ \begin{array}{l} \sqrt{\pi} nL \cdot erf\left(\frac{nL}{\sqrt{D_A t}}\right) + \sqrt{\pi}(n+1)L \cdot erf\left(\frac{(n+1)L}{\sqrt{D_A t}}\right) \\ + \sqrt{D_A t} \exp\left(-\frac{L^2\left(2n^2+2n+1\right)}{D_A t}\right)\left[\exp\left(\frac{L^2(n+1)^2}{D_A t}\right) + \exp\left(\frac{L^2 n^2}{D_A t}\right) \right] \end{array} \right\}_0^t$$

$$P_A(0,t) = P_{A0} - \frac{2P_{A0} SRTA}{V\sqrt{\pi}} \sum_{n=0}^{\infty} \left\{ \begin{array}{l} \sqrt{\pi} nL \cdot erf\left(\frac{nL}{\sqrt{D_A t}}\right) + \sqrt{\pi}(n+1)L \cdot erf\left(\frac{(n+1)L}{\sqrt{D_A t}}\right) \\ + \sqrt{D_A t}\left[\exp\left(\frac{-L^2(n+1)^2}{D_A t}\right) + \exp\left(\frac{-L^2 n^2}{D_A t}\right) \right] \end{array} \right\}_0^t$$

Now apply the upper and lower bounds, resulting in the final form of the pressure profile with Eq. (A.25):

$$p_A(0,t) = p_{A0} - \frac{2p_{A0} SRTAL}{V} \sum_{n=0}^{\infty} \left\{ \begin{array}{l} n \cdot erf\left(\frac{nL}{\sqrt{D_A t}}\right) + (n+1) \cdot erf\left(\frac{(n+1)L}{\sqrt{D_A t}}\right) - 2n - 1 \\ + \frac{\sqrt{\pi D_A t}}{L}\left[\exp\left(\frac{-L^2(n+1)^2}{D_A t}\right) + \exp\left(\frac{-L^2 n^2}{D_A t}\right) \right] \end{array} \right\} \qquad \text{(A.25)}$$

A.3.3 Fick's 2nd Law of Diffusion: Analytical Solution [Semi-infinite Slab]

At the upstream side of the medium where the diffusion occurs, and during short early times, the flux profile can be approximated as if it were a semi-infinite slab.

So before proceeding with the short time solution for the inflow, it is necessary to obtain the space-time concentration profile in a semi-infinite slab.

$$\frac{\partial C_A}{\partial t} = D_A \frac{\partial^2 C_A}{\partial x^2} \qquad \text{Boundary Conditions: } \begin{cases} C_A(x,0) = C_{Ai} \\ C_A(0,t) = C_{Ao} \\ C_A(\infty,t) = C_{A\infty} \end{cases}$$

Solution performed using Laplace Transforms:

LHS: $$L\left[\frac{\partial C_A}{\partial t}\right] = \int_0^\infty \exp(-st)\frac{\partial C_A}{\partial t}dt$$

RHS: $$L\left[\frac{\partial^2 C_A}{\partial x^2}\right] = \int_0^\infty \exp(-st)\frac{\partial^2 C_A}{\partial x^2}dt$$

Perform integration:

$$\frac{d^2 C_A}{dx^2} = s\overline{C_A} - C_A(x,0) \qquad \Rightarrow \qquad \overline{C_A} = A\exp\left(-\sqrt{\frac{s}{a}}x\right) + B\exp\left(\sqrt{\frac{s}{a}}x\right) + \frac{D}{s} \qquad \text{(A.26)}$$

Where the initial condition: $C_A(x,0) = C_{Ai}$

Note that the 2 boundary conditions in the Laplace Domain are as follows:

At $x = 0$, $\overline{C_A} = \frac{C_{Ao}}{s}$

At $x = \infty$, $\overline{C_A} = \frac{C_{A\infty}}{s}$

Now, back to Eq. (A.26), apply *second* boundary condition:

Implication that $B = 0$, and $D = C_{A\infty}$

First boundary condition:

$$\overline{C_A} = A\exp\left(-\sqrt{\frac{s}{a}}x\right) + \frac{C_{A\infty}}{s} \qquad \Rightarrow \qquad \frac{C_{Ao}}{s} = A + \frac{C_{A\infty}}{s}$$

Therefore: $A = \frac{C_{Ao} - C_{A\infty}}{s}$

Finally

$$\overline{C_A} = \left(\frac{C_{Ao} - C_{A\infty}}{s}\right)\exp\left(-\sqrt{\frac{s}{a}}x\right) + \frac{C_{A\infty}}{s}$$

Perform inverse Laplace transform of the equation above:

$$C_A(x,t) = \left[C_{Ao} - C_{A\infty}\right] erfc\left(\frac{x}{2\sqrt{D_A t}}\right) + C_{A\infty} \qquad \text{(A.27)}$$

A.3.4 Flux profile (In Semi-Infinite Slabs):

Fick's 1st law of diffusion:

$$J_A(x,t) = -D_A \frac{\partial C_A}{\partial x}$$

$$J_A(x,t) = -D_A\left[C_{Ao} - C_{A\infty}\right]\frac{\partial}{\partial x}\left\{erfc\left(\frac{x}{2\sqrt{D_A t}}\right) + C_{A\infty}\right\}$$

After obtaining the derivative of the concentration profile:

$$J_A(x,t) = \left[C_{Ao} - C_{A\infty}\right]\sqrt{\frac{D_A}{\pi t}}\exp\left(\frac{x^2}{4D_A t}\right) \quad \text{(A.28)}$$

In cases where $C_{A\infty} = 0$

$$J_A(x,t) = C_{Ao}\sqrt{\frac{D_A}{\pi t}}\exp\left(\frac{x^2}{4D_A t}\right) \quad \text{(A.29)}$$

A.3.5 "Short Time" solution at the inflow (x = 0) using semi-infinite assumption:

At $x = 0$, the equation simplifies to the following.

$$J_A(0,t) = C_{Ao}\sqrt{\frac{D_A}{\pi t}} \tag{A.30}$$

This can also be defined as a linear function of the following:

$$J_A(0,t) = C_{Ao}\sqrt{\frac{D_A}{\pi}}\frac{1}{\sqrt{t}}$$

Thus $J_A(0,t)$ will be plotted vs. $1/\sqrt{t}$:

- Slope: $C_{Ao}\sqrt{\frac{D_A}{\pi}}$

A.3.6 Inflow "Short Time" solution using pressure profiles:

This will be done by converting the upstream flux profile in Eq. (A.30) to a pressure profile (based on a semi-infinite slab):

$$p_A(0,t) = p_{A0} - \frac{p_{A0}SRTA}{C_{A0}V}\int_0^t J_A(0,t)dt \tag{A.31}$$

$$p_A(0,t) = p_{A0} - \frac{p_{A0}SRTA}{C_{A0}V}\int_0^t C_{Ao}\sqrt{\frac{D_A}{\pi}}\frac{1}{\sqrt{t}}dt$$

$$p_A(0,t) = p_{A0} - \frac{2p_{A0}SRTA\sqrt{D_A}}{V\sqrt{\pi}}\sqrt{t} \tag{A.32}$$

Where $p_A(0,t)$ will be plotted vs. $\sqrt{t}$:

- Slope: $-\frac{2p_{A0}SRTA\sqrt{D_A}}{V\sqrt{\pi}}$

Appendix B

Supplementary Material for "Shortcut Method for Faster Determination of Permeability Coefficient from Time Lag Experiments"

The following appendix reveals the [corrected] experimental results obtained for the paper in Chapter 2. The application and results obtained for classical and short cut methods is revealed. Firstly, the membrane is characterized using the classical time lag method where all properties are obtained (D, P, and S). The second section will carry out the short time solution for obtaining the diffusivity (D) using the downstream pressure accumulation profile, and lastly the short cut method is employed utilizing the average inflow and outflow fluxes for determining the permeability (P), and consequently solubility (S).

B.1 Transient Pressure-based permeation data

Table B.1 Transient pressure decay and accumulation data collected under 3 different pressures.

p_{A0} = 3.372*psia*			p_{A0} = 2.546*psia*			p_{A0} = 1.514*psia*		
***t* [s]**	p_A *(0, t)* [torr]	p_A *(l, t)* [torr]	***t* [s]**	p_A *(0, t)* [torr]	p_A *(l, t)* [torr]	***t* [s]**	p_A *(0, t)* [torr]	p_A *(l, t)* [torr]
0	0	0	0	0	0	0	0	0
1	0.004173	0	1	0.002636	0	1.5	0.001791	0
2.5	0.006373	0	2.5	0.005416	0	2.5	0.003531	0
3.5	0.007813	0	4	0.006896	0	3.5	0.004571	0
4.5	0.009013	0	5	0.007776	0	4.5	0.005311	0
5.5	0.010453	0	6	0.008496	0	5.5	0.006151	0
7	0.011473	0	7	0.009236	0	6.5	0.006691	0
8	0.012233	0	8	0.009916	0	7.5	0.007511	0
9	0.012993	0	9	0.010616	0	9	0.008051	0
10	0.013713	0	10	0.011096	0	10	0.008391	0
11	0.014253	0	11	0.011696	0	11	0.008811	0
12	0.014933	0	12	0.012136	0	12	0.009151	0
13	0.015893	0	13	0.012596	0	13	0.009491	0
14.5	0.016453	0	14	0.013056	0	14.0625	0.010051	0
15.5	0.017033	0	15	0.013856	0	15.5	0.010331	0
16.5	0.017473	0	16.5	0.014136	0	16.5	0.010691	0
17.5	0.018193	0	17.5	0.014616	0	17.5	0.010991	0
19	0.018813	0	18.5	0.014976	0	18.5	0.011551	0
20	0.019233	0	19.5	0.015476	0	20	0.011811	0
21	0.019733	0	21	0.016256	0	21	0.012071	0
22	0.020193	0	22.5	0.016416	0	22	0.012451	0
23	0.020533	0	23.67187	0.017036	0	23.5	0.012651	0
24	0.021273	0	25.21875	0.017416	0	24.5	0.012891	0
25.5	0.021693	0	26.5	0.018056	0	25.5	0.013211	0
26.5	0.022053	0	28	0.018296	0.0001	26.5	0.013311	0.0001
27.5	0.022473	0.0001	29	0.018656	0.0001	27.5	0.013591	0.0001
28.5	0.023033	0.0001	30	0.018776	0.0001	28.5	0.013771	0.0001
29.5	0.023333	0.0001	31	0.019156	0.0001	29.5	0.014131	0.0001
30.5	0.023853	0.0001	32	0.019876	0.0001	31	0.014291	0.0001
31.5	0.024193	0.0001	33.5	0.020076	0.0001	32	0.014411	0.0001
32.5	0.024453	0.0001	34.5	0.020236	0.0001	33	0.014631	0.0001
33.5	0.024893	0.0002	35.625	0.020616	0.0002	34	0.014851	0.0001

34.5	0.025413	0.0003	37	0.020876	0.0003	35	0.015171	0.0001
36	0.025773	0.0003	38	0.021256	0.0002	36.5	0.015391	0.0002
37	0.026073	0.0003	39	0.021656	0.0002	37.5	0.015491	0.0002
38	0.026373	0.0003	40	0.021636	0.0003	38.5	0.015631	0.0002
39	0.026793	0.0004	41	0.022196	0.0003	39.5	0.015891	0.0002
40	0.027073	0.0004	42	0.022316	0.0004	40.5	0.016071	0.0002
41	0.027593	0.0005	43.5	0.022216	0.0004	42	0.016331	0.0002
42.5	0.027873	0.0005	45	0.022636	0.0004	43	0.016431	0.0002
43.5	0.028153	0.0006	46	0.022896	0.0005	44	0.016511	0.0002
44.5	0.028513	0.0006	47	0.023116	0.0005	45	0.016731	0.0003
45.5	0.028733	0.0007	48	0.023456	0.0005	46	0.016911	0.0003
46.5	0.029093	0.0007	49	0.023676	0.0006	47.5	0.017131	0.0003
47.5	0.029493	0.0008	50.5	0.024056	0.0007	49	0.017351	0.0004
49	0.029853	0.0008	51.5	0.024416	0.0007	50	0.017491	0.0004
50	0.030113	0.0009	52.5	0.024456	0.0007	51	0.017451	0.0004
51	0.030353	0.0009	53.5	0.024896	0.0008	52	0.017811	0.0005
52	0.030773	0.001	55	0.025096	0.0008	53	0.018051	0.0005
53.5	0.031193	0.0011	56	0.025216	0.0009	54.5	0.018011	0.0005
55	0.031493	0.0012	57	0.025556	0.0009	55.5	0.018191	0.0005
56	0.031873	0.0013	58	0.025636	0.001	56.5	0.018411	0.0006
57.5	0.032073	0.0013	59	0.025816	0.001	57.5	0.018551	0.0006
58.5	0.032393	0.0014	60.5	0.026116	0.0011	59	0.018811	0.0006
59.5	0.032653	0.0015	61.5	0.026336	0.0011	60.5	0.018871	0.0007
60.5	0.032933	0.0015	62.5	0.026676	0.0012	61.5	0.018971	0.0007
61.5	0.033173	0.0016	63.5	0.026716	0.0013	62.5	0.019151	0.0007
62.5	0.033393	0.0016	64.5	0.026896	0.0013	63.5	0.019311	0.0008
63.5	0.033633	0.0018	65.5	0.027196	0.0014	65	0.019431	0.0008
64.5	0.033933	0.0018	67	0.027476	0.0015	66	0.019611	0.0009
65.5	0.034153	0.0019	68	0.027656	0.0015	67	0.019671	0.0009
66.5	0.034393	0.002	69	0.027816	0.0016	68	0.019751	0.0009
67.5	0.034633	0.002	70.5	0.027956	0.0017	69	0.019891	0.0009
68.5	0.034913	0.0021	71.5	0.028316	0.0017	70	0.020111	0.001
69.5	0.035293	0.0022	73	0.028516	0.0018	71.5	0.020231	0.001
71	0.035493	0.0023	74	0.028656	0.0019	72.5	0.020351	0.001
72	0.035713	0.0024	75	0.028896	0.0019	73.5	0.020591	0.0011
73	0.035893	0.0025	76.5	0.029076	0.002	74.5	0.020711	0.0011
74	0.036113	0.0025	77.5	0.029356	0.0021	76	0.020811	0.0012
75	0.036473	0.0027	78.51562	0.029556	0.0021	77.5	0.020931	0.0012
76.5	0.036713	0.0028	80	0.029736	0.0022	78.5	0.021071	0.0012
77.5	0.036933	0.0028	81	0.029936	0.0023	79.5	0.021231	0.0013

78.5	0.037153	0.0029	82	0.030156	0.0024	80.5	0.021291	0.0013
79.5	0.037353	0.003	83.5	0.030316	0.0025	82	0.021511	0.0014
80.5	0.037593	0.0031	84.5	0.030456	0.0026	83	0.021771	0.0014
81.5	0.037933	0.0032	85.5	0.030596	0.0026	84	0.021651	0.0015
83	0.038113	0.0033	86.5	0.030836	0.0027	85	0.021831	0.0015
84	0.038333	0.0034	87.5	0.030956	0.0027	86	0.021951	0.0015
85	0.038493	0.0035	88.5	0.031236	0.0028	87	0.022131	0.0016
86	0.038873	0.0036	90	0.031376	0.0029	88.5	0.022311	0.0017
87.5	0.039113	0.0037	91	0.031516	0.003	89.5	0.022191	0.0017
88.5	0.039253	0.0038	92	0.031696	0.0031	90.5	0.022331	0.0018
89.5	0.039493	0.0039	93	0.031936	0.0031	91.5	0.022331	0.0018
90.5	0.039633	0.004	94.5	0.032016	0.0033	92.71875	0.022551	0.0019
91.5	0.039873	0.0041	95.5	0.032316	0.0033	94	0.022711	0.0019
92.5	0.040153	0.0043	97.09375	0.032596	0.0034	95	0.022911	0.002
94	0.040453	0.0043	98.5	0.032696	0.0036	96	0.022971	0.002
95	0.040573	0.0044	99.5	0.032896	0.0036	97	0.023071	0.002
96	0.040813	0.0045	101.0313	0.033216	0.0037	98.5	0.023191	0.0021
97	0.041033	0.0047	102.5	0.033316	0.0038	99.5	0.023351	0.0021
98.5	0.041373	0.0049	103.5	0.033476	0.0039	100.5	0.023431	0.0021
100	0.041593	0.0049	104.5	0.033656	0.004	101.5	0.023491	0.0022
101	0.041833	0.005	105.5	0.033876	0.0041	102.5	0.023511	0.0023
102	0.041973	0.0051	107	0.034036	0.0042	103.5	0.023631	0.0023
103	0.042213	0.0052	108	0.034216	0.0043	104.5	0.023771	0.0023
104	0.042533	0.0054	109	0.034396	0.0043	106	0.023891	0.0024
105.5	0.042673	0.0055	110.5	0.034556	0.0044	107	0.023991	0.0025
106.5	0.042893	0.0056	111.5	0.034776	0.0045	108	0.024071	0.0025
107.5	0.043073	0.0057	113	0.034916	0.0046	109	0.024171	0.0026
108.5	0.043293	0.0058	114	0.035036	0.0047	110	0.024231	0.0026
109.5	0.043593	0.006	115	0.035256	0.0048	111.5	0.024411	0.0027
111	0.043753	0.0061	116	0.035376	0.0049	112.5	0.024531	0.0027
112	0.043973	0.0061	117	0.035596	0.005	113.5	0.024591	0.0028
113	0.044093	0.0062	118.5	0.035756	0.0051	114.5	0.024711	0.0028
114	0.044293	0.0063	119.5	0.035876	0.0052	115.5	0.024731	0.0028
115	0.044573	0.0065	120.5	0.035956	0.0052	117	0.025011	0.0029
116.5	0.044813	0.0066	121.5	0.036216	0.0053	118	0.025011	0.0029
117.5	0.044993	0.0068	123	0.036376	0.0054	119	0.025211	0.003
118.5	0.045173	0.0068	124	0.036536	0.0055	120	0.025271	0.003
119.5	0.045433	0.007	125	0.036696	0.0056	121.5	0.025351	0.0031
121	0.045653	0.0072	126	0.036756	0.0057	122.5	0.025451	0.0032
122.5	0.045853	0.0073	127	0.036916	0.0058	123.5	0.025511	0.0032

123.5	0.046053	0.0074	128	0.037156	0.0059	124.5	0.025611	0.0033
124.5	0.046293	0.0075	129.5	0.037236	0.0059	125.5	0.025751	0.0033
125.5	0.046533	0.0076	130.5	0.037416	0.006	126.5	0.025831	0.0034
127	0.046813	0.0078	131.5	0.037516	0.0061	128	0.025971	0.0034
128.5	0.046913	0.0079	132.5	0.037716	0.0062	129	0.026031	0.0035
129.5	0.047073	0.008	133.5	0.037836	0.0063	130	0.026111	0.0035
130.5	0.047313	0.0082	134.5	0.038076	0.0064	131.1719	0.026211	0.0036
131.5	0.047453	0.0082	136	0.038096	0.0065	132.5	0.026391	0.0037
132.5	0.047813	0.0084	137	0.038316	0.0066	133.5	0.026451	0.0037
134	0.047953	0.0085	138	0.038456	0.0067	134.5	0.026511	0.0038
135	0.048093	0.0086	139	0.038556	0.0068	135.5	0.026611	0.0038
136	0.048233	0.0087	140	0.038796	0.0068	136.5	0.026691	0.0038
137	0.048473	0.0089	141.5	0.038916	0.0069	137.5	0.026871	0.0038
138	0.048653	0.009	142.5	0.039056	0.007	139	0.026871	0.004
139	0.048793	0.0091	143.5	0.039196	0.0071	140	0.027091	0.004
140	0.048933	0.0092	144.5	0.039336	0.0072	141	0.027111	0.0041
141	0.049153	0.0093	145.5	0.039536	0.0073	142	0.027111	0.0041
142	0.049273	0.0094	147	0.039716	0.0074	143	0.027271	0.0042
143	0.049433	0.0095	148	0.039776	0.0075	144.5	0.027311	0.0042
144	0.049833	0.0097	149	0.039916	0.0076	145.5	0.027531	0.0043
145.5	0.049853	0.0098	150	0.040036	0.0076	146.5	0.027591	0.0044
146.5	0.050153	0.0099	151	0.040276	0.0078	147.5	0.027591	0.0044
147.5	0.050253	0.01	152	0.040356	0.0078	148.5	0.027751	0.0044
148.5	0.050553	0.0102	153	0.040436	0.0079	149.5	0.027891	0.0045
150	0.050713	0.0103	154	0.040616	0.008	151	0.027891	0.0045
151	0.050933	0.0104	155	0.040776	0.0081	152	0.028011	0.0046
152	0.051093	0.0105	156	0.040936	0.0082	153	0.028091	0.0047
153	0.051193	0.0106	157.5	0.041116	0.0083	154	0.028231	0.0047
154	0.051513	0.0108	158.5	0.041196	0.0084	155	0.028271	0.0047
155.5	0.051733	0.0109	159.5	0.041296	0.0085	156	0.028431	0.0048
156.5	0.051793	0.0111	160.5	0.041456	0.0086	157.5	0.028551	0.0049
157.5	0.052013	0.0111	161.5	0.041656	0.0086	158.5	0.028531	0.0049
158.5	0.052153	0.0112	163	0.041816	0.0088	159.5	0.028751	0.005
159.5	0.052453	0.0114	164.5	0.042056	0.0089	161	0.028851	0.0051
161	0.052633	0.0115	166	0.042236	0.0091	162	0.028751	0.0051
162	0.052793	0.0117	167.5	0.042456	0.0091	163	0.029051	0.0052
163	0.052913	0.0118	169	0.042576	0.0093	164	0.029131	0.0052
164	0.053113	0.0119	170	0.042756	0.0094	165.5	0.029071	0.0053
165	0.053213	0.012	171.5	0.042896	0.0095	166.5	0.029311	0.0053
166	0.053513	0.0122	172.5	0.043016	0.0096	168	0.029311	0.0054

167.5	0.053773	0.0123	173.5	0.043196	0.0096	169	0.029551	0.0054
169	0.053973	0.0124	175	0.043356	0.0098	170	0.029591	0.0055
170	0.054193	0.0126	176	0.043416	0.0099	171	0.029671	0.0056
171.5	0.054453	0.0128	177	0.043676	0.01	172	0.029711	0.0056
173	0.054613	0.0129	178.5	0.043776	0.0101	173.5	0.029851	0.0057
174	0.054753	0.013	179.5	0.043976	0.0102	174.5	0.029951	0.0057
175	0.054973	0.0131	181	0.044136	0.0103	175.5	0.029991	0.0058
176	0.055113	0.0132	182	0.044176	0.0104	176.5	0.030051	0.0058
177	0.055393	0.0134	183	0.044356	0.0105	178	0.030271	0.0059
178.5	0.055553	0.0135	184	0.044536	0.0106	179.5	0.030271	0.006
179.5	0.055713	0.0136	185	0.044736	0.0106	180.5	0.030471	0.0061
180.5	0.055833	0.0137	186.5	0.044796	0.0108	181.5	0.030491	0.0061
181.5	0.056033	0.0138	187.5	0.044976	0.0109	183	0.030631	0.0062
182.5	0.056153	0.014	188.5	0.045076	0.011	184.5	0.030831	0.0063
183.5	0.056373	0.0141	189.5	0.045216	0.011	185.5	0.030811	0.0063
184.5	0.056673	0.0143	191	0.045476	0.0112	186.5	0.030951	0.0063
186	0.056773	0.0144	192.5	0.045616	0.0113	188	0.031051	0.0064
187	0.056953	0.0144	193.5	0.045696	0.0114	189.5	0.031111	0.0065
188	0.057193	0.0146	194.5	0.045856	0.0115	190.5	0.031291	0.0066
189.5	0.057433	0.0148	195.5	0.045976	0.0116	192	0.031391	0.0066
190.5	0.057513	0.0149	196.5	0.046176	0.0116	193	0.031451	0.0067
191.5	0.057693	0.015	198	0.046276	0.0118	194	0.031571	0.0067
192.5	0.057853	0.0151	199	0.046396	0.0119	195.5	0.031651	0.0068
193.5	0.058033	0.0152	200.1094	0.046556	0.012	196.5	0.031771	0.0069
194.5	0.058213	0.0154	201.5	0.046736	0.0121	197.5	0.031791	0.0069
196	0.058433	0.0155	202.6406	0.046916	0.0122	198.5	0.031791	0.007
197	0.058613	0.0156	204	0.047056	0.0123	199.5	0.032011	0.007
198	0.058873	0.0158	205	0.047176	0.0124	201	0.032071	0.0071
199.5	0.059033	0.0159	206	0.047336	0.0125	202	0.032151	0.0071
200.5	0.059273	0.0161	207	0.047356	0.0126	203	0.032231	0.0072
202	0.059453	0.0162	208	0.047596	0.0127	204	0.032231	0.0072

B.2 Characterization using Classical Time Lag Method

B.2.1 Diffusion Coefficient

The diffusivity is measured by extrapolating the linear steady state portion of the pressure profiles to the x-axis, where the time lag θ, is obtained. The time lags of the downstream (θ_d) and upstream (θ_u) are evaluated. The diffusivity is estimated using the following expression

$$D = \frac{l^2}{6\theta_d} \qquad or \qquad D = -\frac{l^2}{3\theta_u} \tag{B.1}$$

Where, the thickness l = 0.0042 cm. So, in the case of calculating the diffusivity from the downstream pressure profile, where θ_d = 65.1 s.

$$D = \frac{(0.0042cm)^2}{6(65.1s)}$$

$$D = 4.52 \times 10^{-8} cm^2 s^{-1}$$

Table B.2 Estimated diffusivities using the upstream and downstream time lag methods

p_{A0} [psig]	From Downstream Time Lag		From Upstream Time Lag	
	θ_d [s]	D [cm²/s]	θ_u [s]	D [cm²/s]
3.372	65.1	4.52 x 10^{-8}	-155.2	3.788 x 10^{-8}
2.546	64.8	4.54 x 10^{-8}	-172.4	3.410 x 10^{-8}
1.514	65.7	4.51 x 10^{-8}	-155.9	3.770 x 10^{-8}

B.2.2 Permeability Coefficient

The permeability is measured by taking the slope of the linear steady state portion of the pressure profiles. The steady state slope of the downstream $\left(\left.\frac{dp_A(l,t)}{dt}\right|_{\infty}\right)$ and upstream $\left(\left.\frac{dp_A(0,t)}{dt}\right|_{\infty}\right)$ are evaluated. The permeability is estimated using the following expression

$$P = \left.\frac{dp_A}{dt}\right|_{\infty} \frac{V \cdot l}{A_f RT\Delta p} \tag{B.2}$$

Where, the thickness l = 0.0042 cm. The membrane cross-sectional area is A = 12.57 cm^2, and the operating temperature is T = 295.3 K. So for example, the downstream permeability is evaluated based on a reservoir volume of V = V_2 = 115.1 cm^3. In the case where the trans-membrane pressure is $\Delta p = p_{A0}$ = 3.372 psia, the pressure drop due to expansion is 17%, and the steady state slope is $\left.\frac{dp_A(l,t)}{dt}\right|_{\infty}$ = 0.0001095 torr/s.

$$P = [0.0001095\ \text{torr/s}]\frac{(115.1\ \text{cm}^2)(0.0042\ \text{cm})}{(12.57\text{cm}^2)(8.314\ \text{J/mol}\cdot\text{K})(295.3\ \text{K})(3.372\ \text{psia})} \times \left(\frac{1\text{m}}{10^6\ \text{cm}}\right) \times \left(\frac{22400\ \text{cm}^3(\text{STP})}{1\ \text{mole}}\right)$$
$$\times \left(\frac{1013251\ \text{pa}}{760\ \text{torr}}\right) \times \left(\frac{76\ \text{cmHg}}{14.696\ \text{psia}}\right) \times \left(\frac{1\ \text{Barrer}}{10^{-10}\ \text{cm}^3(\text{STP})\cdot\text{cm}\cdot\text{s}^{-1}\text{cm}^{-2}\cdot\text{cmHg}}\right) \times \left(\frac{1}{1-0.17}\right) = 3.69\ \text{Barrer}$$

Table B.3 Estimating steady state permeabilities using the upstream and downstream

p_{A0} [psig]	From Downstream St. State Slope		From Upstream St. State Slope	
	slope [torr/s]	***P*** [Barrer]	***slope*** [torr/s]	***P*** [Barrer]
3.372	0.0001095	3.69	0.0001630	3.70
2.546	0.0001110	3.74	0.0001622	3.69
1.514	0.0001105	3.72	0.0001648	3.77

B.3 Estimating the Diffusion Coefficient using the Downstream Short Time Solution

The pressure-based short time solution is expressed below

$$\ln\left[\frac{p_A(l,t)}{\sqrt{t}}\right] = \ln\left[\frac{4p_{A0}SRTA_f\sqrt{D_A}}{V_2\sqrt{\pi}}\right] - \frac{l^2}{4D_A}\frac{1}{t} \tag{B.3}$$

The diffusivity is obtained via the slope (m) of plotting the linear relationship between $y = \ln\left(p_A(l,t)/\sqrt{t}\right)$ against $x = t^{-1}$. The diffusivity is therefore

$$D_A = -\frac{l^2}{4m} \tag{B.4}$$

Table B.4 Application of the downstream short time solution at 3 different pressures

$p_{A0} = 3.372 psia$		$p_{A0} = 2.546 psia$		$p_{A0} = 1.514 psia$	
x	***y***	***x***	***y***	***x***	***y***
0.029850746	-10.273	0.035714	-10.8764426	0.032258	-10.9273
0.028985507	-9.88221	0.02807	-10.303717	0.024691	-10.3678
0.025641026	-9.65583	0.025	-9.95616781	0.021739	-10.026
0.025	-9.66849	0.02439	-9.96851412	0.02	-9.78006
0.024390244	-9.45769	0.02381	-9.69288082	0.018868	-9.58605
0.023529412	-9.47565	0.022989	-9.71042648	0.018349	-9.6
0.022988506	-9.30496	0.022222	-9.72737726	0.017391	-9.44447
0.02247191	-9.31633	0.021739	-9.51522316	0.01626	-9.32395
0.021978022	-9.17329	0.021277	-9.52597626	0.015748	-9.20642
0.021505376	-9.18416	0.020833	-9.53650296	0.015385	-9.21809
0.021052632	-9.06126	0.020408	-9.36449105	0.032258	-10.9273
0.020408163	-9.07681	0.019802	-9.22541689	0.024691	-10.3678
0.02	-8.96913	0.019417	-9.23522113	0.021739	-10.026
0.019607843	-8.97903	0.019048	-9.24483681	0.02	-9.78006
0.019230769	-8.88338	0.018692	-9.12073966	0.018868	-9.58605
0.018691589	-8.80229	0.018182	-9.13456542	0.018349	-9.6
0.018181818	-8.7291	0.017857	-9.02579164	0.017391	-9.44447

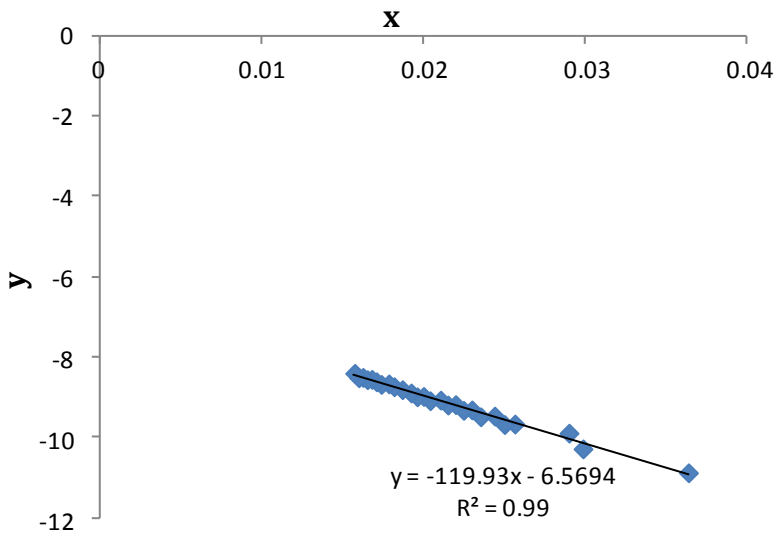

Figure B.1 Application of downstream short time solution, p_{A0} = 3.372 psia

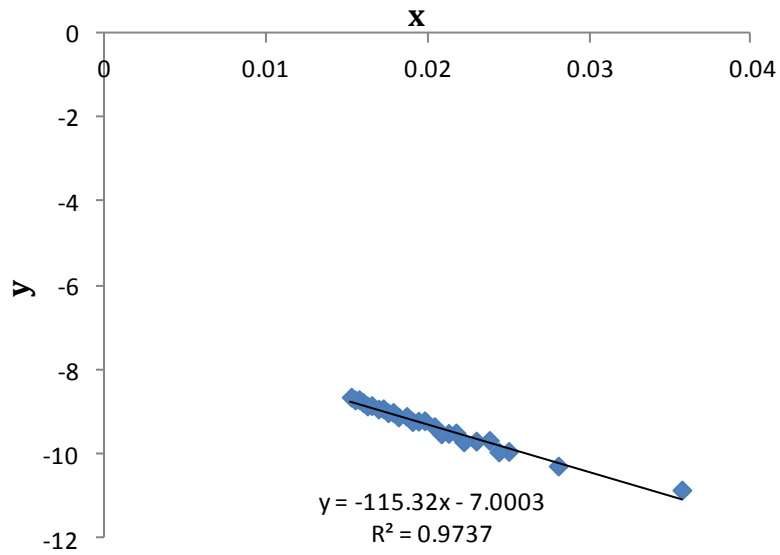

Figure B.2 Application of downstream short time solution, p_{A0} = 2.546 psia

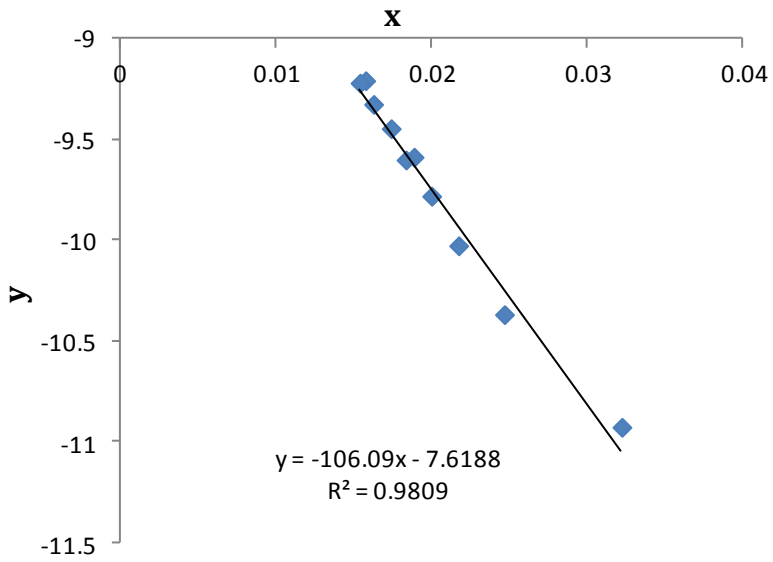

Figure B.3 Application of downstream short time solution, p_{A0} = 1.514 psia

Table B.5 Summary of applied short time solution for estimating the diffusivities attempted at 3 different pressures

p_{A0} [psig]	From Downstream St. State Slope	
	slope	***D*** [cm²/s]
3.372	-119.93	4.16 x 10^{-8}
2.546	-115.32	4.39 x 10^{-8}4
1.514	-106.09	4.59 x 10^{-8}

B.4 Estimating the Permeability Coefficient using the Short Cut Method

The actual permeability (P) of the membrane is based on the slope at the steady state (∞) portion of pressure profile $\left(\left.\frac{dp_A}{dt}\right|_{\infty}\right)$ in either the downstream $\left(\left.\frac{dp_A(l,t)}{dt}\right|_{\infty}\right)$ or the upstream $\left(\left.\frac{dp_A(0,t)}{dt}\right|_{\infty}\right)$

The short cut method is based on utilizing the average transient-based (t) pressure derivative:

$$\left.\frac{dp_{A,AVG}}{dt}\right|_t = \frac{1}{2}\left[\left.\frac{dp_A(0,t)}{dt}\right|_t\left(\frac{V_2}{V_1}\right)+\left.\frac{dp_A(l,t)}{dt}\right|_t\right] \tag{B.5}$$

Where a transient value of the permeability (P_t) is obtained

$$P_t = \left.\frac{dp_{A,AVG}}{dt}\right|_t \frac{V_2 \cdot l}{A_f RT\Delta p} \tag{B.6}$$

The fraction $\left(\frac{V_2}{V_1}\right)$ is the ratio of the downstream (V_2 = 115.1 cm^3) and upstream volumes (V_1 = 77.6 cm^3).

The time scale re-expressed in terms of the Fourier number $Fo = \left(\frac{Dt}{l^2}\right)$, and a correction factor (G) is applied to each estimated value of the transient permeability. The correction is a function of the Fourier number.

$$G = f(Fo) \tag{B.7}$$

Table B.6 Application of the short cut method by correcting for the transient permeabilities

p_{A0} = 3.372*psia*				p_{A0} = 2.546*psia*				p_{A0} = 1.514*psia*			
t **[s]**	***Fo***	P_t **[Barrer]**	***Corrected*** P_t **[Barrer]**	***t*** **[s]**	***Fo***	P_t **[Barrer]**	***Corrected*** P_t **[Barrer]**	***t*** **[s]**	***Fo***	P_t **[Barrer]**	***Corrected*** P_t **[Barrer]**
0	0	46.21612506	4.177747039	0	0	31.70791573		0	0	36.16565477	4.081782612
1	0.0026	23.11118045	3.793232213	1	0.0026	42.40645971	7.665703702	1.5	0.003733	41.59895904	3.906921787
2.5	0.005201	14.83796767	3.836190793	2.5	0.005201	27.10011801	6.927973082	2.5	0.006222	28.07872028	4.303513179
3.5	0.007801	12.25235466	4.820431286	4	0.007801	13.41428828	4.199990173	3.5	0.00871	16.38746871	3.676521235
4.5	0.010401	13.33324591	4.661829445	5	0.010401	9.251943834	3.344898894	4.5	0.011199	15.72400844	3.766287771
5.5	0.013002	11.53324109	3.477833496	6	0.013002	8.922253185	3.606446989	5.5	0.013688	13.4350705	3.629775305
7	0.015602	7.854404157	3.258546931	7	0.015602	8.778013526	3.886796358	6.5	0.016176	13.50141653	3.966900448
8	0.018202	6.813274562	3.546123392	8	0.018202	8.695590864	4.15879188	7.5	0.018665	14.33074187	4.283603419
9	0.020803	6.935760396	3.063681272	9	0.020803	7.191377279	3.676815479	9	0.022398	8.160561343	4.312499986
10	0.023403	5.649659131	3.001594438	10	0.023403	6.614418643	3.586848349	10	0.024887	7.364409017	3.293110427
11	0.026003	5.251580168	4.762561632	11	0.026003	6.531995981	3.733429211	11	0.027375	7.696139153	3.334887244
12	0.028604	7.946268534	4.493569709	12	0.028604	5.398684375	3.2356781	12	0.029864	6.269699569	5.088338148
13	0.031204	7.180732066	3.279068288	13	0.031204	5.357473044	3.352607836	13	0.032353	9.42113586	4.60918859
14.5	0.033804	5.037229957	3.027916966	14	0.033804	8.324688884	5.419094137	14.0625	0.034997	8.59181052	3.146466275
15.5	0.036405	4.4860437	3.696666616	15	0.036405	6.820475299	4.603573717	15.5	0.038574	6.00431546	4.675765203
16.5	0.039005	5.297512356	4.693065516	16.5	0.039005	4.285978435	2.990806314	16.5	0.041063	6.269699569	
17.5	0.041605	6.522370704	3.433639101	17.5	0.041605	5.254444716	3.78075004	17.5	0.043552	8.95671367	4.483673805
19	0.044206	4.639150994	3.117066161	18.5	0.044206	4.904148402	3.629775305	18.5	0.04604	8.59181052	3.693887164
20	0.046806	4.103275466	3.550032397	19.5	0.046806	8.695590864	6.60563305	20	0.049773	4.478356835	4.234854598
21	0.049406	4.562597347	2.654891663	21	0.049406	5.625346696	4.376928644	21	0.052262	6.667775732	4.855425841
22	0.052007	3.337738999	4.150865937	22.5	0.052007	4.430218094	3.523867231	22	0.054751	5.904796419	2.029619942

23	0.054607	5.113783604	4.697315482	23.67187	0.054607	6.387756322	5.184951532	23.5	0.058484	3.947588617	2.973016715
24	0.057207	5.68028059	2.674618463	25.21875	0.057207	6.321519067	5.227588481	24.5	0.060972	5.754296508	3.962887198
25.5	0.059808	3.179553404	3.601867675	26.5	0.059808	6.624754787	5.57269818	25.5	0.063461	5.764067308	4.830335151
26.5	0.062408	4.215377224	4.7951451	28	0.062408	4.584793897	3.917519135	26.5	0.06595	5.332818131	2.990806314
27.5	0.065009	5.532099948	3.316720075	29	0.065009	2.674316264	2.318059082	27.5	0.068438	4.327856924	4.36162443
28.5	0.067609	3.776671848	3.293110427	30	0.067609	2.493285532	2.189634289	28.5	0.070927	5.53989327	1.625222358
29.5	0.070209	3.705196503	3.755732657	31	0.070209	7.60349059	6.75784243	29.5	0.073416	5.53989327	3.927588785
30.5	0.07281	4.179829113	2.149096101	32	0.07281	6.078671339	5.461913356	31	0.077149	2.288937938	4.200680314
31.5	0.07541	2.368084748	3.449129165	33.5	0.07541	1.314342337	1.192798524	32	0.079637	3.317301359	4.285435881
32.5	0.07801	3.766287771	5.763099352	34.5	0.07801	4.312499986	3.94934492	33	0.082126	4.378837794	4.081782612
33.5	0.080611	6.24132015	4.486748895	35.625	0.080611	6.289214875	5.8073243	34	0.084615	5.289874318	3.906921787
34.5	0.083211	4.822728096	2.619753291	37	0.083211	3.66338821	3.408175347	35	0.087103	7.489064015	4.303513179
36	0.085811	2.79678517	2.361850458	38	0.085811	4.040139453	3.784405304	36.5	0.090836	4.702530873	3.676521235
37	0.088412	2.505881312	3.980984418	39	0.088412	2.961366577	2.791155739	37.5	0.093325	1.740361864	3.927588785
38	0.091012	4.200066494	3.617265976	40	0.091012	4.25068299	4.028960677	38.5	0.095813	4.179799712	3.917519135
39	0.093612	3.79690923	4.234854598	41	0.093612	5.9197419	5.639661016	39.5	0.098302	4.445183821	3.966900448
40	0.096213	4.424649133	4.355661317	42	0.096213	0.175181468	0.16766709	40.5	0.100791	4.511529848	4.283603419
41	0.098813	4.531824239	2.895084824	43.5	0.098813	1.619007062	1.556072359				
42.5	0.101413	3.000751303	4.177747039	45	0.101413	5.82113383	5.616152259				
		Average =	3.71 Barrer			**Average =**	3.95 Barrer			**Average =**	3.95 Barrer